Cell Migration on Opposing Rigidity-Protein Gradients: Single Cell and Co-culture Studies

Gaurav Jain

Dissertation submitted to the faculty of the Virginia Polytechnic Institute and State University in partial fulfillment of the requirements for the degree of

Doctor of Philosophy
In
Biomedical Engineering and Sciences

Padmavathy Rajagopalan
Rafael V. Davalos
Richey M. Davis
Scott S. Verbridge
Shay Soker

September 23 2014
Blacksburg, VA

Keywords: Cell Migration, Gradients, Durotaxis, Haptotaxis

Cell Migration on Opposing Rigidity-Protein Gradients: Single Cell and Co-culture Studies

Gaurav Jain

ABSTRACT

Cell migration is a complex physiological process that is important from embryogenesis to senescence. *In vivo*, the migration of cells is guided by a complex combination of signals and cues. Directed migration is typically observed when one of these cues is presented to cells as a gradient. Several studies have been conducted into directed migration on gradients that are purely mechanical or chemical. Our goal was to investigate cellular migratory behavior when cells are presented with a choice and have to choose between increasing substrate rigidity or higher protein concentration. We chose to focus on this unique environment since it recapitulates several interfacial regions *in vivo*. We have designed novel hydrogels that exhibit dual and opposing chemical and mechanical profiles using photo-polymerization. Our studies demonstrate that durotaxis, a well-known phenomenon, can be reversed when cells sense a steep protein profile in the opposite direction.

Fibroblasts were co-cultured with macrophages to obtain an understanding on how migration occurs when two different cell types are present in the same microenvironment. First, we investigated the migratory behavior of macrophages. These cell types exhibited a statistically significant preference to move towards the rigid/low collagen region of the interface. Interestingly, fibroblasts when co-cultured with macrophages, exhibited a preference for the low modulus-high collagen region of the interface. However, with the current sample size, these trends are statistically insignificant. On the contrary, the

presence of fibroblasts in the cellular microenvironment did not result in the reversal of durotaxis exhibited by macrophages. Macrophages secreted significantly higher levels of secreted tumor necrosis factor (TNF-alpha) in mono-cultures in contrast to fibroblast-macrophage co-cultures. This trend could be an indication of macrophage plasticity between mono- and co-cultures. In summary, we have designed dual and opposing rigidity-protein gradients on a hydrogel substrate that can provide new insights into cellular locomotion. These results can be used to design biomimetic interfaces, biomaterial implants and for tissue engineering applications.

ACKNOWLEDGEMENTS

I would like to express my sincere gratitude to my advisor Prof. Padma Rajagopalan for her guidance, motivation, knowledge and extreme patience throughout my graduate studies. Without her continuous support during research, this work would not have been possible. I would also like to thank my committee members Professors Rafael Davalos, Richey Davis, Scott Verbridge and Shay Soker for their guidance, insightful comments and suggestions during meetings and examinations. I would also extend my greatest thanks to Ms. Tess Sentelle, Ms. Pamela Stiff and Mr. David Ashwell (School of Biomedical Engineering and Sciences), Ms. Diane Cannaday, Ms. Tina Russell, Ms. Nora Bentley, and Mr. Mike Vaught (Chemical Engineering), Mr. Steve McCartney (Nanoscale Characterization and Fabrication Laboratory at the Institute for Critical Technologies and Applied Sciences,) Dr. Kristi DeCourcy (Confocal facility at the Fralin Life Science Institute) and Mr. Donald Leber (Micro & Nano Fabrication Laboratory) at Virginia Tech for providing their help in various forms in getting work done in time.

I would also like to thank my friend and labmate, Andrew Ford for his help with experiments. I consider myself fortunate to have met awesome lab mates during this time who cheered me up whenever I felt dull and made the lab a joyful place to work. This includes Dr. Adam Larkin, Cigdem Arca, Dr. Era Jain, Lucas Vu, Brandon Veres, Maggie Cassin, Sophia Orbach and Rebekah Less.

Words will not be enough to describe my heartfelt thanks to my very good friends Dr. Abhijit Gurjarpadhye, Dr. Hazitha Samuel, Somya Jain, Amrapali Dengada, Dr. Gurtej Singh, Dr. Neha Arya, Shilpa Soni, Dr. Nrusingh Mohapatra and Siddharth Sharma outside the lab who were my support system during all these four years. I also thank my sport buddies William Hubbard,

Prasad Vaidya, Dr. Satyavrata Samavedi, Hardik Zatakia and Harsh Deshpande with whom I played several sports and kept me sane.

This work would not have been possible without the unconditional support provided by my parents and grandparents during this entire time. I thank them for staying by me in times of need. They have encouraged me the most during these times and I am sure are they are the happiest of all today, when I submit this work for the degree.

Finally, I would also like to thank that invisible power for lighting my path, showing me the way and carrying me through it!

Gaurav Jain

Table of Contents

List of Figures

Chapter 1

Chapter 2

Chapter 3

Chapter 4

List of Tables

Chapter 2

Chapter 3

Chapter 4

Glossary

ADP - Adenosine diphosphate

AFM - Atomic force microscopy

APS - Ammonium persulphate

ATP - Adenosine triphosphate

Arp2/3 - Actin related protein 2 and 3

ADF - Actin depolymerizing factor

Cas - CRK - Crk-associated signaling

Cdc42 - cell division control protein 42 homolog

CCL2 - chemokine cysteine-cysteine motif ligand 2 (also called as Monocyte Chemotactic Protein-1

CCL7 - Cysteine-cysteine motif ligand 7 (also called as monocyte chemotactic protein 3)

CXCL4 - Cysteine-X-cysteine motif ligand 4 (also called Platelet factor 4)

CXCL12 - Cysteine-X-cysteine motif chemokine 12 (also called Stromal cell-derived factor 1)

DG1- Dual Gradient 1 (4-fold increase in surface-immobilized collagen on the low modulus side)

DG2- Dual Gradient 2 (7-fold increase in surface-immobilized collagen on the low modulus side)

DOCK - 180- dedicator of cytokinesis 180

DOPA - 3,4-dihydroxyphenyl-L-alanine

EGF - Epidermal growth factor

ECM - Extracellular matrix

ERK - Extracellular signal-regulated kinases

FAK - Focal adhesion kinase – FAK

FITC - Fluorescein isothiocyanate

FBS - Fetal bovine serum

GAPs - GTPase activating proteins

GEFs - Guanine nucleotide exchange factors

GRB2 - Growth-factor-receptor-bound protein 2

GTPases - Guanosine triphosphate (GTP)-binding protein

HEPES - 4-(2-hydroxyethyl)-1-piperazineethanesulfonic acid

IgG - Immunoglobulin

IL - Interleukin

iNOS - Inducible nitric oxide synthase

MEK- Mitogen-activated protein kinases

MLCK - Myosin light chain kinase

MTOC - Microtubule-organizing center

PAK - p21- activated Kinase

PAAM - Polyacrylamide

PDGF- Platelet derived growth factor

PDMS - Polydimethylsiloxane

PEG – Polyethylene glycol

PHEMA - Poly (2-hydroxyethyl methacrylate)

PKC - Protein kinase C

PIP-2 - Phosphatidylinositol 4,5-bisphosphate

PIP-3Ks - Phosophoinositide 3-kinases

Rac - Ras-related C3 botulinum toxin substrate

Raf kinase - Rapidly accelerated fibrosarcoma kinase

RGD - Arginine- glycine- aspartic acid

RG1- Rigidity gradient 1 (Young's modulus on the soft end is ~48kPa; Young's modulus on the rigid end is ~80kPa)

RG2- Rigidity gradient 2 (Young's modulus on the soft end is ~46kPa; Young's modulus on the rigid end is ~126kPa)

Rho A - Ras homolog gene family, member A

RhoG - Ras homolog gene family, member G

Shc - Src homology 2 domain containing

TGF-β - Transforming growth factor - beta

TNF- α - Tumor necrosis factor - alpha

TNFR-II - Tumor necrosis factor receptor- alpha

VASP - Vasodilator-stimulated phosphoprotein

VEGF - Vascular endothelial growth factor

WASP - Wiskott–Aldrich Syndrome Protein

WAVE - WASP-family verprolin-homologous protein

YM - Young’s modulus

Chapter 1. Background and Significance

Section 1.1 Introduction

Cell migration plays an important role in several processes in an organism's lifetime. For example, tissue development [1, 2], wound healing [3], inflammation [4] and disease progression [5-7] are regulated by cellular locomotion. Cells move in a coordinated manner that results in the formation of tissues, organs and limbs during embryonic development [6, 8]. The migration of cells plays a role in defining the correct architecture of tissues and organs [9, 10]. The locomotion of cells results in the formation of distinct embryonic layers that further differentiate into tissues of epithelial, muscular, nervous or mesenchymal origin [1].

When pathogens cause infections, the first step in restoring tissue homeostasis is accomplished by the migration of leukocytes into the wound region [11, 12]. These cells kill the invading pathogens and subsequently clear the wound of debris [11, 13]. Tissue repair is initiated through the migration of cell types such as keratinocytes, endothelial cells, macrophages, and fibroblasts [3, 14]. These cells types synthesize ECM proteins that aid wound closure [12]. On the other hand, altered inflammatory responses during healing can lead to the formation of scar or fibrotic tissues [15, 16].

Cancer metastasis involves the migration of tumor cells to other organs through blood vessels [17]. Tumor progression is a multi-stage process in which cancer cells migrate to different locations within the body through blood vessels [7, 18]. These cells acquire an invasive, migratory phenotype associated with increased expression of several genes involved in cell

motility [19-21]. Several chemical and physical cues provide guidance to cancer cells to migrate to other locations within the body. For example, EGF acts as a chemoattractant for breast cancer invasion [22]. Similarly, the cytokine CXCL12, is highly expressed by osteoblasts and bone marrow stromal cells and is important for tumor colonization in the bone [23]. Metastatic ovarian cancer cells exhibit preferential adherence to soft substrates, increased migration, proliferation and an enhanced malignant phenotype on such materials [24].

Therefore, studies on cell migration have significant physiological relevance. The migration of a cell involves a coordinated chain of events that includes cell polarization, membrane extension, formation of cell adhesions, cell traction, and the release of focal adhesions at the trailing edge [25]. A detailed description of each of these events is provided in **Section II**.

Section 1.2 A summary of migratory processes

Cell migration is a cyclic process where a cell undergoes a series of steps [25, 26]. These steps include polarization, protrusion formation, adhesion, translocation and retraction [25, 27]. A migrating cell on a 2D substrate is shown in **Figure 1.**

1.2.1 Cellular Protrusions: Protrusions are extensions of the cell membrane comprised of actin filaments that determine the overall shape [28]. These filaments are the backbone of cell extensions and are composed of arrays of monomeric globular G protein subunits that undergo ATP catalyzed hydrolysis to form polymeric chains. In this process, ATP bound to G-actin is hydrolyzed to ADP that binds to F-actin + inorganic phosphate (P_i) forming the bond between the actin monomers [29] . Hence, cleavage of ATP results in a highly stable filament with bound

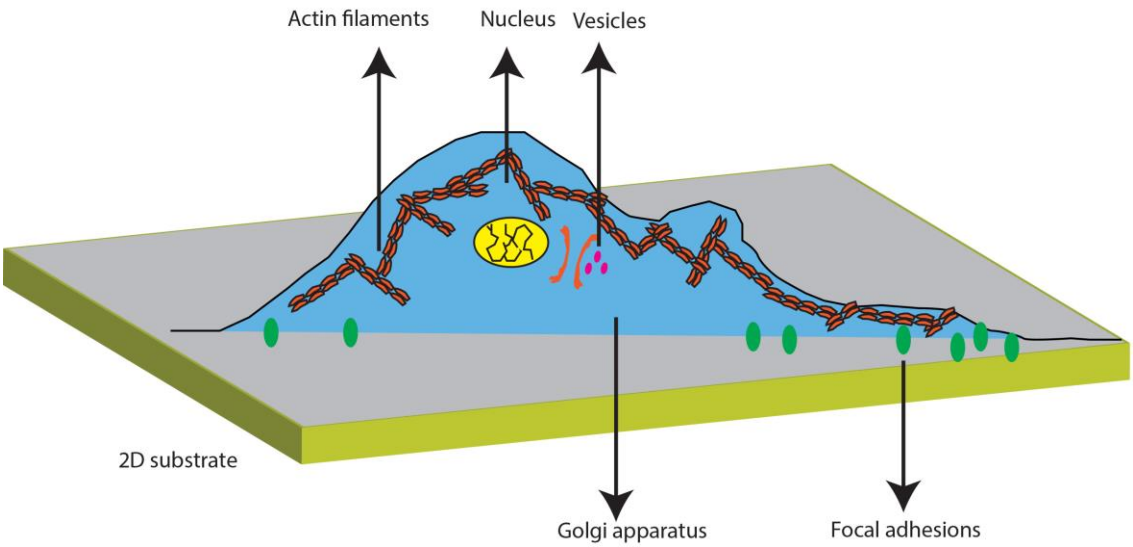

Figure 1. Schematic of a migrating cell on a flat 2D substrate.

ADP + Pi while the release of Pi results in depolymerization [30]. Actin filaments are polarized filaments displaying an oriented, head-to-tail structure of the binding monomers. The new actin monomers are added to the 'fast' growing barbed ends while the slow growing 'pointed' ends serve as the origin of the growing filament [31]. Actin filaments associate laterally with other filaments, forming bundles through actin binding proteins such as α-actinins and filamins [26]. The polarity between the two ends of the actin filament drives membrane protrusions resulting in lamellipodia, filopodia or stress fibers (**Figure 2**).

There are fundamental differences in the structure of these membrane extensions when they are involved in different processes such as leading-edge protrusions, contraction of the cell body and adhesion.

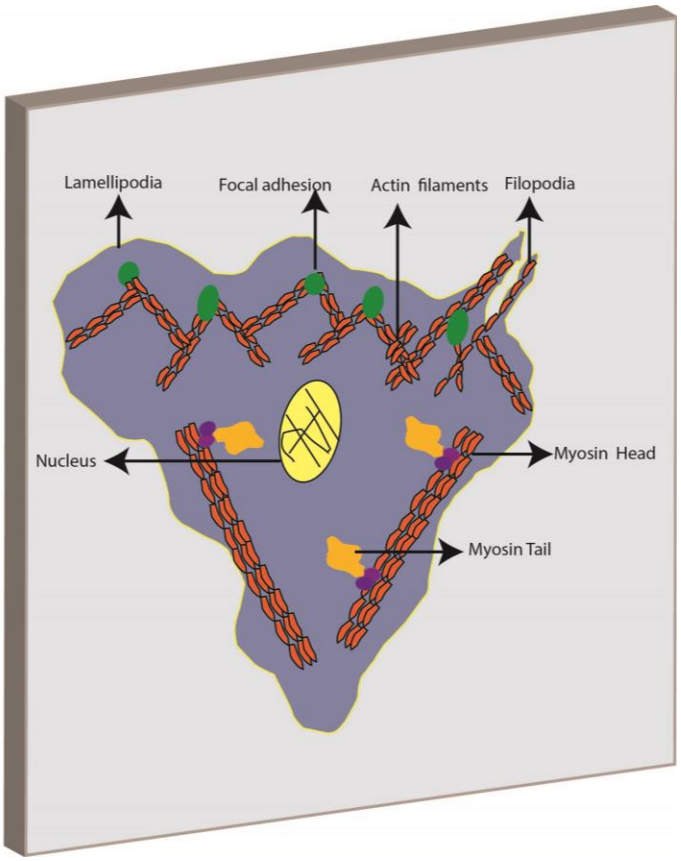

Figure 2. Schematic of a migrating cell showing membrane protrusions.

i. **Lamellipodia:** Lamellipodia are comprised of broad, sheet-like protrusions of thin, short actin filaments. These extensions contain actin in the form of bundles. Depending on the cell type, the lamellipodium can vary from ~1-5 μm in width. Lamellipodia are typically aligned along the direction of migration [32]. A study by Koestler *et al* showed that actin filaments in protruding lamellipodia subtend angles from 15–90° at the frontal region of the cell, and that cell motion terminates with the formation of actin bundles parallel to the cell edge [33].

ii. **Filopodia:** Filopodia contain long parallel bundles of actin filaments and multiple actin-associated proteins [34, 35] . These protrusions are elongated and resemble finger-like

projections emerging from the edge of a cell. The extensions are unbranched and are involved in cell-cell signaling, guidance toward chemoattractants, and adhesion to the ECM [34]. Filopodia contain receptors that detect guidance cues in the extracellular microenvironment. For example, filopodia can detect and sense the concentration of EGF and mediate cellular responses through activated cell receptors [36].

iii. **Stress fibers:** Stress fibers are thick, short, contractile actin filament bundles found at the basal portion of the cell. These fibers are studded with myosin II which allows for the contractile behavior of the cells [37]. Three different types of stress fibers are present. "Ventral" stress fibers are connected to the substrate via focal adhesions while "transverse" arcs are not anchored directly. "Dorsal" stress fibers terminate in the transverse arcs [38].

Actin is the dominant structural protein of the cell cytoskeleton [31]. Actin filaments acquire polarity which is critical to their assembly in cells. Actin filaments elongate at their barbed end and release actin monomers at the pointed ends within the bundle [30]. Actin polymerization leads to the formation of membrane protrusions such as lamellipodia and filopodia as shown in **Figure 3**. When extracellular ligands bind to membrane receptors, signaling transduction pathways are activated that produce active Rho GTPases and PIP2 which in turn activates WASP/scar proteins. WASP proteins and Arp2/3 along with actin monomers initiate the formation of a branch next to a pre-existing actin filament [30].

Two different pools of monomeric actin exist for polymerization. One is *de novo* synthesis at the protrusion sites and the other is monomer recycling during depolymerization [39]. Actin polymerization is mediated by the Arp2/3 complex, which binds to a pre-existing filament [40].

Arp2/3 is a seven sub-unit protein that plays a major role in actin cytoskeletal polymerization. It serves as the major nucleation site for new filament formation [30]. Several actin binding proteins regulate the rate of polymerization by affecting the pool of available monomers and free ends of the filaments to which the Arp2/3 binds [41, 42]. This process pushes the membrane forward forming membrane extensions such as lamellipodia or filopodia (**Figure 3**) [30]. Capping proteins terminate the growing filament. The aging of filaments leads to the hydrolysis of ATP-actin, disassociating phosphate groups and resulting in ADP-actin [30]. ADF/cofilin severs the ADP-actin from the growing filament [43]. Profilin prevents self-nucleation by binding to available actin monomers and catalyzing the exchange of ADP for ATP [44]. These profilin bound actin monomers are then returned to the pool to be added to the newly growing filaments at the barbed ends. Rho GTPases have been shown to activate PAK and Lin11, Isl-1 & Mec-3 kinase (LIM kinase) which phosphorylates ADF/cofilin that slows down its function [30]. Filopodia protrusion occurs through a "treadmilling" mechanism [28]. Proteins such as VASP help in continuous elongation of the filaments [45] Fascin helps in bundling the filaments and in generating the mechanical stiffness needed to push the plasma membrane into the filopodia [28]. The Rho family of small GTPases regulate actin and adhesion organization [37, 42, 46]. They also control the formation of membrane protrusions such as lamellipodia and filopodia [42]. When bound by GTP, Rho proteins become active and interact with downstream target proteins such as protein kinases [42]. Rho GTPases are activated by GEFs and inactivated by GAPs [42]. Cdc42, Rac, and RhoG enable the protrusion of lamellipodia and filopodia [42]. Rac stimulates lamellipodial extension by activating WAVE proteins while Cdc42 binds to WASP proteins inducing the formation of filopodia through actin polymerization [28].

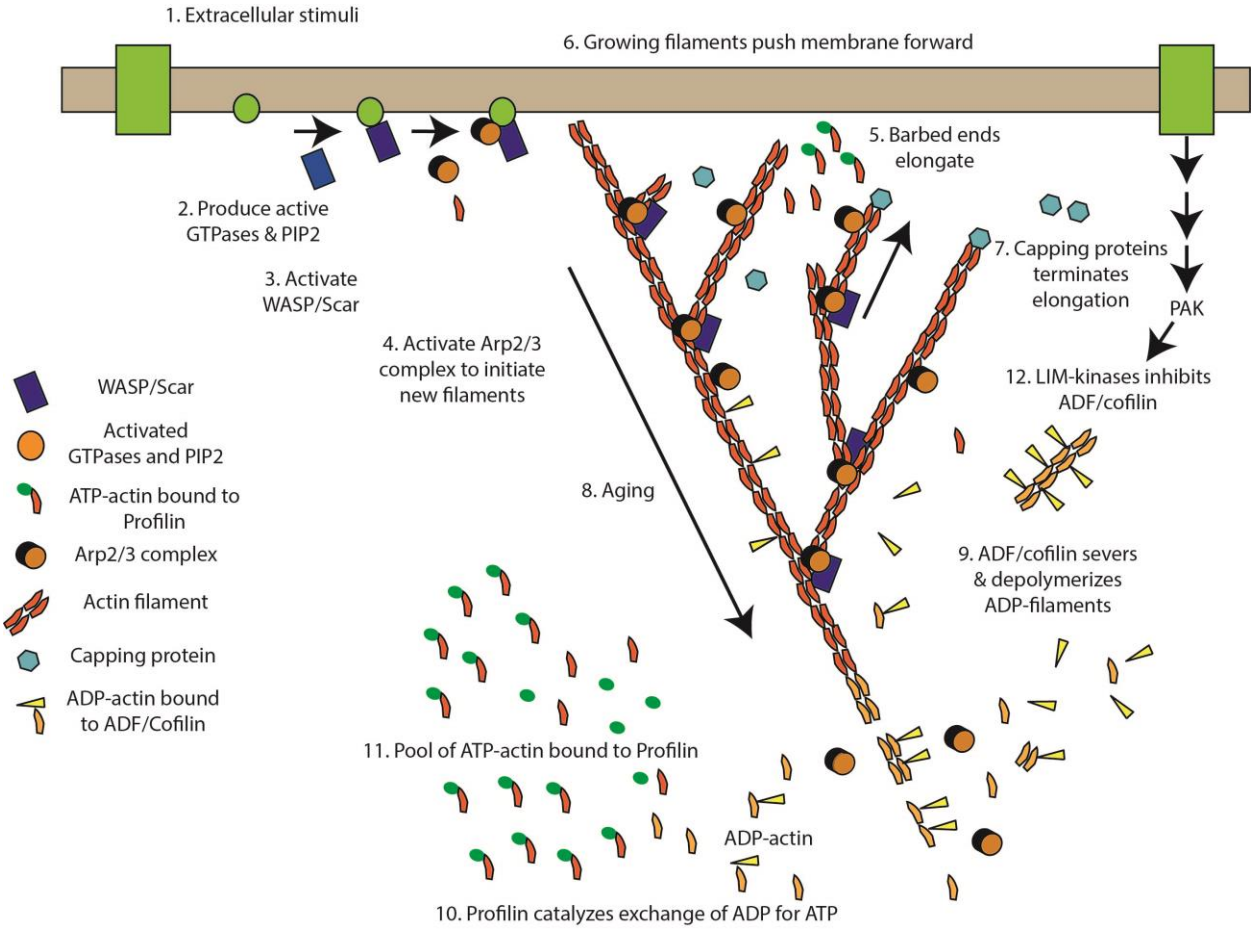

Figure 3. A signaling pathway for actin polymerization, depolymerization and treadmilling [30].

1.2.2 Cell polarization: The second step in cell migration is polarization, wherein protein concentration and compositions are different at the front and rear of cells [47]. Cell polarization can occur due to internal mechanisms or can be dictated by signals in the cellular microenvironment [48]. An external influx of extracellular, soluble signals leads to asymmetric recruitment or activation of signaling proteins within the cell [26]. Similarly, asymmetric guidance cues promote activation of cells receptors that induce polarized signals generating a protrusion in the front and in the rear [49]. The maintenance of cell polarity is mediated by a set of interlinked positive feedback loops involving the Rho family of GTPases, P1P3Ks, integrins, microtubules and vesicular transport. Cdc42 regulates cell polarity in eukaryotic organisms

which is active at the front of the cells [50]. It regulates actin polymerization and recruits other signaling PKC proteins to the front of the cell [51]. Cdc42 influences polarity by defining the location of the lamellipodia on the cell. [52]. Cdc42 also activates Rac and together they promote lamellipodia formation in the direction of migration. Cdc42 localizes the MTOC and Golgi apparatus in front of the nucleus, pointing them towards the leading edge of cells [53]. Cdc42-induced MTOC orientation may contribute to polarized migration by facilitating microtubule growth into the lamella. These microtubules also mediate the delivery of Golgi-derived vesicles to the leading edge, hence providing the membrane the required proteins needed for forward protrusion [53].

Rac activity correlates inversely with the activation of the small GTPase RhoA [42]. RhoA activation contracts actin filaments that lead to contraction of myosin II to form larger, thicker actomyosin bundles [46]. These bundles then form stable adhesions that define the rear of the cell. Rho also stabilizes microtubules in the tail, promoting focal adhesion turnover [53]. A study by Evers *et al* has reported that Rho and Rac can exhibit mutually antagonistic behavior in migrating cells [46]. Active Rac at the leading edges of cells suppress Rho activity whereas Rho is more active at the sides and rear of the cell and suppress Rac activity. This prevents Rac-mediated protrusions at the sites other than the leading edge [54, 55]. However, there are also reports that Rac can also be involved in cellular detachment [56].

1.2.3 Cell adhesion and Integrins

1.2.3.1 Cell adhesion: Adhesion is the physical interaction of cells with another cell or the ECM and is essential for cell migration and tissue integrity [57]. Cell matrix adhesions are binding sites between the actin cytoskeleton and the ECM. Such adhesions are called focal adhesions [58]. Different types of matrix adhesions have been described such as nascent adhesions, focal

complexes, focal adhesions, podosomes and invadopodia [26]. These different types of focal adhesions share many components, such as adhesion receptors that are the physical links between cells and the ECM [59]. Cell surface receptors called “integrins” play a major role in cell adhesion. These transmembrane proteins are regarded as the ‘feet’ of a migrating cell [60]. Focal adhesion formation is initiated with small-scale clustering of integrins [61]. Fast migrating cells exhibit fewer integrin clusters and small adhesions at the leading edge [58]. However, non-migratory or slow moving cells exhibit large integrin clusters (focal adhesions) and are tightly adherent [6]. A brief description of different types of focal adhesions is provided below.

i. **Nascent focal adhesions:** Nascent focal adhesions are small and highly transient structures observed within lamellipodium. These are formed along lamellipodial protrusions and can transform into focal adhesions [62, 63].

ii. **Focal Complexes:** Focal complexes are immature adhesions. These complexes are myosin dependent, and are present at the edge of lamellipodia [61]. Focal complexes are present in motile cells and their rapid turnover is correlated with high velocity [26].

iii. **Focal adhesions:** Focal adhesions are mature adhesions that elongate over time. These adhesions are linked to large, contractile actomyosin stress fibers. Their concentration is linked inversely with cell motility [64].

iv. **Podosomes:** Podosomes are ring or dot shaped adhesions found in rapidly moving cells such as macrophages, endothelial cells and dendritic cells [65].

v. **Invadopodia:** Invadopodia is the term used for podosomes in cancer cells. These are specialized actin structures that are similar to podosomes but possess proteolytic activity[65]. These structures appear as irregular dots in the vicinity of the nucleus and the Golgi complex.

1.2.3.2 Integrins: Integrins are heterodimeric receptors consisting of α and β chains with large ligand-binding extracellular and short cytoplasmic domains [66]. The binding of ligands to the extracellular region of integrins leads to conformational changes and clustering that initiates intracellular signaling leading to protein tyrosine phosphorylation and GTPase activation [67]. This signaling step regulates the formation of adhesions, cell polarity and the dynamics of the cytoskeleton during cell movement [67]. Furthermore, activated integrins preferentially localize at the leading edge forming new adhesions [68] . The alterations in the conformation of the extracellular domains resulting from interactions at the integrin cytoplasmic tail change the integrin affinity [69]. An important characteristic of integrins is their ability to recognize multiple ligands such as fibronectin, collagen, fibrinogen, laminin and additional proteins (**Figure 4**) [70]. Studies on integrin-ligand interactions have led to the identification of small recognition sequences from large ECM proteins that bind to these cell surface receptors [70, 71]. One of the most widely used peptide sequence is RGD that binds to integrins α5β1, αvβ3, α8β1, αvβ1, αvβ5, αvβ6, αvβ8, and αIIbβ3 to name a few [71]. Similarly, collagen binds to α1β1 and α2β1 integrins [70].

1.2.3.3 The interplay between integrins and adhesions: Several proteins and signaling molecules are involved in the integrin signaling pathways that lead to cell migration. A brief description of these proteins is provided below.

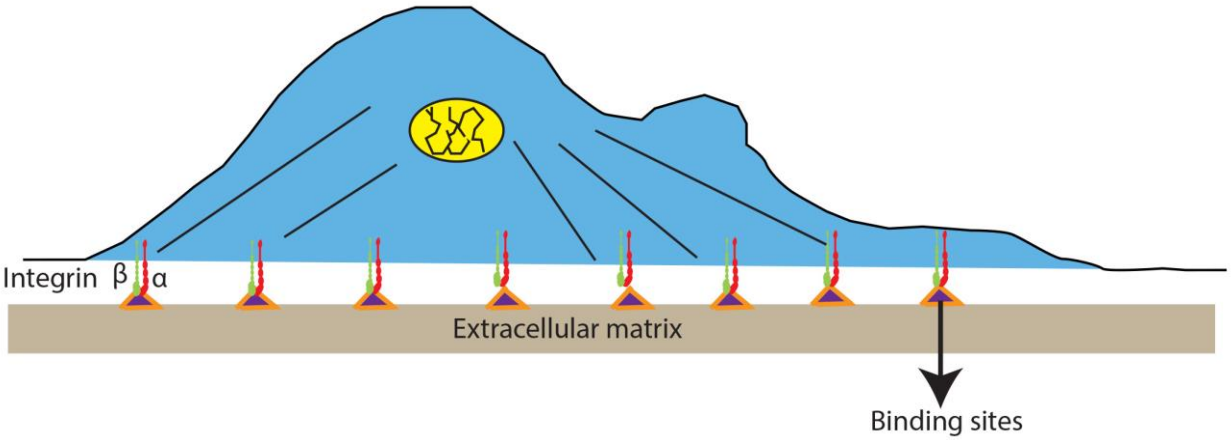

Figure 4. Schematic of a cell depicting integrin-binding to sites on ECM proteins.

i. **Focal adhesion kinase (FAK):** FAK is a cytoplasmic protein kinase that co-localizes with integrins at focal adhesions [72]. After integrin clustering, FAK is auto-phosphorylated, recruiting Src family kinases to focal adhesions [73]. This step has been shown to be required for integrin-mediated cell motility in fibroblasts [74].

ii. **Crk-associated signaling (Cas-CRK):** The Cas-CRK system is a component of the cell migration machinery that is localized to the leading edge of the motile cells. Inhibition of the Cas-CRK complex can prevent haptotaxis and chemotaxis [75, 76].

iii. **Src homology 2 domain containing (Shc):** Shc family is a group of adaptor proteins that are recruited to activate tyrosine kinases in response to integrin clustering. These proteins are composed of three interaction domains: a carboxy-terminal SRC homology 2 (Shc 2) domain, a central collagen homology (CH) domain, and an amino-terminal phosphor-tyrosine binding (PTB) domain [77, 78].

Integrins act as mechanosensory sites, integrating signals from ECM to the intracellular cytoskeleton [68]. Focal adhesion complexes are composed of integrins, protein kinases such as FAK and Src, adaptor proteins such as Shc, signaling intermediates such Rho and Rac GTPases,

and actin binding cytoskeletal proteins such as vinculin, paxillin, talin and tensin [79] (**Figure 5**). Integrin (α and β chains) clustering due to ligand binding activates FAK which activates multiple downstream signaling proteins [67]. The engagement of surface integrin receptors with fibronectin on NIH 3T3 cells has been shown to cause FAK tyrosine phosphorylation [79]. This was shown by anti-phosphotyrosine blotting of quiescent NIH 3T3 lysates. FAK auto-phosphorylation causes it to bind to GRB2 and activate Ras, a small G protein that leads to Ras/MAPK activation. Anti-GRB2 immunoblotting confirmed the association of GRB2 with FAK in both NIH 3T3 and v-Src transformed 3T3 cells. The evidence for coupling of integrin mediated signal transduction to activation of Ras pathway was proved by investigating the activation of MAPK pathway. A MAPK band was detected in a Western blot with monoclonal anti-ERK antibody showing integrin mediated cell adhesion led to activation and nuclear translocation of MAPKs.

Activated Ras recruits Raf kinase to the cytoplasmic membrane where it is activated by protein kinases such as Src leading to activation of mitogen-activated protein kinase MEK/ERK pathway [80, 81]. This ERK activation leads to phosphorylation and enhancement of MLCK activity while inhibition of MEK by inhibiting ERK phosphorylation dramatically reduced FG carcinoma cell migration [82]. MLCK phosphorylation activates myosin, resulting in increased contractility and transmission of tensions to the sites of adhesion [59]. Gu *et al* showed that activated Src phosphorylates Cas, leading to its binding to CRK and DOCK-180, causing Rac activation [76]. They compared the integrin dependent Rho and Rac activation by laminin-10/11 and fibronectin. It was observed that the laminin-10/11 preferentially activated Rac, through an $\alpha_3\beta_1$ integrin-dependent pathway involving a $p130^{Cas}$-CrkII-DOCK180 complex, thereby strongly promoting cell migration through enhanced lamellipodia formation. On the other hand, fibronectin

preferentially activated Rho forming stress fibers and focal contacts on the substrate [76]. Integrin dependent adhesion in NIH 3T3 cells showed rapid activation of PAK, a downstream effector of GTPases, cdc42 and Rac [83]. Further experiments with dominant negative mutants of Rac and Cdc42 suggested that integrins first activate cdc42, which subsequently activated Rac and contributed to cell spreading [84].

Adhesion assembly is observed both at the leading and at the rear edges of cells. Adhesions are continuously assembled and disassembled [85]. Protein kinases and phosophatases play a major role in the regulation of adhesion turnover and assembly [86]. Adhesion turnover is also regulated by Rac-associated proteins [87] and by the MEK/ERK [88]. At the rear, adhesions tend to tether strongly to the substrate resulting in a long tail of the cell at the site of attachment [25]. The integrins are left behind when the tension overcomes the physical linkage between the integrin and cell cytoskeleton leading to detachment. The role of myosin II is in the maintenance of polarity as well as retraction. In addition, calcium has been implicated in the disassembly of adhesions at the rear [89]. The tension generated leads to the opening of stretch-activated calcium channels which severs focal adhesion proteins including vinculin, talin and FAK [90, 91].

Studies on mouse knockouts of cell cytoskeletal proteins, such as actin, have shown early embryonic lethality with embryonic weight loss [9]. Mouse knockouts of focal adhesion proteins such as paxillin and vinculin, leads to abnormal development of mesodermal structures or premature death of the embryo [9]. Knockouts of cell surface receptors, specifically, β1 integrins, resulted in abnormal vascular patterning and fetal growth retardation. In humans, a number of disorders have been linked to inefficient migration of cells [92, 93].

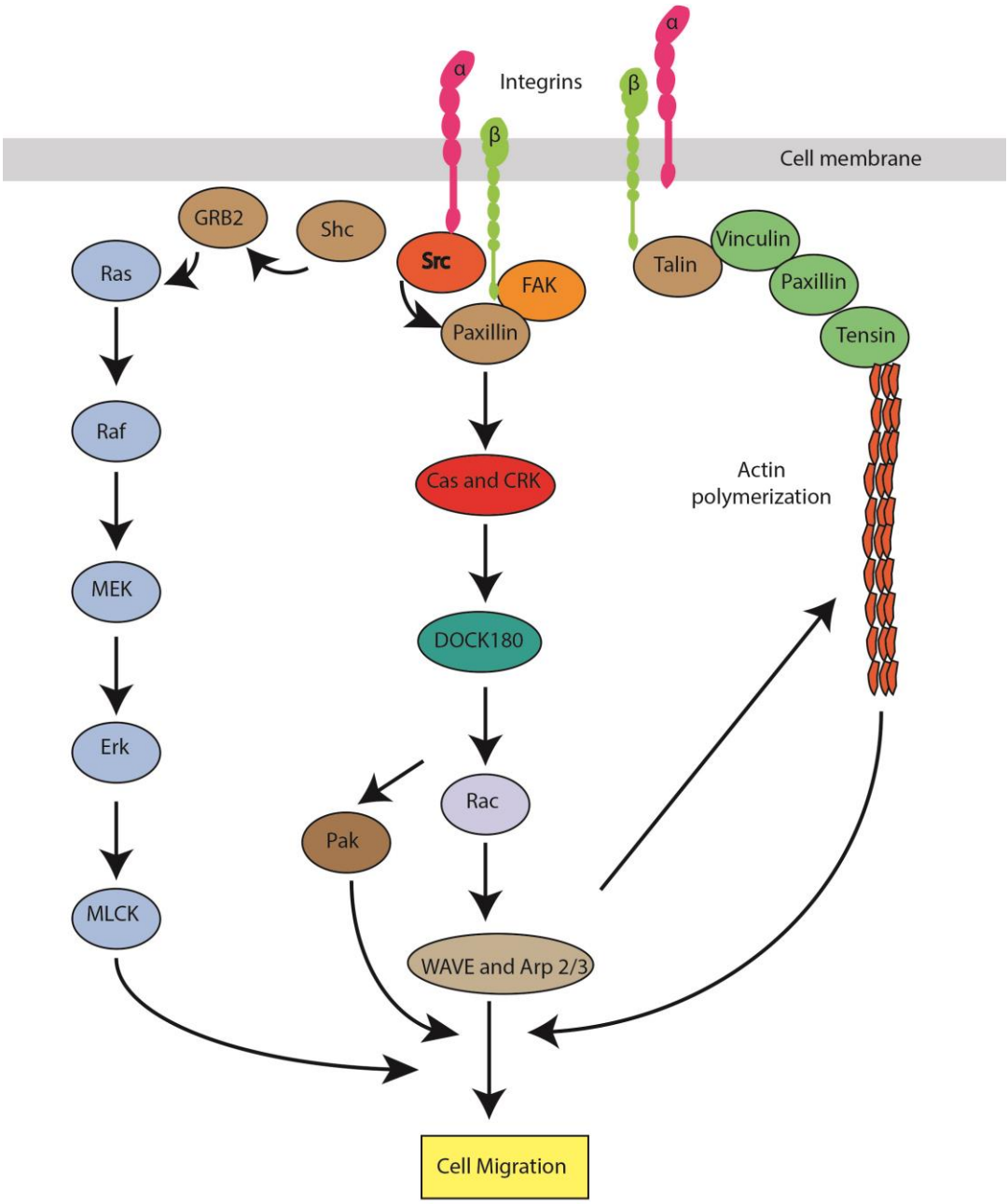

Figure 5. A pathway showing the signaling molecules and proteins involved in cell migration [94, 95].

Abnormally slow migration of cardiac neural crest cells due to a mutation in the Pax3 gene leads to the absence of or defects in heart septation [96-98]. DiGeorge syndrome is caused by chromosome deletions on chromosome 22 that result in migratory defects of the neural crest cells

causing heart defects, poor immune system function, a cleft palate, complications related to low levels of calcium in the blood and behavioral disorders [99].

Section 1.3 Directed cell migration

Cell migration can be either random or directed. Random migratory patterns of cells resemble Brownian motion of particles, wherein, a cell or a group of cells do not exhibit a preferred direction of motion [100, 101]. Directed migration occurs when cells respond to a specific cue and move towards it [101-104]. Since our research objectives are focused on directed migration, we will discuss this mode of migration in greater detail. Several directional cues exist *in vivo* that influence a cell's decision to migrate in a particular direction. These directional cues can be mechanical [105, 106], electrical [107], optical [108] or chemical [109, 110] in nature. It is well known that cell migration *in vivo* is guided by a combination of such signals. Cell locomotion may occur due to soluble chemoattractants (chemotaxis), immobilized molecules (haptotaxis) and the biophysical properties of the underlying matrix (durotaxis) [111, 112]. In developmental biology, cells move in response to gradients of morphogens [113, 114]. Among these external stimuli, the most widely studied cues for cellular locomotion are mechanical and chemical in nature [105, 106, 115-117].

1.3.1 Haptotaxis and Chemotaxis: Studies have shown that cells can sense chemical stimuli and migrate in the direction of increasing or decreasing chemical concentration [115, 118, 119]. The term "haptotaxis" was first reported when mouse fibroblasts migrated away from a less adherent substrate (cellulose acetate) to a more adherent substrate (glass) [120]. Several ECM components such as fibrin and collagen and integrins such as $\alpha v\beta 3$ and $\alpha v\beta 5$, are involved in driving haptotactic cell migration [121]. Directed migration can be obtained through

immobilized, soluble, whole protein, or polypeptide sequences. PDGF has been shown to elicit directed migration by fibroblasts during wound repair [122]. Human microvascular endothelial cells exhibited increased drift speed with increasing fibronectin concentration [115]. A study by Dimilla *et al* showed that cell speed exhibits a biphasic relationship with immobilized protein concentration [123]. A higher concentration of protein or immobilized chemical moieties resulted in higher adhesion and consequent obstruction in the release of cell adhesions. In contrast, cells on substrates with lower protein concentrations exhibited higher speeds. Migration requires adhesion for cells to be adherent on the substrate, however, highly adhesive surfaces can retard cellular locomotion. Due to these reasons, maximal migratory speed has been observed at an intermediate level of cell-substratum adhesiveness [123-125]. A study by Huttenlocher *et al* investigated the effects of altered integrin affinity and cytoskeletal linkages on random and haptotactic migration. The authors showed that alterations in the integrin affinity for extracellular ligands played an important role in regulating cell migration. For example, locking the integrin receptor in a high affinity state by an activating antibody or a mutation in the integrin cytoplasmic domain significantly inhibited both types of cell migration [126].

Studies on chemotaxis have shown that fragments of ECM proteins or minimal peptide recognition sequences can also result in directed motion [104, 127]. When the chemotactic responses of collagens I, II and III and collagen derived peptides were investigated using human dermal fibroblasts [128], it was reported that the responses were similar for collagens I, II, III but the constituent α chains were less efficient. Furthermore, peptides containing hydroxyproline derived from the collagen type I, II and III degradation by bacterial collagenase also elicited

chemotactic responses from dermal fibroblasts [128]. Burdick *et al* studied the migratory behavior of human umbilical vascular endothelial cells cultured on hydrogels exhibiting RGD gradients [129]. These cells exhibited greater cell attachment and migration towards the high RGD concentration side of the hydrogel compared to low RGD domains. These studies demonstrate that similar modes of directed cell migration can be obtained through polypeptide and protein-conjugated materials.

1.3.2 Durotaxis: The mechanical properties of the matrix on which cells are adherent have also been shown to regulate directionality and speed of moving cells. Durotaxis is exhibited by various cell types including fibroblasts [105, 106, 130-135], myofibroblasts [136], vascular smooth muscle cells [137], and neurons [138].

A pioneering study by Pelham *et al* showed that substrate stiffness could be used to modulate cell migration [106]. The results from this study showed reduced spreading but higher fibroblast motility on soft PAAM matrices compared to stiff substrates. Another study demonstrated that cell movement can be guided by matrix rigidity alone [105, 106]. Cells in the vicinity of an interface that exhibited a sharp change in elastic moduli migrated away from soft region (14 kPa) towards the stiffer side (30 kPa). Such cells also exhibited increased projected cell areas and contractile forces. In contrast, cells on the 30kPa side of the interfacial region did not cross over to the soft side [105].

Rat aortic smooth muscle cells cultured on polyelectrolyte multilayers assembled layer-by-layer with poly(allylamine hydrochloride) (PAH) and poly(acrylic acid) (PAA) migrated away from soft regions (elastic modulus: 38 MPa) to stiff regions (elastic modulus: 120 MPa) [139]. Micro-structured PDMS substrates containing dense arrays of micropillars were designed to create an

anisotropic stiffness gradient [140]. Epithelial cells seeded on these substrates migrated towards the regions of highest rigidity. Cells migrating towards the high modulus regions exhibited large contractile forces that correlated to their focal adhesion sizes and actin cytoskeleton [140]. NIH 3T3 fibroblasts migrated towards more rigid posts on PDMS micropost arrays exhibiting two different step-rigidity gradient profiles (15 - 39 nN/μm and 7.5-40 nN/μm). Furthermore, cells bridging two rigidities across the PDMS micropost array developed stronger traction forces on the more rigid side of the substrate indistinguishable from forces generated by cells exclusively seeded on rigid regions of the micropost array [141]. Smooth muscle cells cultured on PAAM hydrogels that exhibited an elastic modulus gradient varying from 1.0 to 308 kPa showed a biphasic dependence on substrate compliance suggesting that there exists intermediate substrate stiffness for maximal cell migration [142]. However, it was reported that the optimal stiffness shifted based on the concentration of fibronectin conjugated the PAAM substrates [142]. Substrate elasticity has also been shown to play an important role in the formation of tissue-like clusters on soft surfaces (2.69kPa) [130]. Myosin II dependent contractile forces and weak adhesions on soft substrates enable fibroblast migration towards each other leading to formation and maintenance of tissues.

1.3.3 Directed cell migration under the influence of multiple cues: To date, investigations into cell migration have focused primarily on a single gradient, either chemical or mechanical in nature [105, 106, 115, 122, 143, 144]. A physiological example where both chemical and mechanical cues play important roles is during wound healing. During the early stages of injury, a wound closely resembles a soft tissue at the injured site. When a wound is inflicted, blood rushes to the wounded site [3]. Platelets aid in clot formation, plugging the flow. The signaling molecules released from the platelets help to recruit circulating inflammatory cells including

neutrophils to the wound site [145]. Thereafter, chemotactic signals like PDGF and TGF-β form gradients that help attract fibroblasts and other cells types to the wound. These cell types then remodel the wound by depositing new ECM proteins, leading to wound contraction and stiffening [146]. This change in mechanical properties in the opposite direction also helps accelerate the wound healing. Therefore, both chemotactic and mechanical signals during the wound healing process are critical in promoting wound closure. Another example is cancer cell metastasis. Tumor cell migration is a highly orchestrated process where both mechanical and chemical cues influence locomotion [147-150].

Although, it is well known that the tissue microenvironment exhibits different stimuli, relatively few studies report the migratory behavior of cells when they choose one signal over another [151, 152]. A migrating cell confronts multiple stimuli in its microenvironment. Monitoring cellular motility in the presence of a single external stimulus is not entirely representative of cell motility *in vivo*. Substrates that incorporate multiple stimuli with gradients in different directions could serve as physiologically relevant models to monitor how a cell chooses to move and why one signal may exert a more dominant role than another [100, 111, 152].

In vivo, there are several interfacial regions that exhibit gradients in chemical and mechanical properties. Examples include, the breast cancer-bone [153, 154], bone-ligament/tendon [155], osteochondral [156], and myotendinous regions [157]. Each of these interfacial regions exhibits significantly different mechanical and chemical properties to bridge distinctly varying tissues. [156]. In order to provide more physiologically relevant environments *in vitro*, there is a need for new biomaterials that can incorporate different gradients [111, 151, 152, 158-160]. In the following section, we outline some recent advances in the generation of gradients on soft materials.

Section 1.4 Generation of dual gradients

4.1.1 Immobilized dual gradients: Techniques have been developed to pattern multiple, overlapping biomolecular patterns using photochemistry based approaches. Benzophenone modified PEG surfaces activated on exposure of UV light of λ=365nm formed transient diradicals. These modified materials could then be covalently coupled to biomolecules through non-specific C-H insertions, providing a universal approach to conjugating multiple proteins [161]. An interesting study reported a unique platform to create multi-compartment, layered scaffolds that exhibit multiple interfaces to simultaneously study several chemical and physical cues [162]. These layered scaffolds were created using "Density Gradient Multilayered Polymerization" technique that used a density modifier (iodixanol) to create polymeric layers of PEG exhibiting different values of substrate stiffness. This density modifier can be mixed with bioactive molecules in different concentrations creating a biomolecular gradient within each layer of the scaffold that exhibit dual chemical and mechanical properties. Orthogonal gradients with molecular weight (M_w) and grafting density (σ=number of polymer chains per unit area of grafted surface) of PHEMA increasing in mutually perpendicular directions have been developed to independently study the effect of two system parameters [163]. Nonfouling gels of varying chemical and mechanical functionalities using zwitterionic crosslinkers have been shown to allow for significantly reduced nonspecific cell adhesion relative to PHEMA hydrogels [164]. Our research group has previously designed a PAAM hydrogel which exhibited a sharp interface [152]. On one side of this interface, the hydrogel was more rigid (85kPa) and had a lower concentration of immobilized collagen; the reverse trend was presented on the other side of the interface. In this study, fibroblasts migrated preferentially towards the softer edge (35kPa) of the substrate that had a higher surface concentration of collagen suggesting a more dominant role for

chemical stimuli in directing fibroblast locomotion. However, these gels were synthesized by simply positioning two drops of different polymer solutions side-by-side to achieve dual gradient profiles. Due to difficulties in controlling the extent of diffusion and mixing of two mixtures, it was non-trivial to obtain precise control over mechanical and chemical profiles.

4.1.2 Microfluidic dual gradients: Several studies have shown the design of dual gradients using microfluidic approaches [100, 111, 129, 160, 165]. A parallel plate flow chamber was assembled which allowed multiple proteins to flow through the channel. The protein gradient was created via irradiation of UV light through a photomask containing striped patterns of various widths and spacing. The flow of protein solutions was stopped before exposure to UV light. Simultaneous chemical and mechanical shear stress gradients were incorporated in a single chip to mimic interstitial flow in vivo [166]. A simple osmotic pump was used to provide physiological levels of stress (0.0004-0.0016 Pa) and also a stable chemical gradient [167]. L929 fibroblasts cells cultured under the influence of FBS gradients showed cell alignment in the direction of the flow. Further experimentation showed that the chemical (serum) gradient had a minor effect on cell alignment. However, the alignment of cells was more affected by shear stress levels imposed by the fluid flow. Another study combined osmotic and stiffness gradients in a microfluidic device to study the combinatorial effects of the two gradients on mouse myoblast C2C12 cell lines [168].

Section 1.5 Research objectives

We aim to design interfaces that provide cells with two stimuli, presented as gradients that are in opposing directions (**Figure 6).** Within this interfacial region, cells will have to make a decision

to move in a particular direction. If they choose to move towards the stiffer domains on the substrate, they will experience lower protein concentration. If they migrate towards the softer edge of the substrate, then they are presented with a higher protein concentration. Systematic studies are needed to understand the influence of multiple cues on the motility of cells.

Our goal is to design 2D hydrogel substrates that exhibit dual and opposing rigidity and protein gradients. We have combined UV photopolymerization and conjugation to assemble such gradients on PAAM gels. Our research objectives are

I. **Design and characterize PAAM hydrogels that exhibit dual and opposing rigidity protein gradients.**
II. **Investigate single cell fibroblast migration on dual gradient substrates.**
III. **Investigate fibroblast-macrophage co-culture migration on dual gradient substrates.**

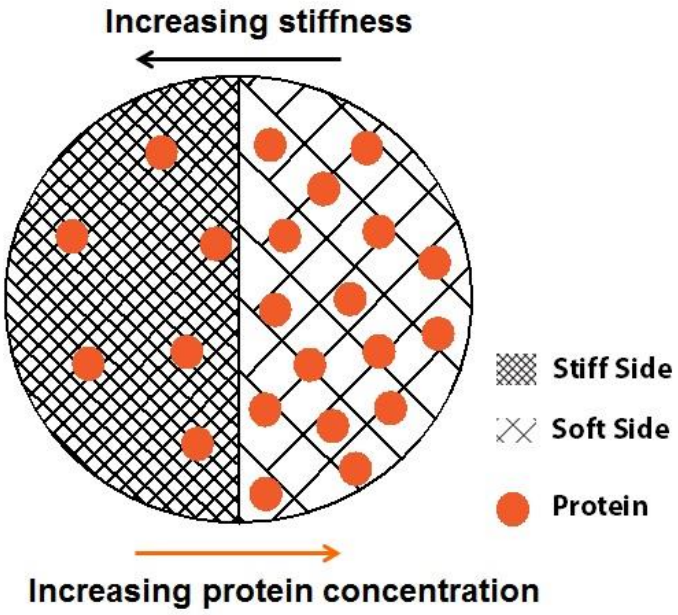

Figure 6. A schematic of a hydrogel substrate exhibiting dual and opposing rigidity-protein gradients.

Chapter 2. The design and characterization of biomimetic interfaces that exhibit chemical and mechanical gradients in opposing directions.

Section 2.1 Introduction

PAAM hydrogels were assembled with dual chemical and mechanical gradients. We chose PAAM as the substrate since it is a very well characterized and studied hydrogel. PAAM has been used quite extensively in cell adhesion studies. [105, 106, 169]. PAAM substrates have several advantages. First, they can be easily tuned to obtain a range of elastic moduli values spanning from 0.1-200kPa [169-171]. Our goal was to mimic tissue interfaces present *in vivo*. Examples include ligament-cartilage, cartilage-bone, tendon-muscle and osteo-chondral interfaces [172]. The YM values vary from low (10-40kPa) on the softer regions of such tissues to (40-100kPa or higher) on the stiffer regions [156]. This enables the use of such hydrogels to study the effect of matrix rigidity on cellular responses. Second, PAAM hydrogels are inert substrates unless chemically modified. Typically, proteins or peptides are conjugated to PAAM substrates to render them biocompatible [137, 173, 174]. Third, they are optically transparent resulting in the ease of visualizing cells and their organelles [175, 176]. PAAM has been extensively used to monitor cell adhesion and migration and is therefore a model substrate to use in our research objective [105, 174, 175, 177].

PAAM can be polymerized through conventional free-radical polymerization [105, 152, 169]. In our work, we have used UV-initiated photopolymerization. Several photo initiators have been used to initiate polymerization with acrylamide [178-180]. Azo-based initiators such as azobisisobutyronitrile (AIBN) can function as thermal and photo initiators [181]. Our goal is to obtain cross-linking solely through UV radiation and therefore initiators that can also induce thermal polymerization were not considered. We chose to use 2-hydroxy-1-[4-

(hydroxyethoxy)phenyl]-2-methyl-1-propanone (Irgacure 2959) over other azo-based initiators since it does not initiate thermal polymerization [182]. Irgacure 2959 was made soluble in water by heating it up to 80°C before polymerization.

For designing chemical gradients, virtually any protein with free primary amine groups can be conjugated to PAAM through the use of hetero-bifunctional cross-linkers. We chose a water-soluble diazirine compound due to the wavelength at which this compound is activated. While polymerization initiated by Irgacure 2959 occurs at a wavelength of 254 nm. Diazirines are activated at 365nm. Therefore, the gels will not continue to polymerize when the protein is being conjugated. We have conjugated Type 1 collagen to PAAM gels in all our studies. Collagen is the most abundant protein *in vivo* and is a very well-studied ECM protein in the context of cell migration [177, 183-185]. The chemical and mechanical properties of dual gradient gels have been characterized using Enzyme linked immunosorbent assay (ELISA), atomic force microscopy (AFM), profilometry and fluorescent methods.

Section 2.2 Materials

FITC labeled collagen **(**$M_w=10^6$ Da), HEPES buffer, Irgacure 2959 (1-[4-(2-Hydroxyethoxy)-phenyl]-2-hydroxy-2-methyl-1-propane-1-one) and 3-triethoxysilylpropylamine were purchased from Sigma Aldrich, St Louis, MO. Glutaraldehyde (25%v/v) was purchased from Electron microscopy Sciences, Hatfield, PA. Phosphate buffered saline, rhodamine-conjugated polystyrene beads (0.5 µm in diameter), penicillin-streptomycin and Dulbecco's modified Eagle medium were purchased from Invitrogen Life Technologies, Carlsbad, CA. Acrylamide (10% v/v), bis-acrylamide (0.72 v/v), and APS were purchased from Bio-Rad, Hercules, CA. All other

chemicals and supplies were purchased from Thermo Fisher Scientific Waltham, MA unless otherwise specified.

Section 2.3 Design of polyacrylamide (PAAM) substrates with opposing rigidity and protein gradients

Glass coverslips were activated using previously published procedures [152, 186].All PAAM hydrogels in this study were polymerized using monomer solutions that contained acrylamide (10%v/v), bis-acrylamide (0.72% v/v) and APS.

2.3.1 Irgacure optimization: Irgacure 2959 compound is known to initiate polymerization only in the presence of UV radiation. The UV wavelength at which it exhibits peak absorbance is at 270nm which is advantageous since this wavelength is distinctly different from the UV wavelength at which the chemical interfaces are created. However, Irgacure 2959 is sparingly soluble in water but its solubility was increased by heating the photoinitiator solution up to 80°C. Several concentrations were varied to optimize the concentration of Irgacure 2959 used to polymerize the solution.

2.3.2 Designing rigidity gradients: High-resolution photo-masks (2μm/pixel) with difference gray scale values were custom-designed on chrome substrates (Benchmark Technologies, Lynnfield, MA). Gray scale masks with four different transmittance values were designed to control the intensity of incident UV radiation. The mask was placed in a custom-designed holder in order to precisely rotate it during hydrogel assembly. Below, the percentage value in a mask represents the amount of light transmitted through the mask (**Figure 1**). A higher percentage value corresponds to a greater light transmittance, which results in higher degrees of crosslinking. The differential absorption of UV light resulted in changes in the extent of cross-

linking and the generation of an interfacial region with two distinct elastic moduli [117, 137]. Rigidity gradients were obtained using two combinations of gray scale values: 70%/40% (denoted as Mask 1) and 80%/30% (denoted as Mask 2).

Polymerization was initiated by Irgacure 2959 (5% w/v) [182] and UV radiation (UVP, Upland CA). The UV wavelength and intensity were 254 nm and 15 mW/cm^2, respectively. Rhodamine-conjugated PS beads (~ 0.5 µm in diameter) were added to all monomer solutions to enable the identification of the rigidity gradient. In the PAAM hydrogel, low and high-crosslinking resulted in "soft" and "stiff" regions, respectively. The interfacial region was defined as the area between the lowest and highest values for substrate rigidity.

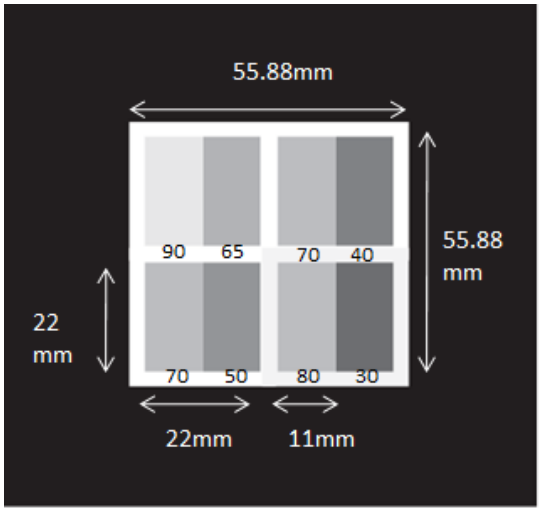

Figure 1. Grayscale values for differential crosslinking to obtain different mechanical gradient profiles.

2.3.3 Designing dual gradients with immobilized collagen: The concentration of surface-immobilized collagen was increased in the opposite direction of the rigidity gradient. FITC-labeled Type 1 collagen was conjugated to PAAM gels using N-hydroxyl succinimide and a hetero bifunctional cross-linker sulfo-succinimidyl-diazirine (**Figure 2**). Reaction time with this

linker molecule and the concentration of collagen were varied to optimize the binding efficiency to PAAM substrates. The collagen gradient was superimposed on the rigidity gradient by rotating the gray scale mask by 180^{o} and exposing to UV light (365nm; Spectroline, Westbury, NY) at an intensity of $27mW/cm^2$ (**Figure 3**). The protein gradients were generated by UV exposure for 10 min and 30 μL of collagen deposited on the "soft" or "stiff" regions. The input collagen concentration varied from 15-50 μg/mL. Our goal was start with low input collagen concentration that can sustain cell adhesion, experiments with lower collagen concentrations than 15 μg/mL did not result in cell adhesion. PAAM gels were rinsed in 50mM HEPES (pH=7) for up to 48h and stored at 4°C.

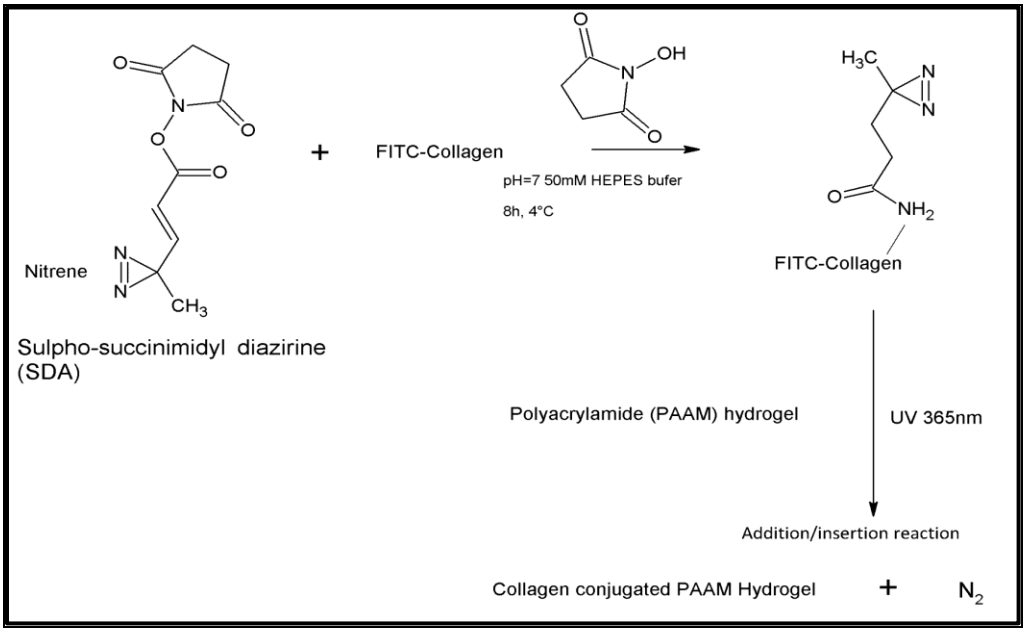

Figure 2. A reaction scheme showing protein conjugation to PAAM hydrogels using SDA.

Section 2.4 Interface characterization

2.4.1 Atomic Force Microscopy (AFM): YM measurements of hydrogels were obtained on hydrated samples using a Veeco MultiMode AFM (Veeco, Santa Barbara CA). All measurements were conducted in contact mode using pyramidal SiN cantilever tips (Bruker AFM Probes, Camarillo, CA) with a spring constant of 0.12 Nm^{-1}. The force-distance curves were obtained at 1 Hz using the blunted tips with a half open angle of 18°. The elastic modulus was obtained by fitting the raw data to a modified Hertz cone model using equations 1 and 2.

$$F = k\,(d\text{-}d_0) \qquad (Equation\ 1)$$

$$F = \frac{2\tan\alpha}{\pi}\left[\frac{E}{1-\nu^2}\right]\delta^2 \qquad (Equation\ 2)$$

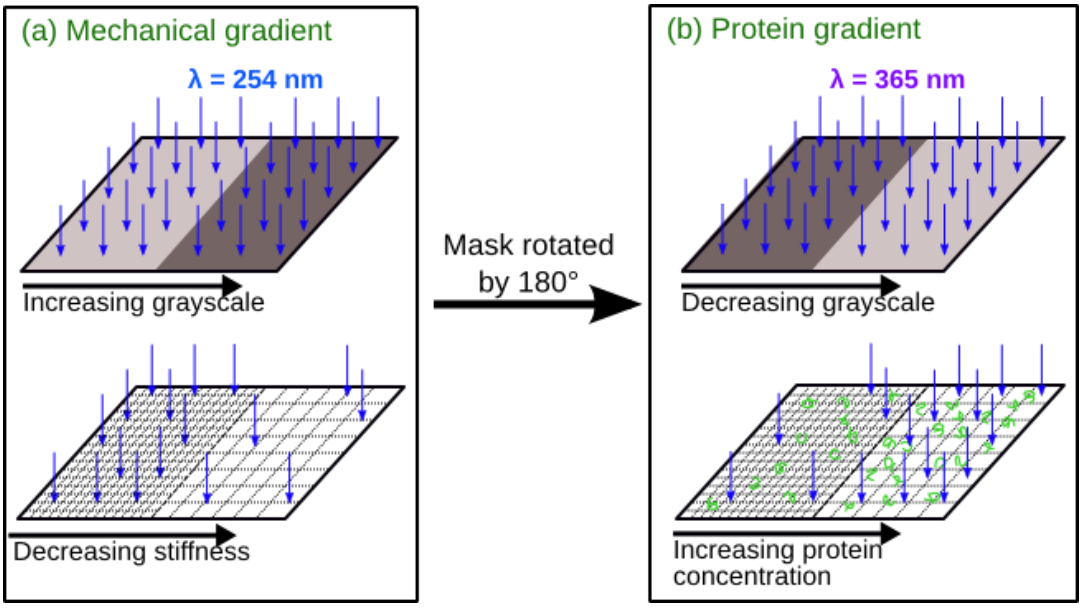

Figure 3. The design and assembly of hydrogels that exhibit opposing rigidity and protein gradients. UV-mediated polymerization and chemical conjugation at two separate wavelengths were used to cross-link and conjugate collagen.

where F = applied force, $\alpha = 18°$, E = YM, k = spring constant of the cantilever, υ = Poisson's ratio (constant = 0.4) [171, 187], d = deflection of the cantilever, and δ = indentation.

2.4.2 Initial identification of the interfacial region using fluorescence microscopy: The YM of gradient gels was determined by initial identification of the interfacial region through fluorescence microscopy. Fluorescent imaging was conducted on a Nikon TE 2000 inverted microscope to determine the intensity of rhodamine beads. Fluorescent intensity was calculated using Nikon Elements™ software. This value was used to determine fluorescent intensities at the high and low cross-linked regions. In hydrogels assembled using either Masks 1 or 2, a 15% difference in intensity was observed between high- and low- cross-linked regions. These values were *only used to identify the initial boundaries of the interfacial region.*

2.4.3 Refinement of the interfacial region using YM measurements: The precise locations of the boundaries were determined by conducting multiple AFM measurements. The center of the interfacial region obtained by fluorescence microscopy was designated as the (0,0) position. Measurements were conducted at ±12.5, 25, 37.5, 50, 100, 150 and 200μm of the center coordinates. The boundaries of the interfacial region were established using the following procedure. In a hydrogel with a rigidity gradient introduced by Mask 1, YM values obtained at each position within the gradient were compared to those obtained from corresponding homogenous gels. YM values were compared (using a *t*-test with α set to 0.05) to those obtained for gels polymerized using only a 70% or a 40% mask. The last position at which the YM value was found to be statistically significant ($p < 0.05$) when compared to a gel polymerized with a 70% or 40% mask was identified as the boundary on the stiffer and softer side, respectively.

Similar measurements were conducted for gradients generated with Mask 2. The migratory behavior of cells was investigated only within this rigidity gradient.

2.4.4 Profilometry: A Veeco Dektak 150 (Bruker, Billerica, Massachusetts) profiler was used to determine the hydrated thickness of PAAM substrates. The location of the interface was first identified and marked. Thereafter, measurements were taken every 50 μm from the interface.

Section 2.5 Concentration of Surface-immobilized Collagen

The surface density of collagen was measured by a fibronectin (FN) binding assay [188]. Briefly, FITC-collagen (Type 1) ranging from 15–50μg/ml in concentration was covalently conjugated to either tissue culture polystyrene (TCPS, control) or PAAM gels. FN (BD Biosciences) was biotinylated using a commercially available kit (Thermo Fisher Scientific) as per the manufacturer's protocol. The substrates were incubated with biotinylated fibronectin and horseradish peroxidase-streptavidin. Thereafter, tetramethylbenzidine (TMZ) was added and the absorbance at 450nm was measured on a microplate reader (Molecular Devices, Sunnyvale, CA).

Section 2.6 Results

Optimization of initiator concentration: We conducted the polymerization of acrylamide using different concentrations of Irgacure 2959, varying the conditions for solubilizing the initiator, and UV exposure times. Based upon our measurements, we identified optimal conditions under which this initiator could be added to the monomer mixture while at the same time maintain its solubility (**Table 1**). For all these reactions, acrylamide was maintained at 10%v/v, bis-acrylamide at 0.72 %v/v, and APS at 0.5% v/v.

Table 1. Optimization of Irgacure 2959 solubility

Irgacure 2959 (%w/v)	Temperature (°C)	Time duration for heating (min)	Solubility
0.5	75	20	Soluble
1	75	20	Soluble
2	75	20	Soluble
3	75	30	Soluble
4	75	30	Soluble
5	75	30	Soluble
6-10	70-90	30-60	Not soluble

Based upon these experiments, PAAM hydrogels were polymerized with Irgacure 2959 at 5% w/v in the monomer solution, where the initiator had been solubilized by heating at 75°C for 30mins (**Table 1**). Further, we also optimized the UV exposure times to achieve polymerization of the acrylamide monomer mixture with 5% w/v Irgacure (**Table 2)**.

Table 2. Conditions optimized to achieve hydrogel polymerization using Irgacure 2959.

Solubilizing Irgacure	% w/v of Irgacure	UV exposure (min)
Heating at 75°C for 30mins	5	10
Heating at 75°C for 30mins	5	20
Heating at 75°C for 30mins	5	30
Heating at 75°C for 30mins	5	45
Heating at 75°C for 30mins	5	60

Design of rigidity gradients: PAAM hydrogels were first polymerized using a photomask with a single gray scale value of 80%, 70%, 40% or 30%. The elasticity of these hydrogels guided the design of rigidity gradients (RGs). The Young's modulus of these hydrogels was 126.7 ± 1.9 kPa (80%, n=3), 80.7 ± 6.2 kPa (70%, n=3), 48.2 ± 2.7 kPa (40%, n=3) and 46.7 ± 1.2 kPa (30%, n=3). Based on these values, two rigidity gradients RG1 and RG2 were obtained using Mask 1 and 2, respectively. The fold change in elastic modulus between the soft and stiff regions was

either ~ 1.7 (RG1) or 2.7 (RG2). The values of YM ratios were in close agreement to the differences in UV transmittance within each mask. In Mask 1 (70%/40%) and Mask 2 (80%/30%), the fold differences in the gray scale values were 1.75 and 2.66, respectively. On RG1, the YM values at 25%, 50% and 75% of the interfacial width were 45.1 ± 4.1 kPa, 57.3 ± 6.9 kPa and 62.8 ± 4.3 kPa, respectively. On RG2, the YM values at 25%, 50% and 75% of the interfacial width were 64.2 ± 5.7 kPa, 68.9 ± 6.2 kPa and 84.0 ± 0.29 kPa, respectively. The gradually increasing values of YM demonstrate that RGs were obtained using the UV photo masks. The widths of the interfacial regions were determined upon immobilizing collagen (Type 1; 15 μg/mL) prior to conducting measurements. The interfacial widths were 95.8±14.4 μm and 158.3±23.6 μm for hydrogels assembled with Masks 1 and 2, respectively (**Table 3**). The interfacial width generated by Mask 2 was significantly higher due to the greater differential in gray scale values and unavoidable refraction of UV light. Together, these factors resulted in crosslinking across a larger cross-section of the gel.

Table 3: Width of rigidity gradients using AFM measurements

Rigidity gradient (RG)	
Substrate	**Width (μm)**
RG1	95.8±14.4 (*n*=3)
RG2	158.3±23.6 (*n*=3)

Design of dual gradients: The input concentration of collagen on the "soft" substrates was either 30 μg/mL or 50 μg/mL. In order to measure the surface density of collagen, standards were prepared by adsorbing different input concentrations of collagen onto TCPS at 37°C for 16h in a humidified environment and then at 40°C for 24h at room temperature. Assuming

100% binding efficiency on TCPS, a calibration curve was obtained which was used to calculate the binding efficiency of collagen conjugated to low and high modulus gels (**Figure 4**). The intensity obtained from proteins adsorbed to the glass coverslips was measured independently and subtracted from the final value. Surface values were calculated by assuming a cylindrical gel with a height of 45 μm (height of a typical PAAM gel in this study) and a diameter of 15mm (diameter of coverslips on which gels were cast).

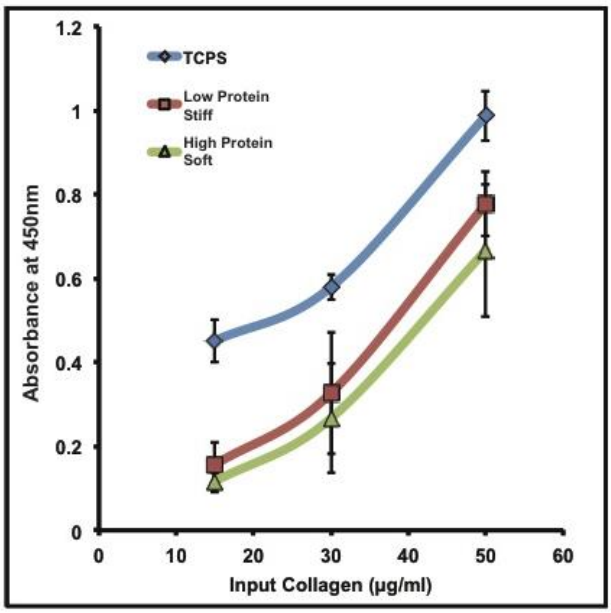

Figure 4. Calculating surface-bound collagen on tissue culture polystyrene (TCPS), and on a ~46kPa (high protein/soft) and 126 kPa (low protein/stiff) hydrogel substrate

RG2 was selected to superimpose a collagen gradient in the opposite direction. This gradient was chosen due to statistically significant durotaxis exhibited by fibroblasts. Moreover, the greater width of this rigidity gradient would pose an additional challenge for cells since they would have to migrate a greater distance away from the stiff side of the RG to reach locations with high collagen concentration. Two different chemical gradients were superimposed in the opposite direction to the rigidity gradient as follows. On the stiff side of RG2 (which exhibited a

YM of 126.7 ± 1.9 kPa), the input concentration of protein was 15 μg/mL. On the soft side of RG2 (YM of 46.7 ± 1.2 kPa), the input concentration of protein was either 30 μg/mL or 50 μg/mL. Upon exposure to UV light, the immobilized protein concentration varied between the low and high YM boundaries of the rigidity gradient. On the stiff side, the surface concentration of collagen was 3.5±1.2 molecules/μm^2 (**Table 4).** On the soft side, the surface concentration of collagen was 12.7±6.2 molecules/μm^2 or 23.9±5.7 molecules/μm^2, corresponding to the input concentrations of 30 μg/mL or 50 μg/mL, respectively (**Table 4).**

Table 4. Estimation of surface concentration of collagen.

[Collagen] (μg/ml)	***Rigid Side***		***Soft Side***	
	Binding efficiency (%)	**molecules/ μm^2**	**Binding efficiency (%)**	**molecules/ μm^2**
15	34.6	3.5±1.2	56.9	5.8±1.2
30	56.4	11.5±5.1	62.1	12.7±6.2
50	87.0	29.7±2.6	70.2	23.9±5.7

Thus, the collagen concentrations increased either four- or seven-fold from the rigid to the soft regions of the substrate. Henceforth, these dual gradients will be denoted as Dual gradient 1 (DG1, four-fold increase) and Dual gradient 2 (DG2, seven-fold increase). The width of RG2 did not undergo a significant change upon superimposing the collagen gradient (**Table 5**). Fluorescent images of a typical dual gradient are presented in **Figure 5**.

Section 2.7 Discussion and conclusions

We designed novel opposing rigidity/protein gradients using photomasks and UV polymerization.

Table 5: Width of dual gradients using AFM measurements

Dual gradient (DG)	
Substrate	**Width (μm)**
DG1	158±11.8 (*n*=3)
DG2	150±20.4 (*n*=3)

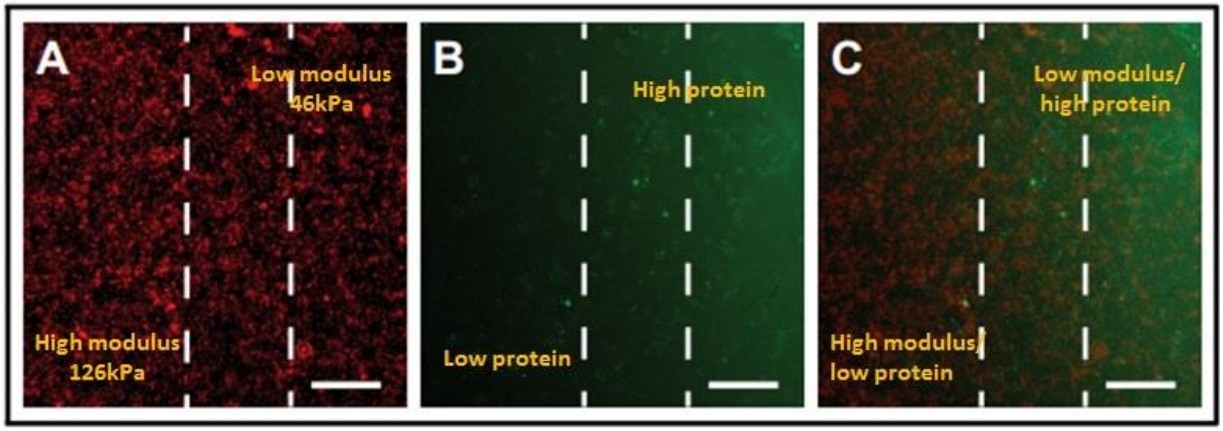

Figure 5. Fluorescent images of: (A) rhodamine-conjugated polystyrene beads imbedded within the PAAM hydrogel; (B) FITC-conjugated type 1 collagen bound to the hydrogel surface; (C) merged fluorescence images of the hydrogel substrate. The vertical dotted lines correspond to the boundaries of the interfacial region. Scale bar = 100μm.

This approach is versatile as it can be extended to design gradients with virtually any protein that has free primary amine groups. Moreover, PAAM hydrogels can exhibit a wide range of elastic moduli that can be easily tuned by changing the gray scale level of the mask and the cross-linker concentration. The wide range of moduli enables the design of physiologically relevant tissues [156, 172]. We assembled two different types of rigidity gradients (RG1 and RG2) using different grayscale levels of the photo-mask exhibiting different modulus values to study cell

migration. Although every attempt was made to obtain mechanical gradients of equal widths, RG2 was significantly wider than RG1. We believe that differential transmission of incident UV between Masks 1 (70%/40%) and 2 (80%/30%) and light scattering led to a wider gradient. Although high-resolution masks (2μm/pixel) were used to control the degree of incident UV light, it is likely that even greater resolution is required to prevent light scattering. Future studies will focus on using masks with even greater resolution or to choose combinations of gray scale values that exhibit the same differential.

To design opposing protein gradient, fluorescently labeled collagen was linked with diazirine cross-linker which was conjugated to the PAAM hydrogel on exposure to UV light through non-specific addition/insertion reactions. We designed two different dual gradient profiles (DG1 and DG2) where the immobilized collagen concentration was varied 4-fold and 7-fold on the low-modulus region while keeping the collagen surface concentration constant on the rigid regions of the interface. We also investigated the height of the hydrogel at the edges of the interface to determine if topography played a role. The height of the hydrogel on the low- and high-modulus edges did not vary significantly as a function of cross-linking. The heights of the high and low modulus edges were within 12% of the thickness at the middle. In summary, two different dual gradient profiles were designed and superimposed on RG2 gradient to study how strong a chemical cue has to be in order for fibroblast to direct its motion away from the rigid region of the biomaterial.

Chapter 3. Investigate fibroblast locomotion in the presence of simultaneous chemical and mechanical stimuli.

Section 3.1 Introduction

The migration of cells is a complex and dynamic process that is governed by several stimuli acting simultaneously. *In vivo*, cells receive and process a wide range of cues that guide their motion and migratory characteristics such as speed and directionality. The design of biomaterials that can recapitulate the combinatorial signaling environment can aid in understanding how migrating cells respond to more than one stimulus and when one cue dominates over the other. We have designed hydrogel substrates that exhibit opposing rigidity- and collagen gradients. Within the boundaries of the interfacial region, the values for substrate modulus decreased in one direction with a concomitant increase in the concentration of surface-bound collagen. The well-known durotactic migration of fibroblasts was first validated on substrates that only exhibit a gradient in modulus while keeping the concentration of surface-bound collagen constant. After durotaxis validation, we investigated the effect of opposing rigidity and protein gradient on directional behavior of fibroblasts.

Section 3.2 Materials and methods

3.2.1 Materials: FITC labeled collagen **(**M_w=10^6 Da), HEPES buffer, Irgacure 2959 (1-[4-(2-Hydroxyethoxy)-phenyl]-2-hydroxy-2-methyl-1-propane-1-one) and 3-triethoxysilylpropylamine were purchased from Sigma Aldrich, St Louis, MO. Glutaraldehyde (25%v/v) was purchased from Electron microscopy Sciences, Hatfield, PA. Phosphate buffered saline, rhodamine-conjugated polystyrene beads (0.5 μm in diameter), penicillin-streptomycin and Dulbecco's modified Eagle medium were purchased from Invitrogen Life Technologies, Carlsbad, CA. Acrylamide (10% v/v), bis-acrylamide (0.72 v/v), and APS were purchased from Bio-Rad,

Hercules, CA. All other chemicals and supplies were purchased from Thermo Fisher Scientific Waltham, MA unless otherwise specified.

3.2.2 Cell culture: Murine Balb/c 3T3 cells (Balb/3T3 clone A31, American Type Culture Collection, Manassas, VA) were maintained between passage numbers 3 to 15 at 37 °C under a humidified atmosphere at 5% CO_2. Cells were maintained in DMEM supplemented with 10%v/v bovine calf serum (Hyclone, Logan, UT) and 2% v/v penicillin-streptomycin.

3.2.3 Time lapse microscopy: PAAM gels were sterilized by exposure to germicidal UV for 1h. Fibroblasts (at a density of ~22000 cells/cm^2) were cultured on the hydrogels for 6-8h prior to conducting microscopy. The gels were placed in a closed observation chamber (Bioptech, Butler, PA) maintained at 37°C. This chamber was perfused with CO_2-enriched culture medium at a rate of 1mL/min [189]. Phase contrast and fluorescent images were obtained on an inverted TE-2000U Nikon microscope every 30 min up to 6h. Cells that underwent death, mitosis, exited the frame, or collided with adjacent cells during the observation period were not taken into consideration for further analysis. To calculate cell speed and displacement, the "*x*" and "*y*" coordinates of the cell centroids were measured at each time point. The mean-squared displacement (<d^2>) was calculated for a cell tracked for a total time $t_{max}= N\,\Delta t$ with a series of real time coordinates (x (nΔt), y (nΔt)) (equation 3) [123]. Here, N is the total number of time-points at which coordinates were obtained, while n and i are intermediate time-points.

$$\langle d^2, t = n\Delta t\rangle = \frac{1}{(N-n+1)} \sum_{i=0}^{i=N-n} [(x((n+i)\Delta t) - x(i\Delta t)]^2 + [(y((n+i)\Delta t) - y(i\Delta t)]^2$$

(*Equation 1*)

Only those cells that exhibited a minimum mean square displacement of 30 μm over the 6h observation period were further investigated for directionality of locomotion. This cutoff value was very close to the width of fibroblasts on the hydrogel substrates.

3.2.4 Immunofluorescence staining for actin and vinculin: PAAM hydrogels were polymerized with 0.5 μm fluorescent blue beads (Polysciences Inc, Warrington PA). Fibroblasts were fixed using a 0.75% glutaraldehyde in 1X PBS (v/v, Electron Microscopy Sciences, Hatfield PA) solution. A 0.1% Triton X-100 (Sigma-Aldrich) solution was added to enhance membrane permeability. Samples were incubated at 37^{o}C for 2h in a 0.1% AlexaFluor® 350 phalloidin (Invitrogen Life Technologies) solution and a monoclonal antibody to vinculin (Abcam; 1:100 dilution) followed by a FITC-conjugated secondary antibody (Abcam; 1:100 dilution). Images were obtained on a Zeiss LSM 510 Laser scanning confocal microscope placed on an inverted Axio Observer Z1 base.

3.2.5 Statistical analysis: Statistical significance and *p*-values between sample groups (e.g. evaluating trends in cell areas and displacement) were determined by t-test analysis with alpha set to 0.05. All data are reported as mean ± standard deviation. Sample sizes are denoted by *n*.

The binomial test was performed to assess the statistical significance of the cell count trends in cell migration. For rigidity gradients, the null hypothesis was that cells would not show a preference to migrate towards either side of the interface. Hence, according to the null hypothesis, the probability that a cell would move towards the high modulus side of the interface was 0.5. Suppose that out of a total of *l* cells, we observed *k* cells moving towards the high modulus side, where *k* was larger than *l/2*. Then the alternative hypothesis was that cells showed a preference to move towards the high modulus side. Under the null hypothesis, the probability

that we would observe *k* or more out of *l* cells moving towards this side is provided in equation (4). This quantity is the *p*-value of the one-sided binomial test. The one-sided binomial test was appropriate here because of the way in which the alternative hypothesis is posed: that the cells moved towards the high modulus side. Alpha was maintained at a value of 0.05. Cells exhibiting random walk motion near the high-modulus edge of the interfacial region were not included in *k*.

$$Bin(l,k,\frac{1}{2}) = \sum_{i=k}^{l} \binom{l}{i} \left(\frac{1}{2}\right)^{i} \left(\frac{1}{2}\right)^{l-i} = \sum_{i=k}^{l} \binom{l}{i} \left(\frac{1}{2}\right)^{l} \quad Equation\ (2)$$

Based on the results described later for rigidity gradients, the null hypothesis for dual gradients was that cells would show a preference to migrate towards the high modulus/low protein side of the interface. Hence, according to the null hypothesis, the probability that a cell would move towards the low modulus/high protein side of the interface was *p*, where this probability was calculated from the cell counts for rigidity gradients. Suppose that out of a total of *l* cells, we observed *k* cells moving towards the low modulus/high protein side, with *k* being at least *l/2*. The alternative hypothesis was that the cells showed a preference for the low modulus/high protein side. Then, under the null hypothesis, the probability that we would observe *k* or more out of *l* cells moving towards this side is provided in equation (5). This quantity is the *p*-value of the one-sided binomial test. Alpha was maintained at a value of 0.05. Cells exhibiting random walk motion near the low-modulus/high collagen edge of the interfacial region were not included in *k*.

$$Bin\ (l,k,p) = \sum_{i=k}^{l} \binom{l}{i} p^{i}(1-p)^{l-i} \quad Equation\ (3)$$

Section 3.3 Results

Fibroblast migration on rigidity gradients: Durotaxis was monitored on two different rigidity gradients. Approximately 65% (RG1) and 74% (RG2) of cells either migrated towards the stiffer regions of the hydrogel or exhibited random walk motion at the rigid edge of the gradient (**Table 1**, **Figure 1**).

Table 1: Direction of fibroblast migration on rigidity gradients.

Direction of motion	**RG1** ***n* = 23**	**RG2** ***n* = 34**
Soft to Stiff	13	20
Stiff to Soft	8	9
Exhibiting random walk motion near the high-modulus edge of the interfacial region	2	5
p-value of binomial test	0.2	0.03

The average values for total displacement were 45 ± 17.8 μm (RG1) and 71.5 ± 25.3 μm (RG2). However, when the displacements over each 2h period were calculated, significant differences were observed between the two gradients (**Figures 2A and 2D**). On RG1, the average displacement was 32.9 ±11.0 μm, 17.1±7.2 μm and 9.6±5.9 μm from 0–2h, 2-4h and 4-6h, respectively. In contrast, on RG2, fibroblasts exhibited average displacements of 25.6±10.8 μm, 21.3 ±14.6 μm and 25.1±14.9 μm in the same time periods. These trends indicate that fibroblasts remained motile on RG2 throughout the observation period in contrast to the large decrease in speed observed on RG1 in the second half. Moreover, changes in spread cell areas (**Figures 2B and 2E**) were observed between the two gradients.

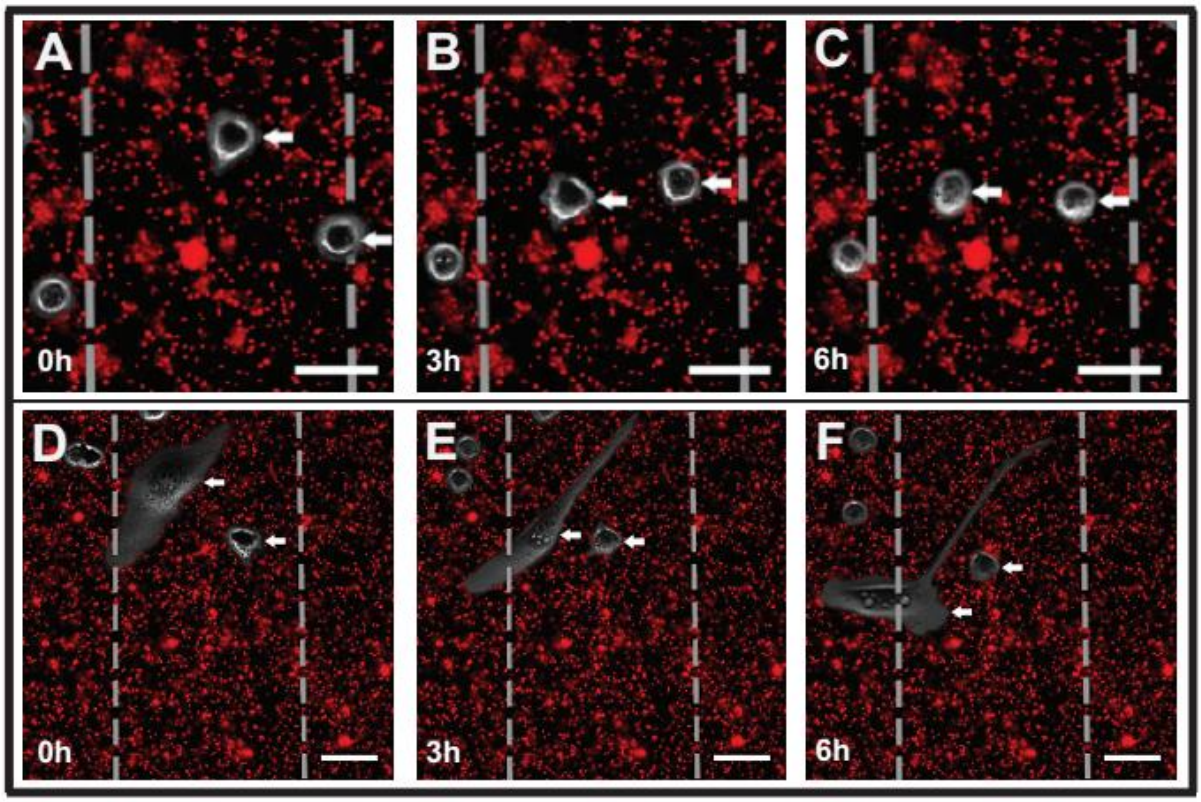

Figure 1. Merged phase-contrast and fluorescence time-lapse images of fibroblasts migrating on RG1 (A-C) and RG2 (D-F). Durotactic motion is observed on both rigidity gradients over a 6h period. Scale bars = 50µm.

Approximately 43% (RG1), and 35% (RG2) of cells exhibited increased cell areas ($Area_{t=6h}/Area_{t=0h} > 1$) (Figures 2B and 2E). The higher cell areas on RG1 suggest that the cell adhesion to the substrate is better when compared to RG2. When the average trajectory of all cells was calculated, there is a clear preference exhibited by fibroblasts for the high-modulus regions of the interface (Figures 2C and 2F). The extended migratory behavior of fibroblasts on RG2 compared to RG1 can be attributed to the differences in the widths of the two interfacial regions. Fibroblasts moving on RG2 have to migrate a wider distance in order to reach the rigid edge of the interface and would therefore remain motile for longer time periods. Upon applying the one-sided binomial test to the data show in **Table 1**, the *p*-values for RG1 and RG2 were

calculated to be 0.2 and 0.03, respectively. Therefore, the results obtained on RG1 were not significant. In contrast, migration to the high modulus region was statistically significant for RG2 at the 0.05 level.

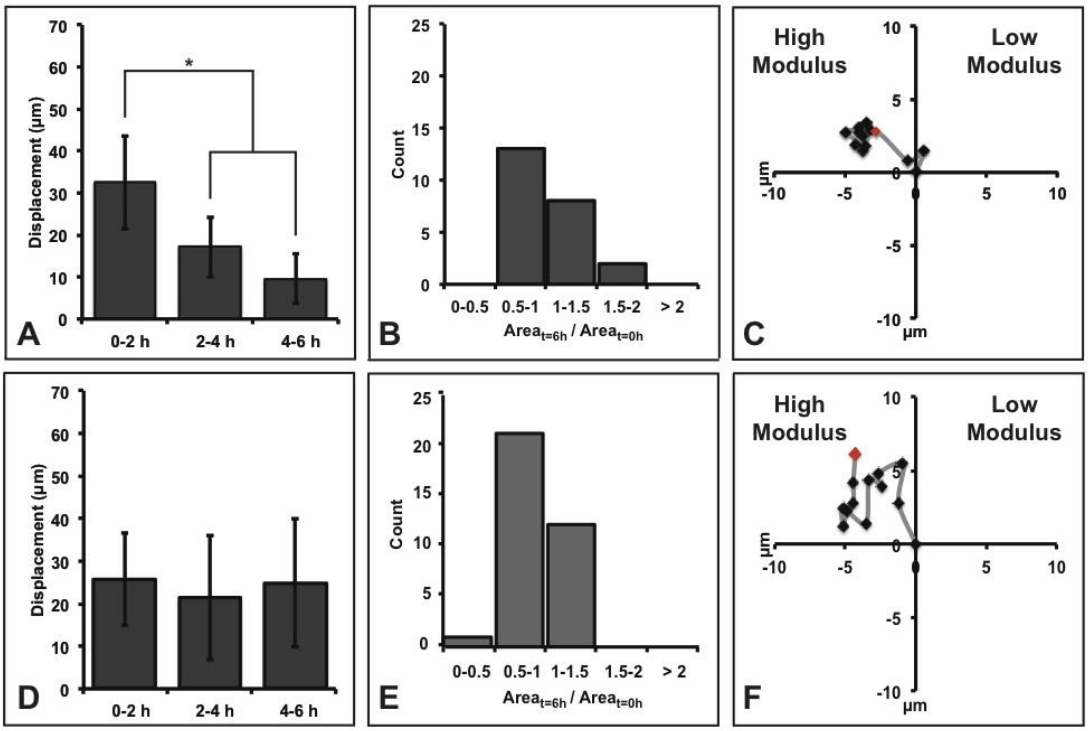

Figure 2. Average displacements exhibited by fibroblasts over 2h increments on RG1 (A) and RG2 (D). Histograms of the area fold change exhibited by fibroblasts over 6h on RG1 (B) and RG2 (E). The average trajectory of cells analyzed on the rigidity gradients. The diagrams show positions at each time-point relative to the cell's initial position (t=0) on RG1 (C) and RG2 (F). An asterisk (*) indicates a statistically significant difference (p < 0.05). n=23 (RG1) and n=34 (RG2).

Fibroblast migration on opposing rigidity/protein gradients: Fibroblasts migrating across DG1 or DG2 were monitored to determine their preference for directed motion towards the 46kPa (soft) edge of the interfacial region (**Figure 3**, **Table 2**). On DG1, approximately 62% of cells either migrated towards the soft edge or exhibited random walks on the soft/high protein edge of the gradient. When a 7-fold increase in collagen was introduced (DG2) a dramatic increase in the preferred direction of migration was noted with 73% of cells clearly exhibiting motion towards

the 46kPa region or performing random walks in this region. Some fibroblasts did indeed move towards the rigid edge of the gradient. Upon tracking the average trajectories of all cells (**Figures 4A and 4B**), both dual gradients elicited cells migrating towards the high collagen/low-modulus regions. However, fibroblasts clearly infiltrated DG2 to a greater extent.

Table 2: Direction of fibroblast migration on opposing rigidity/protein gradients.

Direction of motion	**DG1** ***n* = 29**	**DG2** ***n* = 33**
High-modulus/low collagen to low-modulus/high collagen	15	20
Low-modulus/high collagen to High-modulus/low collagen	11	9
Exhibiting random walk motion near the Low-modulus/high collagen edge of the interfacial region	3	4
p-value of binomial test	0.004	$3x10^{-5}$

The binomial test was repeated for the data in **Table 2**. Since both dual gradients were assembled with the stiffness gradient from RG2, according to the null hypothesis, the probability that a cell would move to the high collagen/low modulus side was 0.31 (9/29; see **Table 1**). The *p*-values of the one-sided binomial test with this probability were for 0.004 for DG1 and $3x10^{-5}$ for DG2. Therefore, fibroblasts on both dual gradients exhibited a reversal of durotaxis.

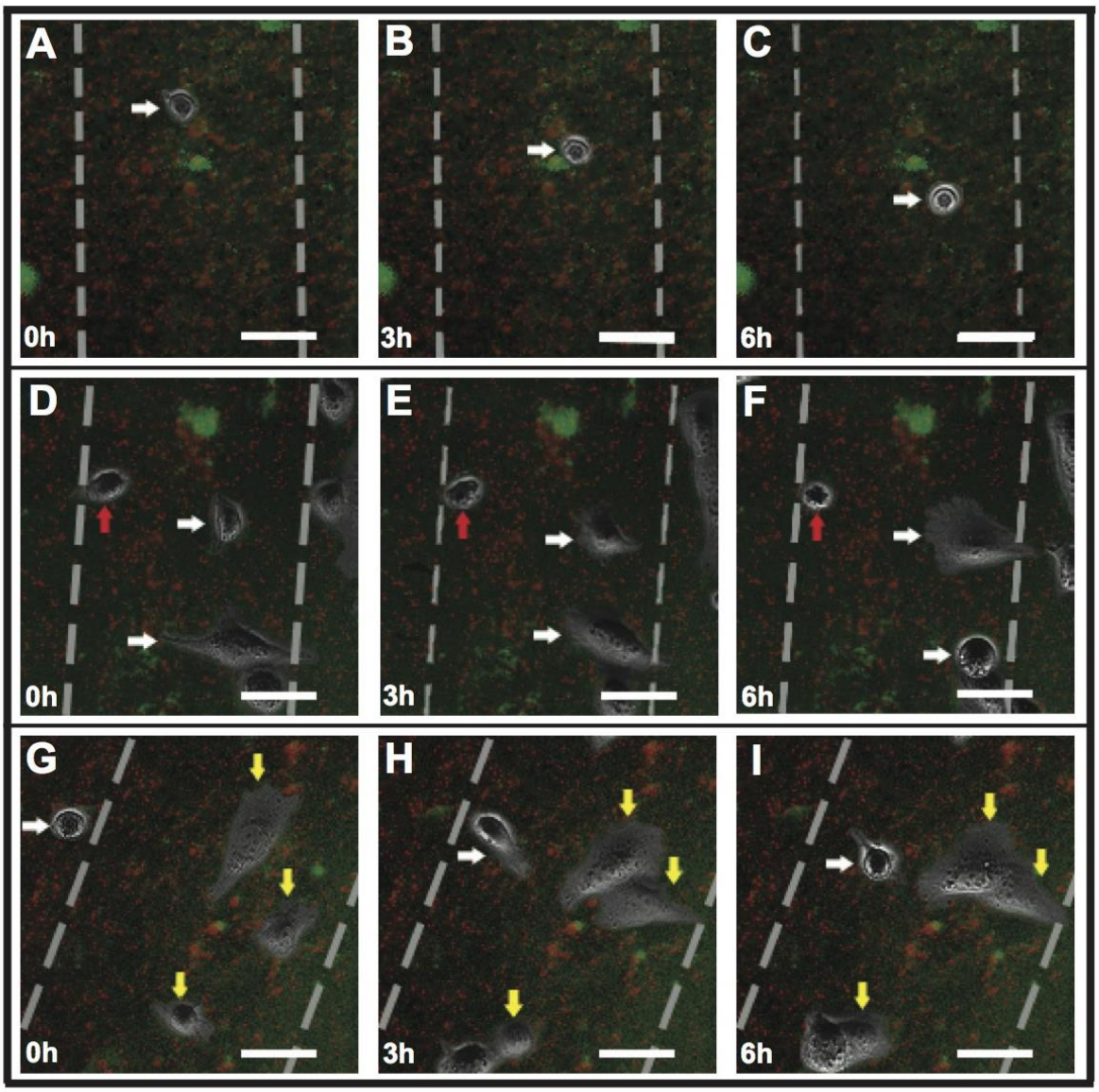

Figure 3. Merged phase-contrast and fluorescence time-lapse images of fibroblasts migrating on DG1 (A-C), DG2 (D-F) and DG2 (G-I). Images 5D-5F depict cells within the gradient exhibiting directed motion towards the low-modulus/high collagen regions. Images 5G-5I depicts one cell that is initially located outside the gradient (on the high-modulus region) moving towards the low-modulus/high regions. Scale bars = 50µm.

Comparing the cell trajectories in **Figure 4A** and **4B**, infiltration of fibroblasts into the low modulus/high collagen regions is greater only when the collagen concentration is 7-fold higher (**Figure 4B**).

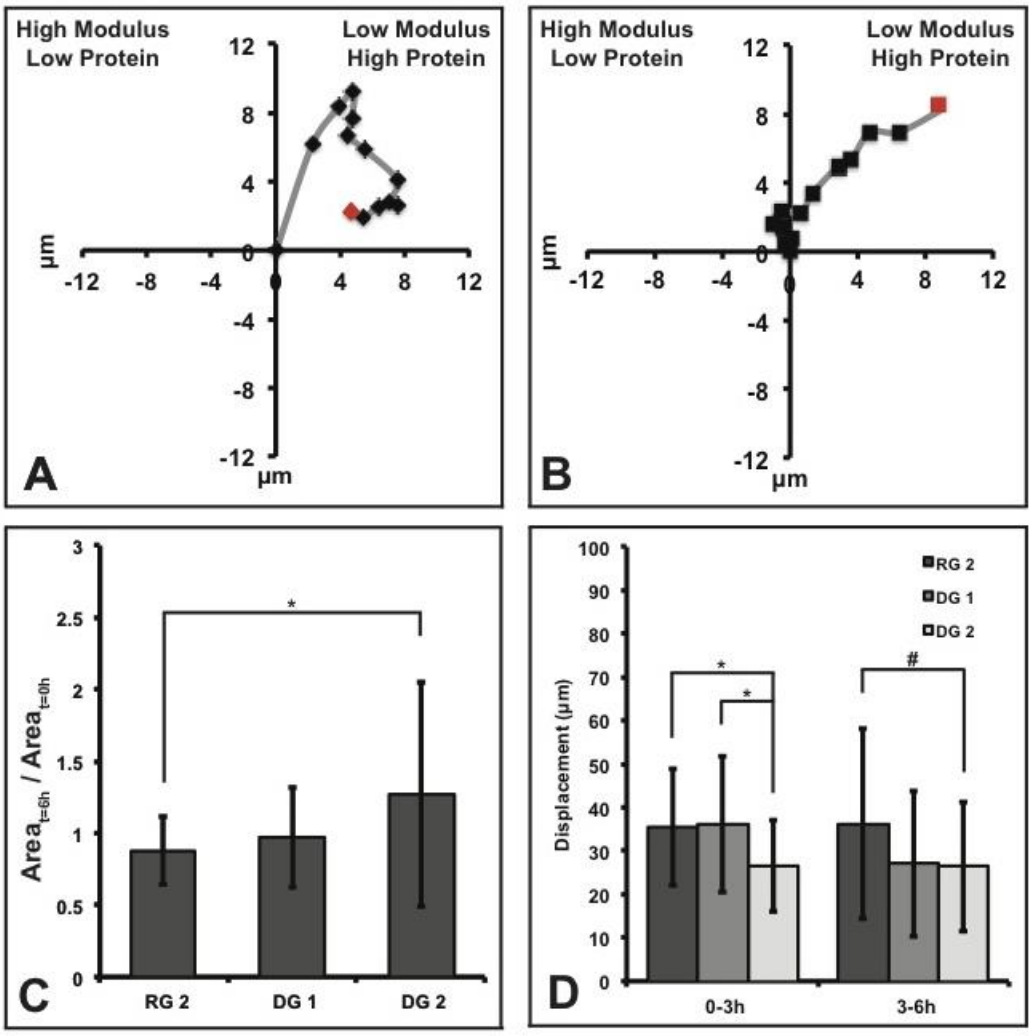

Figure 4. The average trajectory of cells analyzed on dual gradients. The diagrams show positions at each time-point relative to the cell's initial position (t=0) on DG1 (A) and DG2 (B). Average area fold change exhibited by fibroblasts over 6h on RG2, DG1, and DG2 (C). Average displacements exhibited by fibroblasts over 3h increments on RG2, DG1, and DG2 (D). An asterisk (*) or pound (#) sign indicates a statistically significant difference (p < 0.05). n=34 (RG2), n= 29 (DG1), and n=33(DG2).

When the collagen concentration is 4-hold higher (**Figure 4A**), the cells enter the low modulus region but do not infiltrate it to a great extent. The locomotion of cells across the two dual gradients revealed additional interesting contrasts. Projected cell areas on DG2 were statistically higher ($p<0.05$) in comparison to cells moving on the corresponding rigidity gradient (RG2) (**Figure 4C**). The average displacement from 0–3h was also lower for cells on DG2 when compared to RG2 or DG1 (**Figure 4D**). Since cells do not move in a linear manner, the angle (θ) made by the line connecting the final and initial coordinates for each cell with the x-axis was calculated. If this angle ranged between $\pm 45^{o}$ the cell would have moved primarily in the positive "x" direction (toward the soft/high protein side of the dual gradient). Approximately 20%, 34% and 27% of cells exhibited angularities with magnitude at most 45^{o} and therefore horizontal motion on RG2, DG1 and DG2, respectively (**Figures 5A-C**). On both DGs, the trajectory of fibroblasts was primarily radial and not horizontal. It is of interest to note that only on DG2 do cells (~18%) move in a perpendicular manner along the "y" axis. The corresponding value is approximately 3% on RG2 and DG1. The perpendicular motion can be attributed to fibroblasts moving up and down at the low-modulus/ high-collagen edge of the interfacial region.

Actin cytoskeleton and vinculin localization: The actin cytoskeleton on the low-modulus/ high-protein side of the interface did exhibit differences for cells migrating either on DG1 or DG2 (**Figures 6A and 6C**). For cells on DG1, the actin filaments were well defined and were present though the entire cross-section of cells. In contrast, on DG2, the actin filaments were well defined primarily on the peripheral regions of the cell. Vinculin-enriched focal adhesions were found in the frontal regions of cells on both gradients (**Figures 6B and 6D)**. Interestingly, large vinculin-enriched focal adhesions were observed in the tips of cell extensions on the trailing edge

of fibroblasts on DG2. Vinculin is reported to be present in nascent focal adhesion and a critical focal adhesion protein for cell migration [190].

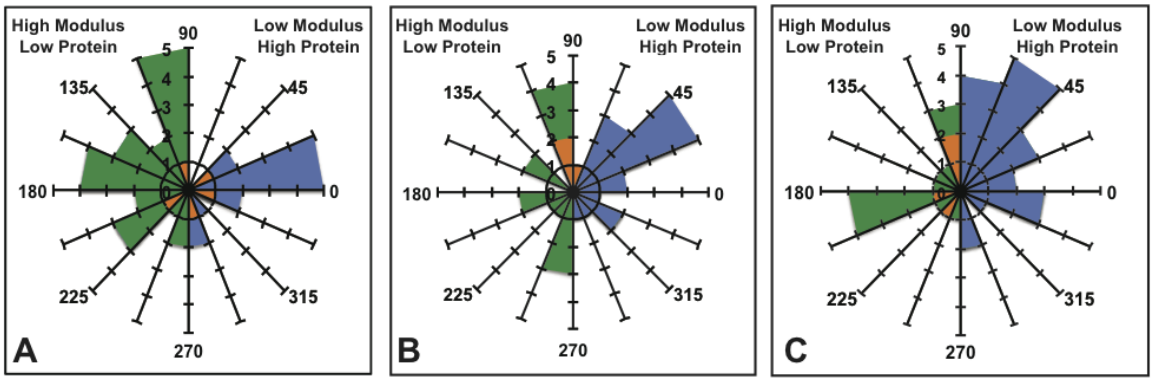

Figure 5. Angularity histograms for RG2 (A), DG1 (B), and DG2 (C), where the angle is determined by the inverse tangent of $(y_f - y_o) / (x_f - x_o)$ where (x_o,y_o) and (x_f,y_f) correspond to the initial (0h) and final (6h) coordinates of cell, respectively. An asterisk (*) or pound sign (#) indicate a statistically significant difference ($p < 0.05$). n=34 (RG2), n= 29 (DG1), and n=33 (DG2).

Section 3.4 Discussion and conclusions

Durotaxis is a well-studied migratory characteristic that has been reported on a wide range of cells and substrates [191]. We have previously reported cells moving away from stiff (high-modulus) regions in favor of softer domains of a hydrogel [152]. In this report, there was a sharp increase in YM values of either side of an interface and the soft regions were modified with high concentrations of collagen-coated microspheres. Previously, fibroblast migration in microfluidics devices was investigated where the cells experienced both protein and shear stress gradients [167]. To the best of our knowledge, there are no migration studies conducted *in vitro* on opposing rigidity-immobilized protein gradients.

We have designed novel opposing rigidity and surface-bound protein gradients using custom designed photomasks and UV-mediated polymerization and conjugation. We assembled two different rigidity gradients to study durotaxis. The broad range of elastic moduli exhibited by the rigidity gradients are of physiological relevance to tissues such as skin breast and collagenous bone [192-194].

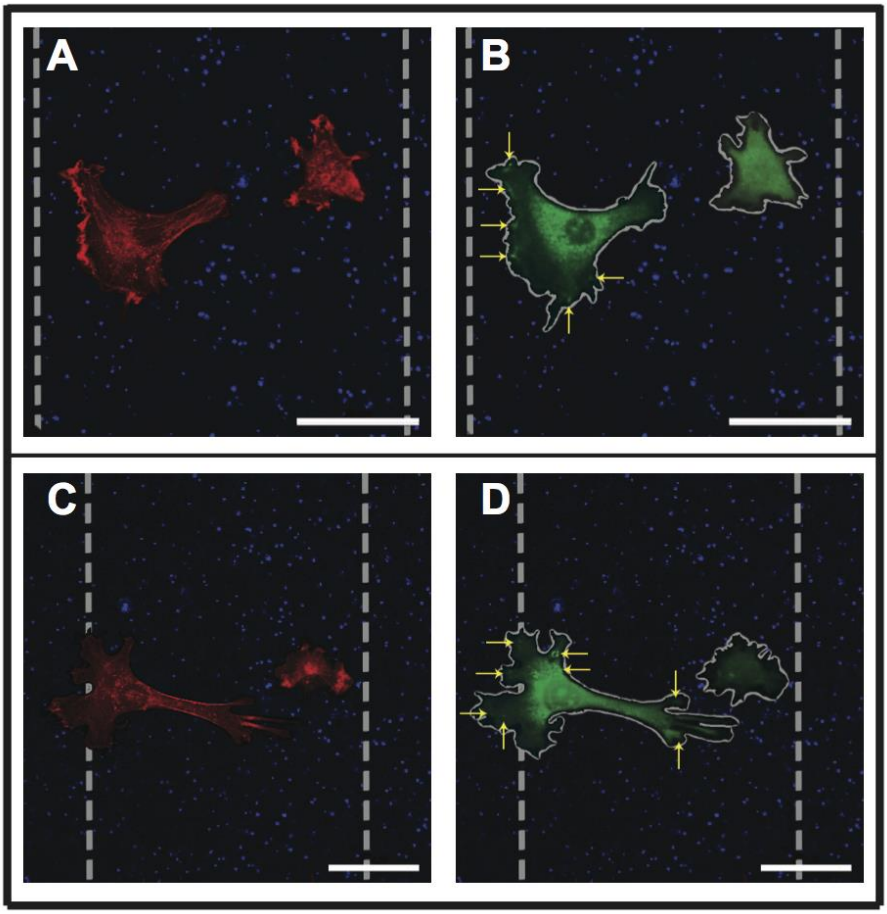

Figure 6. Fluorescent images of actin cytoskeleton and vinculin focal adhesions for fibroblasts on DG1 (A-B) and DG2 (C-D). Actin is depicted in red, vinculin in green, and the embedded polystyrene beads in blue. The vertical dotted lines correspond to the boundaries of the interfacial region. In these images, the high protein, soft side is on the left and the low protein stiff side on the right. Yellow arrows point to focal adhesions (B and D). Scale bars = 50μm.

Upon super-imposing an immobilized collagen gradient in the opposite direction, a reversal of durotaxis was observed. This reversal occurred by increasing the concentration of immobilized collagen by a factor of four or seven from the stiff side to the soft side of the rigidity gradient. It is evident that when fibroblasts preferred low-modulus regions that exhibited a 7-fold increase in collagen. The increased in cell areas and decrease in displacement on DG2 can be correlated to the increased adhesivity of the substrate resulting from higher surface-bound collagen at the middle of the interface and on the low-modulus regions. Since the widths of the DGs were approximately 150μm, the angularity in cell motion was calculated to determine whether cells would choose the quickest route to reach their preferred destination. Based on our data, fibroblasts on RG2 and DG1 primarily exhibited radial motion. Only on DG2 did cells exhibit close to perpendicular motion. These cells were very close to the boundary of the interface on the ~46kPa/high collagen side. There was a moderate difference between cells exhibiting horizontal trajectories on DG1 and DG2. While the precise reasons for the observed differences in angularity of cell motion between the two dual gradients are not fully understood, we hypothesize that the higher collagen concentration on DG2 could have played a role. A significant finding was the extent of infiltration was different on the dual gradients. Fibroblasts migrated further into the low modulus/high protein region only when the collagen concentration was increased by 7-fold. These findings could be of significance to understand wound healing processes and cancer metastasis.

In this study, we have demonstrated that on hydrogels where the substrate elasticity gradually changes in a direction opposite to the rigidity gradient. In the future, substrates that exhibit lower values of elastic modulus (<15kPa) with high concentrations of chemokines, cytokines and

other ECM proteins may provide insights on how cells migrate into diseased tissues. The current work can be extended into understanding cell migration during wound healing. For example, during the early stages of injury, a mechanical gradient is formed from the interior of the wound (low-modulus) to the exterior (high-modulus). In addition to the mechanical gradient, the concentration of signaling molecules is higher in the center of the wound and lower in the periphery [145].

We have designed opposing rigidity-protein gradients. The range of elastic moduli exhibited by these gradients spans a broad range and can therefore be used to investigate cellular migration in different tissues. Since cell locomotion is a dynamic process governed by several stimuli acting simultaneously, we envision that seeking to address how cells move in the presence of dual conflicting stimuli will be of physiological relevance to probe healthy and diseased tissues. The insights obtained on such complex interfaces can aid in the design of future biomaterials and implants that emulate interfacial regions found *in vivo*. Substrates that incorporate multiple stimuli with gradients in different directions could serve as physiologically relevant models to monitor how a cell chooses to move and how one signal may exert a more dominant role than another. In the future, the insights obtained from this work can be extended to investigating migratory behavior during regeneration, cancer metastasis and wound healing.

Chapter 4. Investigate macrophage and fibroblast co-culture locomotion in the presence of simultaneous chemical and mechanical stimuli.

Section 4.1 Introduction

A majority of cellular migration studies have been conducted on single cells [106, 137, 142, 152, 195]. Although, these studies provide insights into locomotion they do not take capture the multi-cellular environment found *in vivo* [106, 170, 196]**.** Since homotypic and heterotypic cell–cell communications play an important role in various cellular functions it is important that migration also be studied in complex cellular mixtures [165, 197-199]. The tissue microenvironment contains different cell types, thus, *in vitro* studies on migration behavior in co-cultures is a step towards future studies of complex cellular mixtures. In this project, we have investigated fibroblast migration in the presence of another motile cell type, murine macrophages. To the best of our knowledge, no study has investigated macrophage-fibroblast co-culture migration on dual and opposing rigidity-protein gradients.

Macrophages are involved in the regulation of the immune and inflammatory responses, as well as in tissue repair and remodeling [15]. These cells can be involved in both pro- and anti-inflammatory processes. Macrophages are involved in apoptosis, promotion of angiogenesis, fibroblast proliferation, synthesis of ECM and tissue formation [15, 200, 201]. Macrophages can be activated via classical (M1) or alternative (M2) pathways [202]. On exposure to pro-inflammatory cytokines such as interferons, lipopolysaccharides or microbial products, macrophages can adopt a classically activated phenotype and produce a large number of cytokines [200]. These cells have high microbicidal and tumoricidal properties and secrete high levels of pro-inflammatory cytokines such as IL-1, IL-6, IL-12, IL-23, TNF-α and iNOS [202]. Alternatively activated macrophages (M2), also called as wound healing macrophages, are

produced in response to IL-4 and other glucocorticoids. M2 macrophages produce anti-inflammatory cytokines (IL-10), growth factors (TGF-β1, VEGF, and PDGF) and ECM, and promote healing [16, 203].

4.1.1 Macrophage responsiveness to the physical properties of biomaterials: Macrophage morphology and cytoskeleton can be modulated by substrate elasticity [195]. Murine macrophages cultured on a soft substrate (elastic modulus: 1.2kPa) exhibited a more rounded shape with fewer filopodial projections compared to cells on a rigid substrate (elastic modulus: 150kPa) that showed increased protrusions. Moreover, these cells exhibited increased phagocytosis of both un-opsonized and IgG coated latex beads. Alveolar macrophages exhibited changes in cell shape when seeded on substrates that exhibited elastic moduli values of 0.1, 40, 160kPa when compared to cells cultured on rigid substrates exhibiting moduli values of 3MPa and 70MPa. Cells on softer substrates were rounded in shape while cells on stiffer substrate exhibited a flattened morphology [204]. RAW 264.7 macrophages on PEG hydrogels exhibited a round morphology on soft substrates (Young's modulus: 130kPa) with localized actin around the periphery of the cell membrane [205]. However, macrophages on stiff substrates (Young's modulus: 240kPa and 840kPa) were well spread with more defined actin on the cell cytoskeleton. Membrane protrusions such as filopodia were also found to be more prominent on cells cultured on stiff substrates. These trends suggest that the mechanical properties of the substrate can influence macrophage morphology and function.

4.1.2 Macrophage response to immobilized molecules: Since collagen type I is the most abundant protein present in the body comprising >60% of the total dry weight of dermal tissue [12] all cells, including macrophages come in contact with this ECM protein. ECM proteins play an important role in cellular adhesion during wound healing [202]. Macrophages encounter

collagen and other ECM proteins that can serve as chemoattractants, thereby, directing them to a wound location [127, 206].

Gowen *et al* reported differences in the adhesion of RAW 264.7 murine macrophages on fibrillar, monomeric and denatured forms of Type I collagen [207]. This study showed that macrophages exhibited poor adhesion on the fibrillar form of collagen while displaying significantly higher adhesion on the denatured form due to a higher number of exposed binding sites. Macrophage scavenger receptor, were found to play a major role in adhesion to monomeric and denatured collagen. However, other reports have implicated the role of integrins in monocytes adhesion to denatured ECM proteins [208-210].

Human peripheral blood monocytes (precursor cells to macrophages) have been shown to be chemotactic towards collagen and collagen-based peptide sequences [211]. It was also found that it is the tertiary structure of native collagen may be responsible for chemotaxis. Native collagen was found to be a more potent chemoattractant than the denatured α-chains of smaller peptides derived from cyanogen bromide, bacterial collagenase or pepsin. Moreover, the chemotactic response of monocytes was concentration-dependent, wherein, increasing concentrations of collagen or α-chains produced a greater chemotactic response [211]. Alveolar macrophages have also been reported to exhibit chemotaxis towards collagen peptides and its degraded products [212].

4.1.3 Studies on macrophage:fibroblast co-cultures: Co-culture studies conducted with macrophages and fibroblasts have shown that these cells can indeed influence each other [213-215]. A study by Zeng *et al* showed that co-culturing fibroblasts with macrophages in a 1:1 ratio induced the proliferation and migration of fibroblasts on the gelatin-oxidized alginate hydrogel.

Moreover, the levels of inflammatory cytokines such as IL-6, IL-13 and TNFR-II increased in the macrophages/fibroblasts co-culture in contrast to monocultures of macrophages [215]. Another report in the literature investigated the effect of differently activated macrophages on a fibroblast cell line WI-38 [216]. Alternatively activated macrophages (M2) increased the proliferation and collagen synthesis of co-cultivated WI-38 cells while classically activated macrophages (M1) reduced collagen production. Similarly, chemokines such as PDGF-AA, PDGF-BB and TGF-β1 production was elevated in alternatively activated macrophages. In contrast, expression and production of TNF-alpha, as well as MMP-7, were enhanced in classically activated macrophages. Previous reports have indicated the production of chemokine (IL-1) by rat bone marrow derived macrophages that enhanced collagenase secretion and collagen degradation by cultured skin fibroblasts of human, mouse and rabbit origin [213, 217]. In a co-culture with primary human macrophages (M1 phenotype) and human dermal fibroblasts, cell-cell signaling resulted in the enhanced secretion of inflammatory cytokines (IL6, CCL2 and CCL7) from fibroblasts [218]. However, fibroblast proliferation increased in the presence of macrophages that exhibited M2 phenotype.

4.1.4 Macrophage plasticity: Recent evidence suggests the presence of both phenotypes can be present in macrophages and that macrophages can switch from one to another [200, 219-221]. The switching from M1 to M2 or vice versa is called plasticity. It has been shown that macrophages can reversibly shift their functional phenotype in response to changes in the levels of cytokines [220, 221]. Even physical properties such as the surface roughness of a biomaterial can initiate this switch [222]. RAW 264.7 macrophages were cultured on polysiloxane substrates filled with epoxy resin that were either polished (average roughness Ra = 0.06μm) or sandblasted, acid-etched (average roughness Ra = 4.33μm). On the rough substrate, markers of

M2 phenotype such as monocyte chemoattractant protein-1 and macrophage inflammatory protein -1 alpha were upregulated. In another report, micropatterned substrates were used to transform cells from M1 to M2 phenotype. Even in the absence of exogenous cytokines, cellular elongation resulted in macrophage plasticity [219]. Although, there are limited studies that clearly exhibit the effect of a biomaterial on macrophage plasticity, there is sufficient evidence to support that biomaterial properties can indeed initiate macrophage plasticity.

Section 4.2 Materials and Methods

4.2.1 Materials: FITC labeled collagen **(**M_w=10^6 Da), HEPES buffer, Irgacure 2959 (1-[4-(2-Hydroxyethoxy)-phenyl]-2-hydroxy-2-methyl-1-propane-1-one) and 3-triethoxysilylpropylamine were purchased from Sigma Aldrich, St Louis, MO. Glutaraldehyde (25%v/v) was purchased from Electron microscopy Sciences, Hatfield, PA. Phosphate buffered saline, rhodamine-conjugated polystyrene beads (0.5 µm in diameter), penicillin-streptomycin and Dulbecco's modified Eagle medium were purchased from Invitrogen Life Technologies, Carlsbad, CA. Acrylamide (10% v/v), bis-acrylamide (0.72 v/v), and APS were purchased from Bio-Rad, Hercules, CA. All other chemicals and supplies were purchased from Thermo Fisher Scientific Waltham, MA unless otherwise specified.

4.2.2 Cell culture: RAW 264.7 macrophages were obtained from ATCC, Manassas, VA. These cells were cultured in DMEM supplemented with 10%v/v fetal bovine serum (Hyclone, Logan, UT) and 1% v/v penicillin-streptomycin at 37 °C under a humidified atmosphere at 5% CO_2. Cells were maintained between passage 3-15 in all experiments.

4.2.3 Time Lapse Microscopy: PAAM gels were sterilized by exposure to germicidal UV for 1h. Macrophages (at a density of ~16000 cells/cm^2) were cultured on the hydrogels for 6-8h prior

to conducting microscopy. For the macrophage-fibroblast co-culture experiments, the two cell types were seeded in the ratio of 1:1 and a total of ~27000 cells/cm^2 cells were cultured on dual gradient hydrogel (DG2).

The gels were placed in a closed observation chamber (Bioptech, Butler, PA) maintained at 37°C. This chamber was perfused with CO_2-enriched culture medium at a rate of 1mL/min [189]. Phase contrast and fluorescent images were obtained on an inverted TE-2000U Nikon microscope every 30 min up to 6h. Cells that underwent death, mitosis, exited the frame, or collided with adjacent cells during the observation period were not taken into consideration for further analysis. To calculate cell speed and displacement, the "*x*" and "*y*" coordinates of the cell centroids were measured at each time point. The mean-squared displacement ($\langle d^2 \rangle$) was calculated for a cell tracked for a total time $t_{max}= N\,\Delta t$ with a series of real time coordinates (x (nΔt), y (nΔt)) (*equation 1*) [123]. Here, N is the total number of time-points at which coordinates were obtained, while n and i are intermediate time-points.

$$\langle d^2, t = n\Delta t\rangle = \frac{1}{(N-n+1)} \sum_{i=0}^{i=N-n} [(x((n+i)\Delta t) - x(i\Delta t)]^2 + [(y((n+i)\Delta t) - y(i\Delta t)]^2$$

(*Equation 1*)

Only those cells that exhibited a minimum mean square displacement of 30 μm over the 6h observation period were further investigated for directionality of locomotion.

4.2.4 Enzyme-linked Immunsosorbent Assays (ELISA): The levels of TNF-α ((R&D systems, Minneapolis) and TGF-β (Abcam, Cambridge, MA) present in spent cell culture medium were measured using ELISA. Spent culture medium was obtained after 8h of cell culture and stored at -20°C until needed. The manufacturer's protocols were followed for each assay and a brief description is provided below.

Concentration of TNF-α: Microwell plates (96w) were coated with a TNF-α antibody. In each well, 50μL of the assay diluent and samples (or standards) were added and the mixture was incubated for 2h at room temperature. A horseradish peroxidase conjugated polyclonal antibody to TNF-α was added and incubated for an additional 2h. Thereafter, tetramethylbenzidine and hydrochloric acid were added. The absorbance at 450 nm was measured on a SpectraMax M2 microplate reader (Molecular Devices, Sunnyvale, CA). Standard curves were generated in culture medium.

Concentration of TGF-β: Microwell plates (96w) were coated with a TGF-β antibody. 100μL of undiluted standards and test samples were added to the wells and then incubated at room temperature. After washing, 100μL of Biotin-conjugated anti-Rat TGF beta 1 detection antibody was added then incubated at room temperature for 2h. Following washing, 100μL of Streptavidin-HRP conjugate was added to each well, incubated at room temperature for 30mins then again washed. 100μL of tetramethylbenzidine was added and then catalyzed by HRP to produce a colored product after adding acidic stop solution. The density of yellow coloration was directly proportional to the amount of Rat TGF beta 1 captured on the plate and amount was measured using a calibration curve.

4.2.5 Statistical analysis: Statistical significance and *p*-values between sample groups (e.g. evaluating trends in cell areas and displacement) were determined by t-test analysis with alpha set to 0.05.

All data are reported as mean ± standard deviation. Sample sizes are denoted by *n*.

The binomial test was performed to assess the statistical significance of the cell count trends in cell migration. For rigidity gradients, the null hypothesis was that cells would not show a preference to migrate towards either side of the interface. Hence, according to the null hypothesis, the probability that a cell would move towards the high modulus side of the interface was 0.5. Suppose that out of a total of *l* cells, we observed *k* cells moving towards the high modulus side, where *k* was larger than *l/2*. Then the alternative hypothesis was that cells showed a preference to move towards the high modulus side. Under the null hypothesis, the probability that we would observe *k* or more out of *l* cells moving towards this side is provided in equation (2). This quantity is the *p*-value of the one-sided binomial test. The one-sided binomial test was appropriate here because of the way in which the alternative hypothesis is posed: that the cells moved towards the high modulus side. Alpha was maintained at a value of 0.05. Cells exhibiting random walk motion near the high-modulus edge of the interfacial region were not included in *k*.

$$Bin(l,k,1/2) \quad = \sum_{i=k}^{l} \binom{l}{i} \left(\frac{1}{2}\right)^{i} \left(\frac{1}{2}\right)^{l-i} = \sum_{i=k}^{l} \binom{l}{i} \left(\frac{1}{2}\right)^{l} \quad Equation\ (2)$$

Based on the results described later for rigidity gradients, the null hypothesis for dual gradients was that cells would show a preference to migrate towards the high modulus/low protein side of the interface. Hence, according to the null hypothesis, the probability that a cell would move towards the low modulus/high protein side of the interface was *p*, where this probability was calculated from the cell counts for rigidity gradients. Suppose that out of a total of *l* cells, we observed *k* cells moving towards the low modulus/high protein side, with *k* being at least *l/2*. The alternative hypothesis was that the cells showed a preference for the low modulus/high protein side. Then, under the null hypothesis, the probability that we would observe *k* or more out of *l*

cells moving towards this side is provided in equation (3). This quantity is the *p*-value of the one-sided binomial test. Alpha was maintained at a value of 0.05. Cells exhibiting random walk motion near the low-modulus/high collagen edge of the interfacial region were not included in *k.*

$$Bin\ (l, k, p) = \sum_{i=k}^{l} \binom{l}{i} p^i (1-p)^{l-i} \quad Equation\ (3)$$

Section 4.3 Results

Our goal was to investigate fibroblast migration when co-cultured with macrophages. As a first step, we monitored the locomotion of macrophages monocultures on PAAM hydrogels to determine if they exhibited directed migration. In Chapter 3, we demonstrated that fibroblasts on RG2 exhibited a statistically significant preference for the high modulus region of the interface. Therefore, we conducted macrophage migration studies only on RG2.

Macrophage mono-culture migration on rigidity gradient (RG2): When monocultures of macrophages were cultured on RG2, the cells appeared to exhibit a slight preference for the rigid (126kPa) region of the interface. Approximately 59.4% of macrophages either migrated towards the stiffer regions of the hydrogel or exhibited random walk motion at the rigid edge of the RG2 gradient (**Figure 1, Table 1**). The average value for total displacement over a 6h period was 60.9 ± 23.5μm (n=31). Upon tracking the average trajectories of all cells for RG2 (**Figure 2**), macrophages appeared to exhibit a slight preference towards the 126 kPa region. However, upon conducting the one-sided binomial test (**Table 1**), the trends were found to be statistically insignificant (*p*-value = 0.13). Therefore, on RG2, macrophages did not exhibit a preference for directed migration towards the low or high YM regions of the interface.

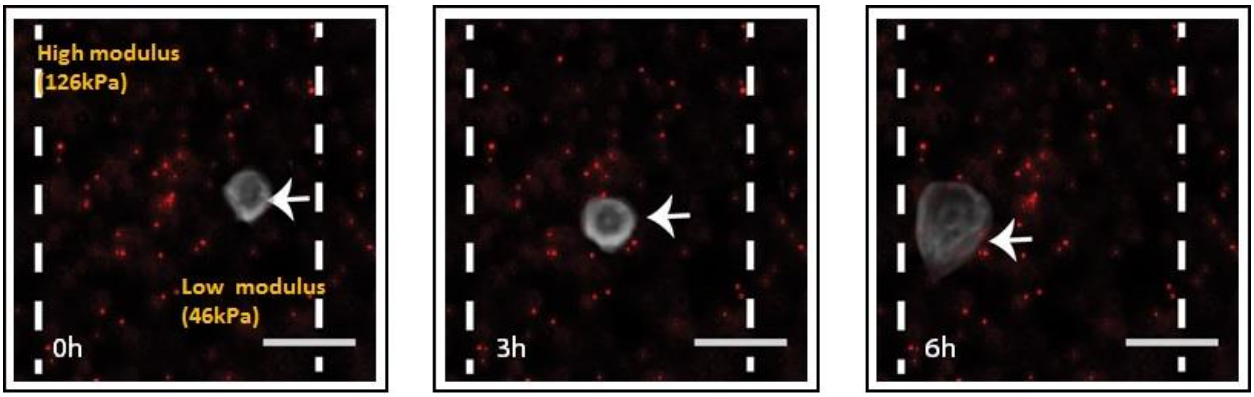

Figure 1. Merged phase-contrast and fluorescence time-lapse images of RAW 264.7 macrophages migrating on RG2 over a 6h period. Scale bars = 50μm

. **Table 1. Direction of macrophage migration on RG2**.

Direction of Motion	RG2 (n=31)
46kPa to 126kPa	18
126kPa to 46kPa	11
Exhibiting random walk motion near the high modulus edge of the interfacial region	2
p-value of one-sided binomial test	0.13

Macrophage mono-culture migration on dual and opposing rigidity-protein gradients: RG2 was selected as the substrate for superimposing a haptotactic gradient in the opposite gradient. The dual gradients were identical to those described in Chapter 3. Two different dual gradient profiles were created in which the collagen concentrations increased either four fold (DG1) or seven-fold (DG2) from the rigid to the soft regions of the substrate. Macrophages migrating across DG1 or DG2 were monitored to determine their preference for directed motion towards the 46kPa (soft) edge or the 126kPa (stiff) edge of the interfacial region.

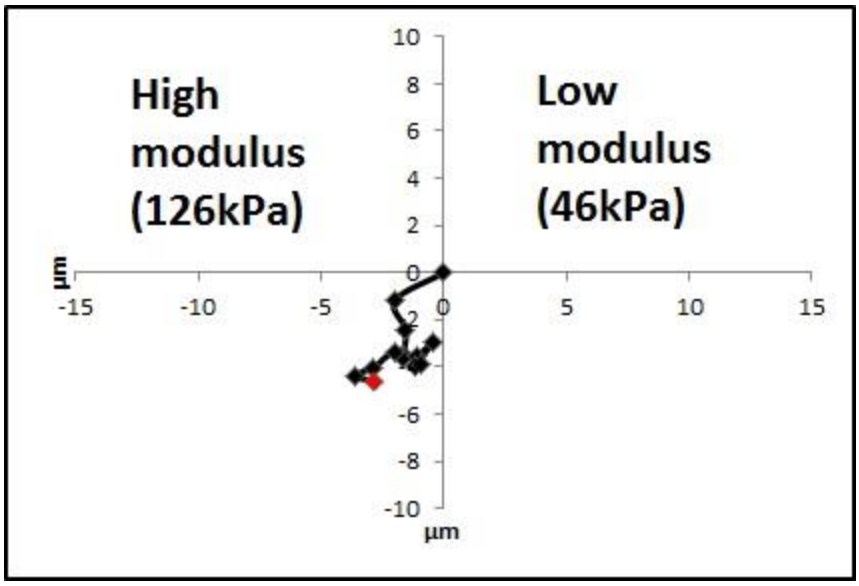

Figure 2. The average trajectory of cells analyzed on the rigidity gradients. The diagrams show positions at each time-point relative to the cell's initial position (t=0) on RG2.

On DG1, approximately 47% of macrophages migrated towards the soft/high protein edge while an equal percentage of cells migrated towards the stiff/low protein edge of the (**Figure 3, Table 2**).

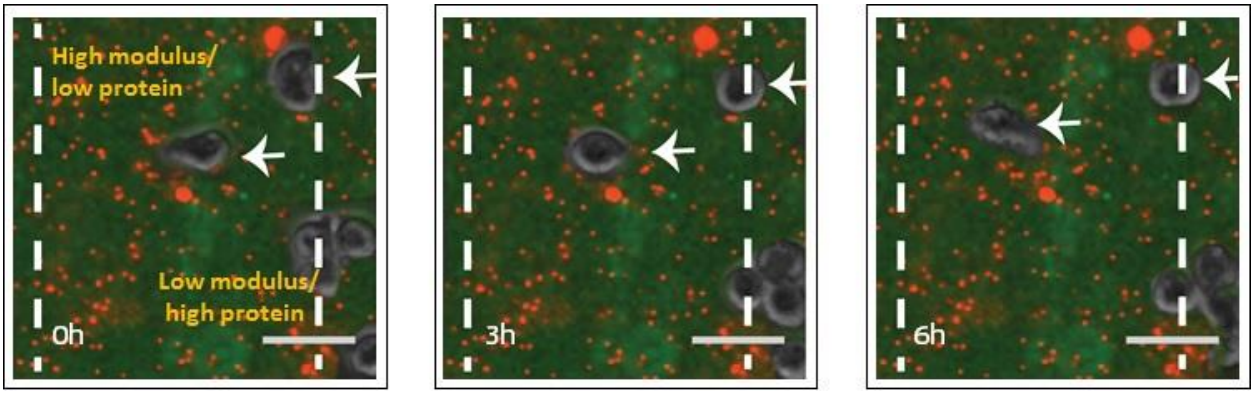

Figure 3. Merged phase-contrast and fluorescence time-lapse images of macrophages migrating on DG1. Scale bar = 50µm

When a 7-fold increase in collagen was introduced (DG2), a dramatic increase in the preferred direction of migration was noted with 66% of cells clearly exhibiting motion towards the low collagen/high-modulus region (**Figure 4, Table 2**).

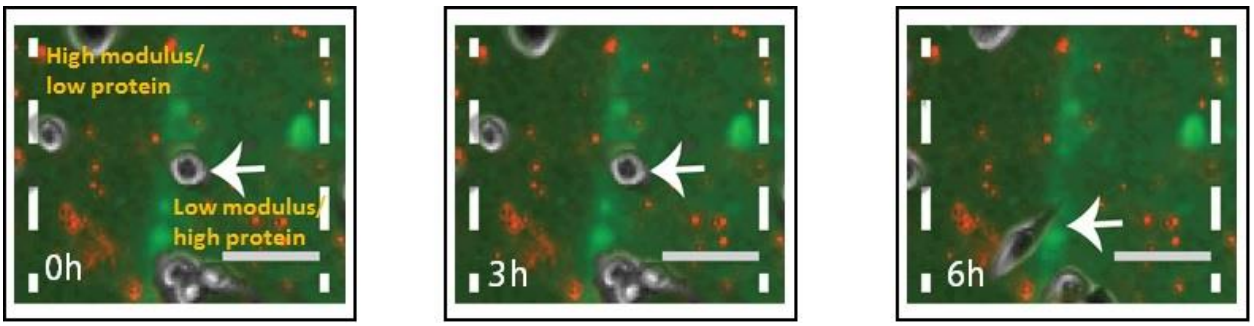

Figure 4. **Merged phase-contrast and fluorescence time-lapse images of macrophages migrating on DG2. Scale bar = 50µm**

The trends were statistically insignificant on DG1 (*p*-value=0.4) and highly significant on DG2 (*p*-value = 0.0003). Upon tracking the average trajectories of all cells, macrophages on DG1 do not appear to infiltrate the low collagen/high-modulus region (**Figures 5A**). However, macrophages on DG2 clearly infiltrated low collagen/high-modulus region to a greater extent (**Figure 5B)**.

Table 2: Direction of macrophage migration on opposing rigidity/protein gradients

Direction of Motion	**DG1 (n=30)**	**DG2 (n = 51)**
Low modulus/high collagen to High-modulus/ low collagen	11	35
High-modulus/low collagen to Low-modulus/high collagen	13	11
Exhibiting random walk motion near the low-modulus/high collagen edge of the interfacial region	2	5
p-value for the one-sided binomial test	0.4	0.0003

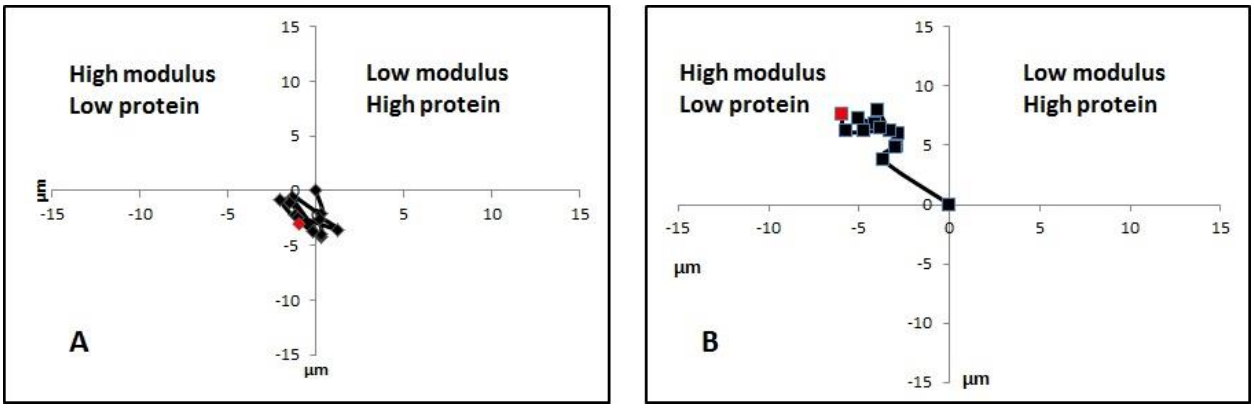

Figure 5. The average trajectory of macrophages analyzed on the rigidity gradients. The diagrams show positions at each time-point relative to the cell's initial position (t=0) on DG1 (A) and DG2 (B)

The locomotion of cells across the two dual gradients also revealed interesting results about the macrophage migration. Projected cell areas of macrophages on RG2 were statistically higher (p<0.05) in comparison to the cells moving on the corresponding rigidity gradient (DG2) (**Figure 6).** The average displacement from 0–3h and 3-6h was also lower for macrophages on DG1 and DG2 when compared to RG2 (**Figure 7**).

Since cells do not move in a linear manner, the angle (θ) made by the line connecting the final and initial coordinates for each cell with the x-axis was calculated. If this angle ranged between ±45° the cell would have moved primarily in the positive "x" direction (toward the soft/high protein side of the dual gradient). Approximately 41%, 69% and 47% of cells exhibited angularities with magnitude at most 45° on RG2, DG1 and DG2, respectively (**Figures 8**).

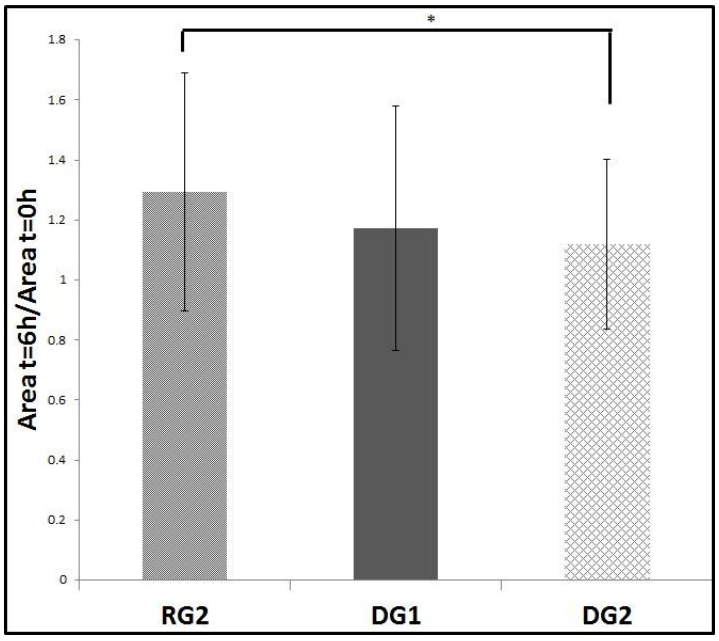

Figure 6. Average area fold change exhibited by macrophages over 6h on RG2, DG1, and DG2. An asterisk (*) sign indicates a statistically significant difference ($p < 0.05$).

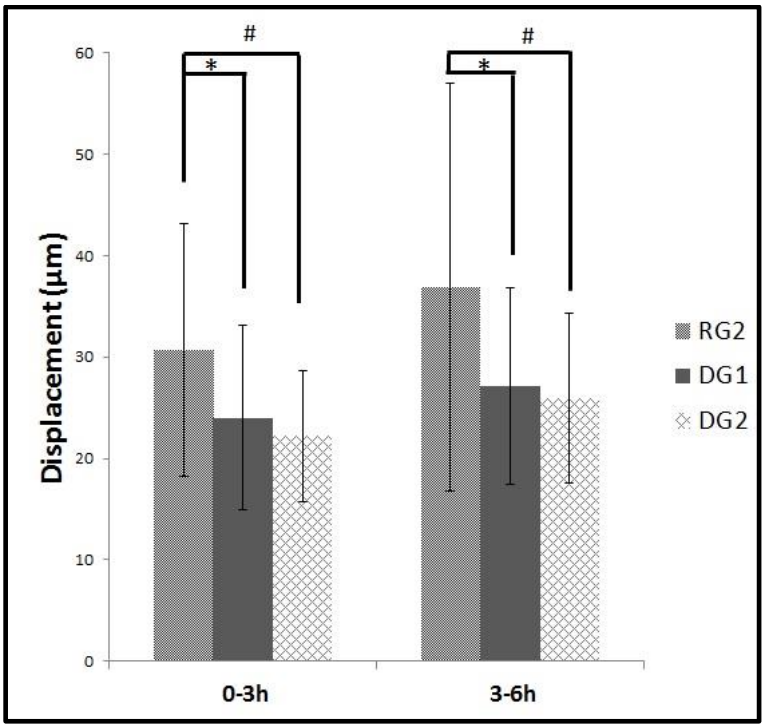

Figure 7: Average displacements exhibited by macrophages over 3h increments on RG2, DG1, and DG2 . An asterisk (*) sign indicates a statistically significant difference ($p < 0.05$).

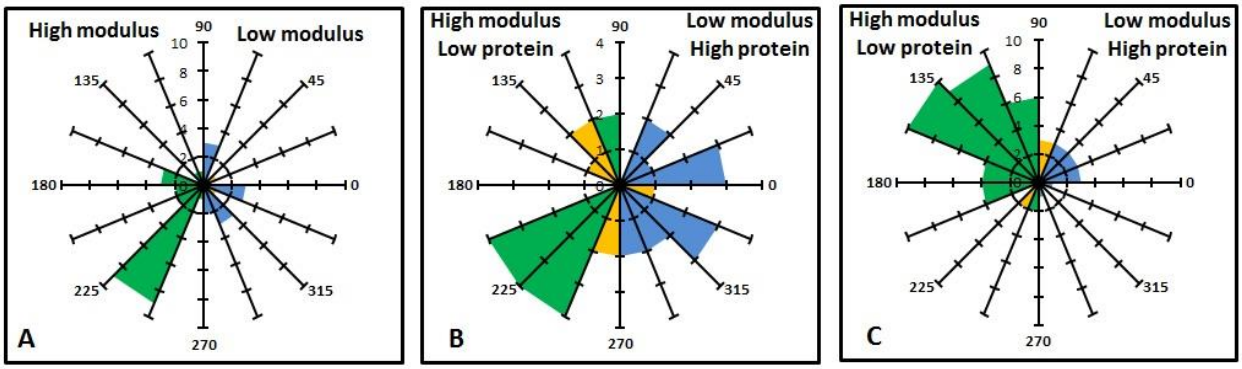

Figure 8. Angularity histograms for RG2 (A), DG1 (B), and DG2 (C), where the angle is determined by the inverse tangent of (yf – yo) / (xf – xo) where (xo,yo) and (xf,yf) correspond to the initial (0h) and final (6h) coordinates of cell, respectively.

Macrophage:fibroblast co-culture migration on dual and opposing rigidity-protein gradients: In order to investigate the effect of macrophages on fibroblast migration, we cultured both cell types in a 1:1 ratio on DG2. We selected this dual gradient substrate since both fibroblasts and macrophages exhibited statistically significant directed migration on this substrate. Macrophages continued to exhibit a statistically significant preference for the high modulus/low protein region of the interface (**Table 3, Figure 9A-C**) wherein 71% of the macrophages exhibited durotaxis. The migratory trends exhibited by fibroblasts were not statistically significant based on the current sample size (**Table 3, Figure 9D-F)**. Approximately 58% of fibroblasts exhibited haptotaxis. It is likely that upon increasing the sample size or the macrophage-fibroblast ratios, statistically significant trends from fibroblasts may be obtained.

The preferred direction of migration from fibroblasts (in co-cultures) appeared to be in the direction similar to their monoculture counterparts. We have only investigated one ratio of macrophages:fibroblasts, the trends may change when we change these ratios. Upon tracking the average trajectories of all cells on DG2 (**Figure 10**), macrophages clearly infiltrated the high modulus-low protein region.

Table 3: Direction of macrophage:fibroblast co-culture migration on DG2 rigidity/protein gradient.

Direction of Motion	Macrophages (n=24)	Fibroblasts (n=26)
Low modulus/high collagen to High-modulus/ low collagen	17	8
High-modulus/low collagen to Low-modulus/high collagen	5	15
Exhibiting random walk motion near the low-modulus/high collagen edge of the interfacial region	2	3
p-value of binomial test	0.008	0.1

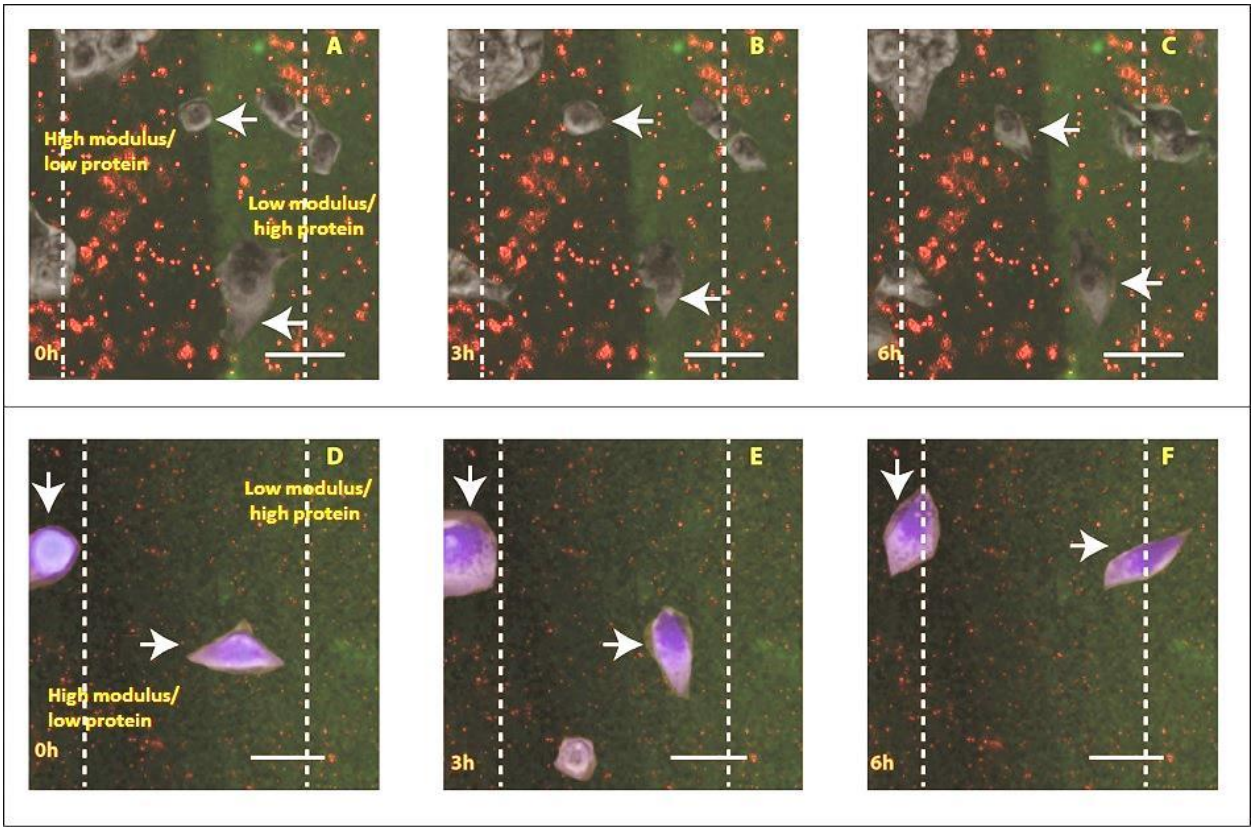

Figure 9. Merged phase-contrast and fluorescence time-lapse images of macrophages (A-C) and fibroblasts (D-F) migrating on DG2. Scale bar = 50µm

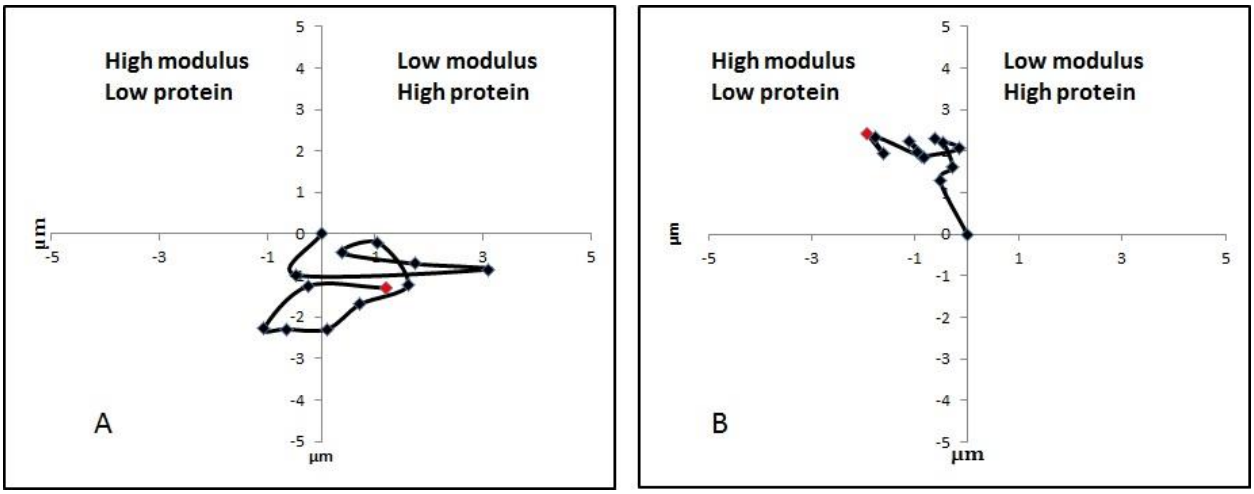

Figure 10. The average trajectory of cells analyzed on the DG2 rigidity/protein gradient. The diagrams show positions at each time-point relative to the cell's initial position (t=0) on DG2 (A) Fibroblasts and (B) Macrophages

Fibroblast displacement was statistically significant in the first 3h increment in co-culture compared to monoculture on DG2 (**Figure 11**). However, the average displacement over 6h exhibited by macrophages was not statistically significant on DG2 alone when compared to macrophages in co-cultures (**Figure 12**). Further, the area fold change was found to be statistically insignificant for both macrophages and fibroblast in both conditions (monocultures vs co-culture) on DG2 (**Figure 13 and 14**).

ELISA on macrophage: fibroblast co-culture: We performed ELISA on spent culture medium samples of fibroblast: macrophage co-cultures and macrophage mono-cultures (on DG2). The samples were tested for a pro-inflammatory cytokine TNF-alpha and a pro-wound healing growth factor TGF-beta. The ELISA results showed statistically significant higher secretion of TNF-alpha in macrophage mono-cultures on DG2 when compared with co-cultures. However,

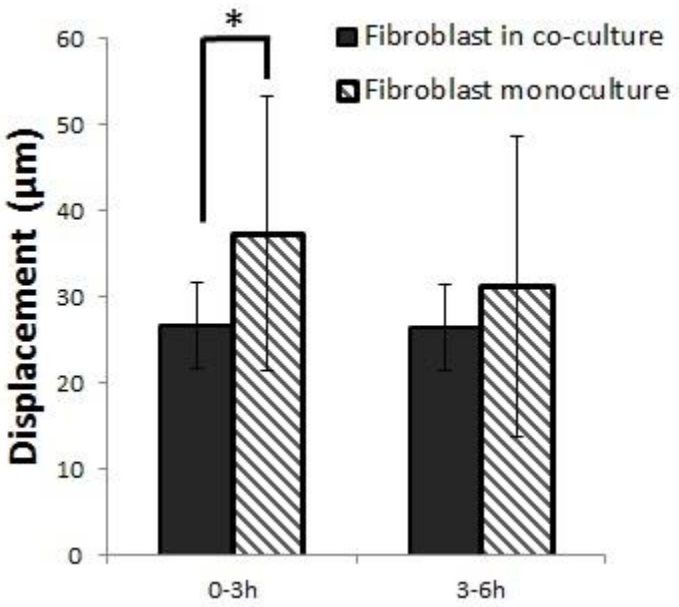

Figure 11: Average displacements exhibited by fibroblast over 3h increments on the DG2 rigidity/protein gradient. An asterisk (*) sign indicates a statistically significant difference ($p < 0.05$).

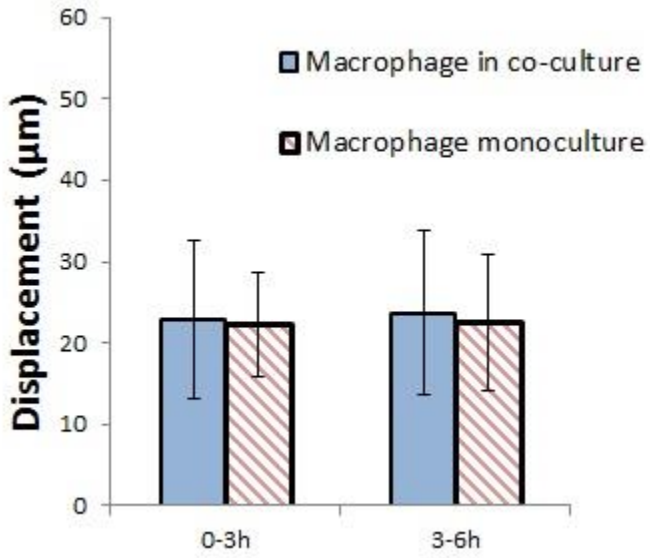

Figure 12: Average displacements exhibited by macrophages over 3h increments on the DG2 rigidity/protein gradient in co-culture studies.

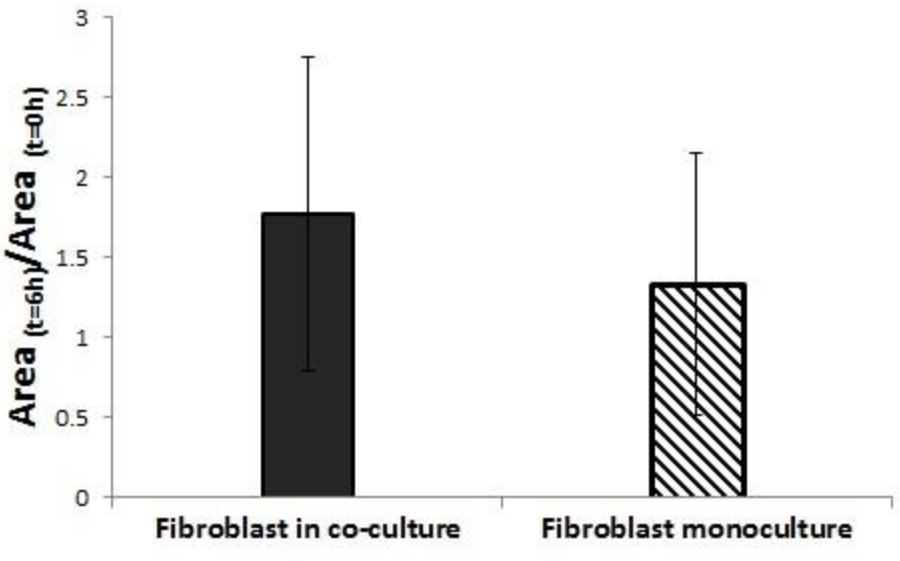

Figure 13: Average area fold change exhibited by fibroblast over 6h on the DG2 rigidity/protein gradient.

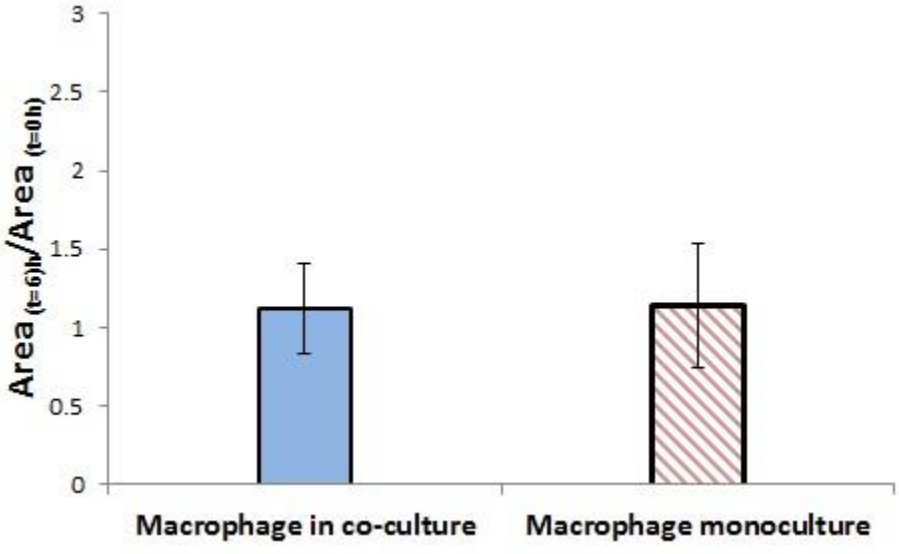

Figure 14: Average area fold change exhibited by macrophages over 6h on the DG2 rigidity/protein gradient

there was no difference in the amount of the pro-wound healing marker, TGF-β secretion in monocultures vs co-cultures (**Table 4**).

Table 4: ELISA estimation of TNF-α and TGFβ

	Macrophage monoculture	Macrophage-fibroblast co-culture
TNF-α (pg/ml)	22.44 ± 4.7*	2.0 ±5.3
TGF-β (pg/ml)	51.5 ±17.4	47.9±11.4

*denotes statistically significant

Section 4.4 Discussion and conclusions

Our research objective was to investigate fibroblast migration when co-cultured with another motile cell type such as macrophages. In order to investigate the directionality of cells in a co-culture, we first studied macrophage directionality on rigidity and dual gradients. We observed that macrophages did not exhibit any preference towards the rigid or soft regions of the interface on RG2 gels (p=0.13, n=31). When macrophage motion was tracked on DG1 dual gradient gels, the trends for directed migration were not significant (p=0.4, n=30). Interestingly, there was a dramatic change in the macrophage direction on DG2 gels upon increasing the concentration of immobilized collagen by 7-fold on the soft regions of the interface. Macrophages exhibited motion away from the high protein-low modulus regions and preferentially moved in the opposite direction. These trends were statistically significant (p=0.0003, n=51). This is very an intriguing result and requires further investigation. Further studies on protein localization, composition and cytokine levels may provide insights into the change in directionality.

In order to study the directionality of fibroblasts in the presence of macrophages we co-cultured them in 1:1 ratio. We observed that fibroblasts appear to migrate towards the high protein-low modulus regions, however the results were statistically insignificant (p=0.1, n=26). In contrast, macrophages continued to move towards the high-modulus/low protein regions of the interface. It is likely that a co-culture ratio of 1:1 may not be optimal to observe a change in macrophage

directionality and additional ratios should be explored. Additionally, longer observation times may be needed. A simpler explanation could be that sample sizes may need to be increased.

We also investigated changes in the levels of two cytokines to determine if the presence of fibroblasts could affect their secretion. We measured the concentration of TNF-α (inflammatory marker; characteristic of M1 phenotype [202]) and TGF-β (pro-wound healing marker, characteristic of M2 phenotype [203]) in the spent culture medium obtained from mono- and co-cultures. The concentration of TNF-α was found to be statistically higher in the mono-cultures compared to macrophage-fibroblast co-cultures. This trend suggests a potential shift in phenotype. However, the concentration of TGF-β was found to be the same (statistically insignificant) under both conditions. In the future, investigating the levels of additional cytokines indicative of M1 and M2 phenotypes may provide more comprehensive information on changes in macrophage phenotype. It is also possible that upon changing the ratio of the two cell types may result in different trends. Studies on cell lysates will also be useful since such samples typically contain higher levels of proteins enabling more accurate measurements.

Chapter 5. Future Research Directions

Cell migration is a dynamic process that occurs in the presence of a wide range of cues. Although a cell receives many different signals from its external environment, it processes them internally and moves in either a random or specific direction. Our research objectives have been focused upon understanding the process of directed motion when a cell encounters dual and opposing rigidity-protein gradients. The studies described in this thesis have been conducted on two rigidity gradients and two dual gradients. In the future, it will be interested to investigate if substrates with lower values of YM (up to 20 kPa) also exhibit similar properties. Such soft tissues are representative of regions in the body where a wound has just been inflicted. We have assembled haptotactic gradients with a single ECM protein i.e. collagen type I. Since, the tissue microenvironment is composed of a wide range of proteins, proteoglycans and other small molecules, it will be of interest to design immobilized gradients comprised of these components. Additionally, peptide sequences derived from ECM proteins can also be incorporated in the chemical gradients.

Hydrogels derived from natural materials such as alginates, chitosan or collagen and synthetic materials such as PEG may also be considered since they may provide a more native environment with greater tunability. Additional studies on obtaining a complete profile in changes in signaling molecules such as Rho GTPases, RAC, Arp2/3 will provide insights into the signaling mechanisms that are activated when cells are cultured on dual gradients. Immunofluorescence staining on additional focal adhesion proteins such as paxillin, tubulin and integrin clustering will also lead to a better understanding on their localization as cells migrate across dual and opposing gradients.

In the research objectives described in this thesis, immortalized murine Balb-c/3T3 fibroblasts and RAW 264.7 macrophages were used. However, it is feasible that primary cells may respond differently to the gradients we have assembled. In the future, studies on primary fibroblasts and macrophages may provide information more relevant to in vivo processes. With the advent of human tissue banks, cells derived from such tissues will lead to information that is more relevant to migratory processes in human beings.

By modifying the hydrogels substrates described in this thesis with suitable chemokines, detailed studies on the migration of cancer cells can also be undertaken. For example, by closely mimicking the mechanical and chemical properties of breast and bone tissues, we may be able to better understand metastasis in these tissues.

A major contribution from the results of our work can be applied to build upon our existing knowledge on how cells at mechanically mismatched tissues survive a high stress environment that exists at these interfaces. The examples of these assemblies of interconnected tissues include bone-ligament, breast-bone and bone-cartilage interfaces. One of the mains reasons of failure of anterior cruciate ligament (ACL) tissue engineered scaffolds is their poor integration into the sub-chondral bone. Strategies to mimic the interfacial architecture fall short of this goal as most of the studies are focused on designing the actual ACL scaffolds without focusing their attention on this interfacial region which is crucial for load bearing activities. These interfacial regions are partitioned into mineralized and non-mineralized zones which is crucial for various mechanical and cellular functions. These zones can be designed with minimal modifications to our existing system by conjugating photo-activatable phosphate and carboxylate groups to the monomer backbone that mimic the glycos-aminoglycans present in the mineralized regions. Quantifying

cell directional behavior along with proteins secreted in this environment could provide us better insights into the how cells navigate in this complex environment where multiple cues are present. The current work on complex interfaces can be applied towards the design of wound-healing biomaterials. The goal is to design adhesives that contain imprinted patterns as guides for the directed migration of cells in a customized manner. A physician can determine the extent of damage or inflammation to the injured site and accordingly determine the gradient patterns that need to be imprinted to the implant or the dressing to allow for cells to either migrate into or out of the wound for accelerated healing. It is hoped that one should be able to get a personalized treatment based on the extent of injury to tissue by imprinted patterns of various guidance cues to the dressing that may aid in hastening of the healing process.

In summary, this versatile method can be easily modified to design models for metastasis, biomimetic interfaces, wound dressings and implants and enhance our understanding of various cellular processes at a multi-tissue interface. The precise immobilization of chemical groups at a micron level using a photo-chemical approach makes this study unique from other contemporary studies. In conclusion, this proposal involves multiple novel approaches which will enhance our understanding of complexities involved at these heterogeneous junctions in designing a novel graded interface and systematically probing multiple cues that may influence cell decision.

References

[1] Keller R. Cell migration during gastrulation. Current Opinion in Cell Biology. 2005;17:533-41.
[2] Locascio A, Nieto MA. Cell movements during vertebrate development: integrated tissue behaviour versus individual cell migration. Current Opinion in Genetics & Development. 2001;11:464-9.
[3] Martin P. Wound Healing--Aiming for Perfect Skin Regeneration. Science. 1997;276:75-81.
[4] Luster AD, Alon R, von Andrian UH. Immune cell migration in inflammation: present and future therapeutic targets. Nat Immunol. 2005;6:1182-90.
[5] Franz CM, Jones GE, Ridley AJ. Cell Migration in Development and Disease. Developmental Cell. 2002;2:153-8.
[6] Ridley AJ, Schwartz MA, Burridge K, Firtel RA, Ginsberg MH, Borisy G, et al. Cell Migration: Integrating Signals from Front to Back. Science. 2003;302:1704-9.
[7] Chambers AF, Groom AC, MacDonald IC. Metastasis: Dissemination and growth of cancer cells in metastatic sites. Nat Rev Cancer. 2002;2:563-72.
[8] Johnston MC, Noden DM, Hazelton RD, Coulombre JL, Coulombre AJ. Origins of avian ocular and periocular tissues. Experimental Eye Research. 1979;29:27-43.
[9] Kurosaka S, Kashina A. Cell biology of embryonic migration. Birth Defects Research Part C: Embryo Today: Reviews. 2008;84:102-22.
[10] Felici M. Origin, Migration, and Proliferation of Human Primordial Germ Cells. In: Coticchio G, Albertini DF, De Santis L, editors. Oogenesis: Springer London; 2013. p. 19-37.
[11] Singer AJ, Clark RAF. Cutaneous Wound Healing. New England Journal of Medicine. 1999;341:738-46.
[12] WERNER S, GROSE R. Regulation of Wound Healing by Growth Factors and Cytokines. Physiological Reviews. 2003;83:835-70.
[13] Weninger W, Biro M, Jain R. Leukocyte migration in the interstitial space of non-lymphoid organs. Nat Rev Immunol. 2014;14:232-46.
[14] Gurtner G, Werner S, Barrandon Y, Longaker M. Wound repair and regeneration. Nature. 2008;453:314 - 21.
[15] Koh TJ, DiPietro LA. Inflammation and wound healing: the role of the macrophage. Expert Reviews in Molecular Medicine. 2011;13:null-null.
[16] Rodero MP, Khosrotehrani K. Skin wound healing modulation by macrophages. International Journal of Clinical and Experimental Pathology. 2010;3:643-53.
[17] Bravo-Cordero JJ, Hodgson L, Condeelis J. Directed cell invasion and migration during metastasis. Current Opinion in Cell Biology. 2012;24:277-83.
[18] Friedl P, Wolf K. Tumour-cell invasion and migration: diversity and escape mechanisms. Nat Rev Cancer. 2003;3:362-74.
[19] Wang W, Goswami S, Lapidus K, Wells AL, Wyckoff JB, Sahai E, et al. Identification and Testing of a Gene Expression Signature of Invasive Carcinoma Cells within Primary Mammary Tumors. Cancer Research. 2004;64:8585-94.
[20] Wang W, Goswami S, Sahai E, Wyckoff JB, Segall JE, Condeelis JS. Tumor cells caught in the act of invading: their strategy for enhanced cell motility. Trends in Cell Biology. 2005;15:138-45.
[21] Weilbaecher KN, Guise TA, McCauley LK. Cancer to bone: a fatal attraction. Nat Rev Cancer. 2011;11:411-25.
[22] Wang W, Wyckoff JB, Frohlich VC, Oleynikov Y, Hüttelmaier S, Zavadil J, et al. Single Cell Behavior in Metastatic Primary Mammary Tumors Correlated with Gene Expression Patterns Revealed by Molecular Profiling. Cancer Research. 2002;62:6278-88.

[23] Kang Y, Siegel PM, Shu W, Drobnjak M, Kakonen SM, Cordón-Cardo C, et al. A multigenic program mediating breast cancer metastasis to bone. Cancer Cell. 2003;3:537-49.
[24] McGrail DJ, Kieu QMN, Dawson MR. The malignancy of metastatic ovarian cancer cells is increased on soft matrices through a mechanosensitive Rho–ROCK pathway. Journal of Cell Science. 2014;127:2621-6.
[25] Lauffenburger DA, Horwitz AF. Cell Migration: A Physically Integrated Molecular Process. Cell. 1996;84:359-69.
[26] Vicente-Manzanares M, Horwitz AR. Cell Migration: An Overview. In: Wells CM, Parsons M, editors. Cell Migration: Developmental Methods and Protocols, Second Edition2011. p. 1-24.
[27] Horwitz R, Webb D. Cell migration. Current Biology. 2003;13:R756-R9.
[28] Welch MD, Mullins RD. Cellular control of actin nucleation. Annual Review of Cell and Developmental Biology. 2002;18:247-88.
[29] Korn E, Carlier M, Pantaloni D. Actin polymerization and ATP hydrolysis. Science. 1987;238:638-44.
[30] Pollard TD, Borisy GG. Cellular Motility Driven by Assembly and Disassembly of Actin Filaments. Cell. 2003;112:453-65.
[31] Pollard TD, Cooper JA. Actin, a Central Player in Cell Shape and Movement. Science. 2009;326:1208-12.
[32] Small JV, Stradal T, Vignal E, Rottner K. The lamellipodium: where motility begins. Trends in Cell Biology. 2002;12:112-20.
[33] Koestler SA, Auinger S, Vinzenz M, Rottner K, Small JV. Differentially oriented populations of actin filaments generated in lamellipodia collaborate in pushing and pausing at the cell front. Nat Cell Biol. 2008;10:306-13.
[34] Gupton SL, Gertler FB. Filopodia: The Fingers That Do the Walking2007.
[35] Bentley D, Toroian-Raymond A. Disoriented pathfinding by pioneer neurone growth cones deprived of filopodia by cytochalasin treatment. Nature. 1986;323:712-5.
[36] Lidke DS, Lidke KA, Rieger B, Jovin TM, Arndt-Jovin DJ. Reaching out for signals: filopodia sense EGF and respond by directed retrograde transport of activated receptors. The Journal of Cell Biology. 2005;170:619-26.
[37] Chrzanowska-Wodnicka M, Burridge K. Rho-stimulated contractility drives the formation of stress fibers and focal adhesions. The Journal of Cell Biology. 1996;133:1403-15.
[38] Hotulainen P, Lappalainen P. Stress fibers are generated by two distinct actin assembly mechanisms in motile cells. The Journal of Cell Biology. 2006;173:383-94.
[39] Kislauskis EH, Zhu X-c, Singer RH. β-Actin Messenger RNA Localization and Protein Synthesis Augment Cell Motility. The Journal of Cell Biology. 1997;136:1263-70.
[40] Mullins RD, Heuser JA, Pollard TD. The interaction of Arp2/3 complex with actin: Nucleation, high affinity pointed end capping, and formation of branching networks of filaments. Proceedings of the National Academy of Sciences. 1998;95:6181-6.
[41] Le Clainche C, Carlier M-F. Regulation of Actin Assembly Associated With Protrusion and Adhesion in Cell Migration. Physiological Reviews. 2008;88:489-513.
[42] Etienne-Manneville S, Hall A. Rho GTPases in cell biology. Nature. 2002;420:629-35.
[43] Svitkina TM, Borisy GG. Arp2/3 Complex and Actin Depolymerizing Factor/Cofilin in Dendritic Organization and Treadmilling of Actin Filament Array in Lamellipodia. The Journal of Cell Biology. 1999;145:1009-26.
[44] Bear JE, Gertler FB. Ena/VASP: towards resolving a pointed controversy at the barbed end. Journal of Cell Science. 2009;122:1947-53.
[45] Trichet L, Sykes C, Plastino J. Relaxing the actin cytoskeleton for adhesion and movement with Ena/VASP. The Journal of Cell Biology. 2008;181:19-25.

[46] Evers EE, Zondag GCM, Malliri A, Price LS, ten Klooster JP, van der Kammen RA, et al. Rho family proteins in cell adhesion and cell migration. European Journal of Cancer. 2000;36:1269-74.
[47] Johnson MH. From Mouse Egg to Mouse Embryo: Polarities, Axes, and Tissues. Annual Review of Cell and Developmental Biology. 2009;25:483-512.
[48] Goldstein B, Macara IG. The PAR Proteins: Fundamental Players in Animal Cell Polarization. Developmental Cell. 2007;13:609-22.
[49] Iglesias PA, Devreotes PN. Navigating through models of chemotaxis. Current Opinion in Cell Biology. 2008;20:35-40.
[50] Etienne-Manneville S, Hall A. Cell polarity: Par6, aPKC and cytoskeletal crosstalk. Current Opinion in Cell Biology. 2003;15:67-72.
[51] Itoh RE, Kurokawa K, Ohba Y, Yoshizaki H, Mochizuki N, Matsuda M. Activation of Rac and Cdc42 Video Imaged by Fluorescent Resonance Energy Transfer-Based Single-Molecule Probes in the Membrane of Living Cells. Molecular and Cellular Biology. 2002;22:6582-91.
[52] Srinivasan S, Wang F, Glavas S, Ott A, Hofmann F, Aktories K, et al. Rac and Cdc42 play distinct roles in regulating PI(3,4,5)P3 and polarity during neutrophil chemotaxis. The Journal of Cell Biology. 2003;160:375-85.
[53] Rodriguez OC, Schaefer AW, Mandato CA, Forscher P, Bement WM, Waterman-Storer CM. Conserved microtubule-actin interactions in cell movement and morphogenesis. Nat Cell Biol. 2003;5:599-609.
[54] Xu J, Wang F, Van Keymeulen A, Herzmark P, Straight A, Kelly K, et al. Divergent Signals and Cytoskeletal Assemblies Regulate Self-Organizing Polarity in Neutrophils. Cell. 2003;114:201-14.
[55] Worthylake RA, Burridge K. RhoA and ROCK Promote Migration by Limiting Membrane Protrusions. Journal of Biological Chemistry. 2003;278:13578-84.
[56] Gardiner EM, Pestonjamasp KN, Bohl BP, Chamberlain C, Hahn KM, Bokoch GM. Spatial and Temporal Analysis of Rac Activation during Live Neutrophil Chemotaxis. Current Biology. 2002;12:2029-34.
[57] Curtis ASG. The mechanism of adhesion of cells to glass: A Study by Interference Reflection Microscopy. The Journal of Cell Biology. 1964;20:199-215.
[58] Geiger B, Yamada KM. Molecular Architecture and Function of Matrix Adhesions. Cold Spring Harbor Perspectives in Biology. 2011;3.
[59] Hynes RO. Integrins: Bidirectional, Allosteric Signaling Machines. Cell. 2002;110:673-87.
[60] Humphries JD, Byron A, Humphries MJ. Integrin ligands at a glance. Journal of Cell Science. 2006;119:3901-3.
[61] Zaidel-Bar R, Ballestrem C, Kam Z, Geiger B. Early molecular events in the assembly of matrix adhesions at the leading edge of migrating cells. Journal of Cell Science. 2003;116:4605-13.
[62] Nobes CD, Hall A. Rho, Rac, and Cdc42 GTPases regulate the assembly of multimolecular focal complexes associated with actin stress fibers, lamellipodia, and filopodia. Cell.81:53-62.
[63] Rottner K, Hall A, Small JV. Interplay between Rac and Rho in the control of substrate contact dynamics. Current Biology.9:S1.
[64] Zaidel-Bar R, Cohen M, Addadi L, Geiger B. Hierarchical assembly of cell-matrix adhesion complexes. Biochemical Society Transactions. 2004;32:416-20.
[65] Gimona M, Buccione R, Courtneidge SA, Linder S. Assembly and biological role of podosomes and invadopodia. Current Opinion in Cell Biology. 2008;20:235-41.
[66] Emsley J, Knight CG, Farndale RW, Barnes MJ, Liddington RC. Structural Basis of Collagen Recognition by Integrin α2β1. Cell.101:47-56.
[67] Askari JA, Tynan CJ, Webb SED, Martin-Fernandez ML, Ballestrem C, Humphries MJ. Focal adhesions are sites of integrin extension. The Journal of Cell Biology. 2010;188:891-903.

[68] Huttenlocher A, Horwitz AR. Integrins in Cell Migration. Cold Spring Harbor Perspectives in Biology. 2011;3.
[69] Geiger B, Bershadsky A, Pankov R, Yamada KM. Transmembrane crosstalk between the extracellular matrix and the cytoskeleton. Nat Rev Mol Cell Biol. 2001;2:793-805.
[70] Plow EF, Haas TA, Zhang L, Loftus J, Smith JW. Ligand Binding to Integrins. Journal of Biological Chemistry. 2000;275:21785-8.
[71] Ruoslahti E. RGD and other recognition sequences for Integrins. Annual Review of Cell and Developmental Biology. 1996;12:697-715.
[72] Frisch SM, Vuori K, Ruoslahti E, Chan-Hui PY. Control of adhesion-dependent cell survival by focal adhesion kinase. The Journal of Cell Biology. 1996;134:793-9.
[73] Schlaepfer DD, Hauck CR, Sieg DJ. Signaling through focal adhesion kinase. Progress in Biophysics and Molecular Biology. 1999;71:435-78.
[74] Sieg DJ, Hauck CR, Schlaepfer DD. Required role of focal adhesion kinase (FAK) for integrin-stimulated cell migration. Journal of Cell Science. 1999;112:2677-91.
[75] Klemke RL, Leng J, Molander R, Brooks PC, Vuori K, Cheresh DA. CAS/Crk Coupling Serves as a "Molecular Switch" for Induction of Cell Migration. The Journal of Cell Biology. 1998;140:961-72.
[76] Gu J, Sumida Y, Sanzen N, Sekiguchi K. Laminin-10/11 and Fibronectin Differentially Regulate Integrin- dependent Rho and Rac Activation via p130Cas-CrkII-DOCK180 Pathway. Journal of Biological Chemistry. 2001;276:27090-7.
[77] Wary KK, Mariotti A, Zurzolo C, Giancotti FG. A Requirement for Caveolin-1 and Associated Kinase Fyn in Integrin Signaling and Anchorage-Dependent Cell Growth. Cell. 1998;94:625-34.
[78] Pelicci G, Lanfrancone L, Grignani F, McGlade J, Cavallo F, Forni G, et al. A novel transforming protein (SHC) with an SH2 domain is implicated in mitogenic signal transduction. Cell. 1992;70:93-104.
[79] Schlaepfer DD, Hanks SK, Hunter T, Geer Pvd. Integrin-mediated signal transduction linked to Ras pathway by GRB2 binding to focal adhesion kinase. Nature. 1994;372:786-91.
[80] Fabian JR, Daar IO, Morrison DK. Critical tyrosine residues regulate the enzymatic and biological activity of Raf-1 kinase. Molecular and Cellular Biology. 1993;13:7170-9.
[81] Li W, Chong H, Guan K-L. Function of the Rho Family GTPases in Ras-stimulated Raf Activation. Journal of Biological Chemistry. 2001;276:34728-37.
[82] Klemke RL, Cai S, Giannini AL, Gallagher PJ, Lanerolle Pd, Cheresh DA. Regulation of Cell Motility by Mitogen-activated Protein Kinase. The Journal of Cell Biology. 1997;137:481-92.
[83] Price LS, Leng J, Schwartz MA, Bokoch GM. Activation of Rac and Cdc42 by Integrins Mediates Cell Spreading. Molecular Biology of the Cell. 1998;9:1863-71.
[84] Manser E, Leung T, Salihuddin H, Zhao Z-s, Lim L. A brain serine/threonine protein kinase activated by Cdc42 and Rac1. Nature. 1994;367:40-6.
[85] Webb DJ, Parsons JT, Horwitz AF. Adhesion assembly, disassembly and turnover in migrating cells - over and over and over again. Nat Cell Biol. 2002;4:E97-E100.
[86] Larsen M, Tremblay ML, Yamada KM. Phosphatases in cell-matrix adhesion and migration. Nat Rev Mol Cell Biol. 2003;4:700-11.
[87] Turner CE, West KA, Brown MC. Paxillin–ARF GAP signaling and the cytoskeleton. Current Opinion in Cell Biology. 2001;13:593-9.
[88] Brahmbhatt AA, Klemke RL. ERK and RhoA Differentially Regulate Pseudopodia Growth and Retraction during Chemotaxis. Journal of Biological Chemistry. 2003;278:13016-25.
[89] Lee J, Ishihara A, Oxford G, Johnson B, Jacobson K. Regulation of cell movement is mediated by stretch-activated calcium channels. Nature. 1999;400:382-6.
[90] Hendey B, Klee C, Maxfield F. Inhibition of neutrophil chemokinesis on vitronectin by inhibitors of calcineurin. Science. 1992;258:296-9.

[91] Glading A, Lauffenburger DA, Wells A. Cutting to the chase: calpain proteases in cell motility. Trends in Cell Biology. 2002;12:46-54.
[92] Hutson MR, Kirby ML. Model systems for the study of heart development and disease - Cardiac neural crest and conotruncal malformations. Seminars in Cell & Developmental Biology. 2007;18:101-10.
[93] Amiel J, Sproat-Emison E, Garcia-Barcelo M, Lantieri F, Burzynski G, Borrego S, et al. Hirschsprung disease, associated syndromes and genetics: a review. Journal of Medical Genetics. 2008;45:1-14.
[94] Hood JD, Cheresh DA. Role of integrins in cell invasion and migration. Nat Rev Cancer. 2002;2:91-100.
[95] Avraamides CJ, Garmy-Susini B, Varner JA. Integrins in angiogenesis and lymphangiogenesis. Nat Rev Cancer. 2008;8:604-17.
[96] Stoller JZ, Epstein JA. Cardiac neural crest. Seminars in Cell & Developmental Biology. 2005;16:704-15.
[97] Epstein JA, Parmacek MS. Recent Advances in Cardiac Development With Therapeutic Implications for Adult Cardiovascular Disease. Circulation. 2005;112:592-7.
[98] Hutson MR, Kirby ML. Neural crest and cardiovascular development: A 20-year perspective. Birth Defects Research Part C: Embryo Today: Reviews. 2003;69:2-13.
[99] Epstein JA. Developing models of DiGeorge syndrome. Trends in Genetics. 2001;17:S13-S7.
[100] Lara Rodriguez L, Schneider IC. Directed cell migration in multi-cue environments. Integrative Biology. 2013;5:1306-23.
[101] Petrie RJ, Doyle AD, Yamada KM. Random versus directionally persistent cell migration. Nat Rev Mol Cell Biol. 2009;10:538-49.
[102] Singer SJ, Kupfer A. The Directed Migration of Eukaryotic Cells. Annual Review of Cell Biology. 1986;2:337-65.
[103] Imitola J, Raddassi K, Park KI, Mueller F-J, Nieto M, Teng YD, et al. Directed migration of neural stem cells to sites of CNS injury by the stromal cell-derived factor 1α/CXC chemokine receptor 4 pathway. Proceedings of the National Academy of Sciences. 2004;101:18117-22.
[104] Green TD, Park J, Yin Q, Fang S, Crews AL, Jones SL, et al. Directed migration of mouse macrophages in vitro involves myristoylated alanine-rich C-kinase substrate (MARCKS) protein. Journal of Leukocyte Biology. 2012;92:633-9.
[105] Lo C-M, Wang H-B, Dembo M, Wang Y-l. Cell Movement Is Guided by the Rigidity of the Substrate. Biophysical journal. 2000;79:144-52.
[106] Pelham RJ, Wang Y-l. Cell locomotion and focal adhesions are regulated by substrate flexibility. Proceedings of the National Academy of Sciences. 1997;94:13661-5.
[107] Brown MJ, Loew LM. Electric field-directed fibroblast locomotion involves cell surface molecular reorganization and is calcium independent. The Journal of Cell Biology. 1994;127:117-28.
[108] Saranak J, Foster KW. Rhodopsin guides fungal phototaxis. Nature. 1997;387:465-6.
[109] Maheshwari G, Brown G, Lauffenburger DA, Wells A, Griffith LG. Cell adhesion and motility depend on nanoscale RGD clustering. Journal of Cell Science. 2000;113:1677-86.
[110] Harris A. Behavior of cultured cells on substrata of variable adhesiveness. Exp Cell Res. 1973;77:285-97.
[111] Wu J, Mao Z, Tan H, Han L, Ren T, Gao C. Gradient biomaterials and their influences on cell migration. Interface Focus. 2012;2:337-55.
[112] Genzer J, Bhat RR. Surface-Bound Soft Matter Gradients. Langmuir. 2008;24:2294-317.
[113] Thiery JP, Duband JL, Tucker GC. Cell Migration in the Vertebrate Embryo: Role of Cell Adhesion and Tissue Environment in Pattern Formation. Annual Review of Cell Biology. 1985;1:91-113.
[114] Jacinto A, Martinez-Arias A, Martin P. Mechanisms of epithelial fusion and repair. Nat Cell Biol. 2001;3:E117-E23.

[115] Smith JT, Tomfohr JK, Wells MC, Beebe TP, Kepler TB, Reichert WM. Measurement of Cell Migration on Surface-Bound Fibronectin Gradients. Langmuir. 2004;20:8279-86.
[116] Zigmond SH. Ability of polymorphonuclear leukocytes to orient in gradients of chemotactic factors. The Journal of Cell Biology. 1977;75:606-16.
[117] Zaari N, Rajagopalan P, Kim SK, Engler AJ, Wong JY. Photopolymerization in Microfluidic Gradient Generators: Microscale Control of Substrate Compliance to Manipulate Cell Response. Advanced Materials. 2004;16:2133-7.
[118] Li Jeon N, Baskaran H, Dertinger SKW, Whitesides GM, Van De Water L, Toner M. Neutrophil chemotaxis in linear and complex gradients of interleukin-8 formed in a microfabricated device. Nat Biotech. 2002;20:826-30.
[119] Chen G, Ito Y. Gradient micropattern immobilization of EGF to investigate the effect of artificial juxtacrine stimulation. Biomaterials. 2001;22:2453-7.
[120] Carter SB. Haptotaxis and the Mechanism of Cell Motility. Nature. 1967;213:256-60.
[121] Lamalice L, Le Boeuf F, Huot J. Endothelial Cell Migration During Angiogenesis. Circulation Research. 2007;100:782-94.
[122] Seppä H, Grotendorst G, Seppä S, Schiffmann E, Martin GR. Platelet-derived growth factor in chemotactic for fibroblasts. The Journal of Cell Biology. 1982;92:584-8.
[123] DiMilla P, Stone J, Quinn J, Albelda S, Lauffenburger D. Maximal migration of human smooth muscle cells on fibronectin and type IV collagen occurs at an intermediate attachment strength. The Journal of Cell Biology. 1993;122:729-37.
[124] Palecek SP, Loftus JC, Ginsberg MH, Lauffenburger DA, Horwitz AF. Integrin-ligand binding properties govern cell migration speed through cell-substratum adhesiveness. Nature. 1997;385:537-40.
[125] Ware MF, Wells A, Lauffenburger DA. Epidermal growth factor alters fibroblast migration speed and directional persistence reciprocally and in a matrix-dependent manner. Journal of Cell Science. 1998;111:2423-32.
[126] Huttenlocher A, Ginsberg MH, Horwitz AF. Modulation of cell migration by integrin-mediated cytoskeletal linkages and ligand-binding affinity. The Journal of Cell Biology. 1996;134:1551-62.
[127] Laskin DL, Kimura T, Sakakibara S, Riley DJ, Berg RA. Chemotactic activity of collagen-like polypeptides for human peripheral blood neutrophils. Journal of Leukocyte Biology. 1986;39:255-66.
[128] Postlethwaite AE, Seyer JM, Kang AH. Chemotactic attraction of human fibroblasts to type I, II, and III collagens and collagen-derived peptides. Proceedings of the National Academy of Sciences. 1978;75:871-5.
[129] Burdick JA, Khademhosseini A, Langer R. Fabrication of Gradient Hydrogels Using a Microfluidics/Photopolymerization Process. Langmuir. 2004;20:5153-6.
[130] Guo W-h, Frey MT, Burnham NA, Wang Y-l. Substrate Rigidity Regulates the Formation and Maintenance of Tissues. Biophysical journal. 2006;90:2213-20.
[131] Kuboki T, Chen W, Kidoaki S. Time-Dependent Migratory Behaviors in the Long-Term Studies of Fibroblast Durotaxis on a Hydrogel Substrate Fabricated with a Soft Band. Langmuir. 2014;30:6187-96.
[132] Wang H-B, Dembo M, Hanks SK, Wang Y-l. Focal adhesion kinase is involved in mechanosensing during fibroblast migration. Proceedings of the National Academy of Sciences. 2001;98:11295-300.
[133] Dokukina IV, Gracheva ME. A Model of Fibroblast Motility on Substrates with Different Rigidities. Biophysical journal. 2010;98:2794-803.
[134] Vicente-Manzanares M. Cell Migration: Cooperation between Myosin II Isoforms in Durotaxis. Current Biology. 2013;23:R28-R9.
[135] Gilbert PM, Havenstrite KL, Magnusson KEG, Sacco A, Leonardi NA, Kraft P, et al. Substrate Elasticity Regulates Skeletal Muscle Stem Cell Self-Renewal in Culture. Science. 2010;329:1078-81.
[136] Rowley JA, Mooney DJ. Alginate type and RGD density control myoblast phenotype. Journal of Biomedical Materials Research. 2002;60:217-23.

[137] Wong JY, Velasco A, Rajagopalan P, Pham Q. Directed Movement of Vascular Smooth Muscle Cells on Gradient-Compliant Hydrogels†. Langmuir. 2003;19:1908-13.
[138] Balgude AP, Yu X, Szymanski A, Bellamkonda RV. Agarose gel stiffness determines rate of DRG neurite extension in 3D cultures. Biomaterials. 2001;22:1077-84.
[139] Martinez JS, Lehaf AM, Schlenoff JB, Keller TCS. Cell Durotaxis on Polyelectrolyte Multilayers with Photogenerated Gradients of Modulus. Biomacromolecules. 2013;14:1311-20.
[140] Saez A, Ghibaudo M, Buguin A, Silberzan P, Ladoux B. Rigidity-driven growth and migration of epithelial cells on microstructured anisotropic substrates. Proceedings of the National Academy of Sciences. 2007;104:8281-6.
[141] Breckenridge M, Desai R, Yang M, Fu J, Chen C. Substrates with Engineered Step Changes in Rigidity Induce Traction Force Polarity and Durotaxis. Cel Mol Bioeng. 2014;7:26-34.
[142] Peyton SR, Putnam AJ. Extracellular matrix rigidity governs smooth muscle cell motility in a biphasic fashion. Journal of Cellular Physiology. 2005;204:198-209.
[143] Lin F, Nguyen CM-C, Wang S-J, Saadi W, Gross SP, Jeon NL. Effective neutrophil chemotaxis is strongly influenced by mean IL-8 concentration. Biochemical and Biophysical Research Communications. 2004;319:576-81.
[144] Stefonek TJ, Masters KS. Immobilized gradients of epidermal growth factor promote accelerated and directed keratinocyte migration. Wound Repair and Regeneration. 2007;15:847-55.
[145] Shaw TJ, Martin P. Wound repair at a glance. Journal of Cell Science. 2009;122:3209-13.
[146] Hinz B. Formation and Function of the Myofibroblast during Tissue Repair. J Invest Dermatol. 0000;127:526-37.
[147] Polacheck W, Zervantonakis I, Kamm R. Tumor cell migration in complex microenvironments. Cell Mol Life Sci. 2012:1-22.
[148] Friedl P, Alexander S. Cancer Invasion and the Microenvironment: Plasticity and Reciprocity. Cell. 2011;147:992-1009.
[149] Kostic A, Lynch CD, Sheetz MP. Differential Matrix Rigidity Response in Breast Cancer Cell Lines Correlates with the Tissue Tropism. PLoS ONE. 2009;4:e6361.
[150] Roussos ET, Condeelis JS, Patsialou A. Chemotaxis in cancer. Nat Rev Cancer. 2011;11:573-87.
[151] Choi JS, Harley BAC. The combined influence of substrate elasticity and ligand density on the viability and biophysical properties of hematopoietic stem and progenitor cells. Biomaterials. 2012;33:4460-8.
[152] Hale NA, Yang Y, Rajagopalan P. Cell Migration at the Interface of a Dual Chemical-Mechanical Gradient. ACS Applied Materials & Interfaces. 2010;2:2317-24.
[153] Suva LJ, Griffin RJ, Makhoul I. Mechanisms of bone metastases of breast cancer. Endocrine-Related Cancer. 2009;16:703-13.
[154] Hussein O, Komarova S. Breast cancer at bone metastatic sites: recent discoveries and treatment targets. Journal of Cell Communication and Signaling. 2011;5:85-99.
[155] Laurencin CT, Freeman JW. Ligament tissue engineering: An evolutionary materials science approach. Biomaterials. 2005;26:7530-6.
[156] Yang PJ, Temenoff JS. Engineering Orthopedic Tissue Interfaces. Tissue Eng Part B-Rev. 2009;15:127-41.
[157] Trotter JA. Structure–function considerations of muscle–tendon junctions. Comparative Biochemistry and Physiology Part A: Molecular & Integrative Physiology. 2002;133:1127-33.
[158] Koo LY, Irvine DJ, Mayes AM, Lauffenburger DA, Griffith LG. Co-regulation of cell adhesion by nanoscale RGD organization and mechanical stimulus. Journal of Cell Science. 2002;115:1423-33.
[159] Singh M, Berkland C, Detamore MS. Strategies and Applications for Incorporating Physical and Chemical Signal Gradients in Tissue Engineering. Tissue Eng Part B-Rev. 2008;14:341-66.

[160] Sant S, Hancock MJ, Donnelly JP, Iyer D, Khademhosseini A. Biomimetic gradient hydrogels for tissue engineering. The Canadian Journal of Chemical Engineering. 2010;88:899-911.
[161] Martin TA, Herman CT, Limpoco FT, Michael MC, Potts GK, Bailey RC. Quantitative Photochemical Immobilization of Biomolecules on Planar and Corrugated Substrates: A Versatile Strategy for Creating Functional Biointerfaces. ACS Applied Materials & Interfaces. 2011;3:3762-71.
[162] Joshi-Barr S, Karpiak JV, Ner Y, Wen JH, Engler AJ, Almutairi A. Density Gradient Multilayered Polymerization (DGMP): A Novel Technique for Creating Multi-compartment, Customizable Scaffolds for Tissue Engineering. 2013:e50018.
[163] Bhat RR, Tomlinson MR, Genzer J. Orthogonal surface-grafted polymer gradients: A versatile combinatorial platform. Journal of Polymer Science Part B: Polymer Physics. 2005;43:3384-94.
[164] Carr LR, Krause JE, Ella-Menye J-R, Jiang S. Single nonfouling hydrogels with mechanical and chemical functionality gradients. Biomaterials. 2011;32:8456-61.
[165] Wu M-H, Huang S-B, Lee G-B. Microfluidic cell culture systems for drug research. Lab on a Chip. 2010;10:939-56.
[166] Park JY, Yoo SJ, Hwang CM, Lee S-H. Simultaneous generation of chemical concentration and mechanical shear stress gradients using microfluidic osmotic flow comparable to interstitial flow. Lab on a Chip. 2009;9:2194-202.
[167] Park JY, Yoo SJ, Hwang CM, Lee SH. Simultaneous generation of chemical concentration and mechanical shear stress gradients using microfluidic osmotic flow comparable to interstitial flow. Lab Chip. 2009;9:2194-202.
[168] Chin-Hsiung T, Po-Ling K. Microfluidic device with dual mechanical cues for cell migration investigation. Engineering in Medicine and Biology Society (EMBC), 2013 35th Annual International Conference of the IEEE2013. p. 842-5.
[169] Beningo KA, Lo C-M, Wang Y-L. Flexible polyacrylamide substrata for the analysis of mechanical interactions at cell-substratum adhesions. Methods in Cell Biology: Academic Press; 2002. p. 325-39.
[170] Raab M, Swift J, P. Dingal PCD, Shah P, Shin J-W, Discher DE. Crawling from soft to stiff matrix polarizes the cytoskeleton and phosphoregulates myosin-II heavy chain. The Journal of Cell Biology. 2012;199:669-83.
[171] Engler A, Bacakova L, Newman C, Hategan A, Griffin M, Discher D. Substrate Compliance versus Ligand Density in Cell on Gel Responses. Biophysical journal. 2004;86:617-28.
[172] Moffat KL, Sun W-HS, Pena PE, Chahine NO, Doty SB, Ateshian GA, et al. Characterization of the structure–function relationship at the ligament-to-bone interface. Proceedings of the National Academy of Sciences. 2008;105:7947-52.
[173] Reinhart-King CA, Dembo M, Hammer DA. Endothelial Cell Traction Forces on RGD-Derivatized Polyacrylamide Substrata†. Langmuir. 2002;19:1573-9.
[174] Wang YL, Pelham RJ. Preparation of a flexible, porous polyacrylamide substrate for mechanical studies of cultured cells. Methods Enzymol. 1998;298:489-96.
[175] Reinhart-King CA, Dembo M, Hammer DA. Cell-Cell Mechanical Communication through Compliant Substrates. Biophysical journal. 2008;95:6044-51.
[176] Damljanovic V, Lagerholm BC, Jacobson K. Bulk and micropatterned conjugation of extracellular matrix proteins to characterized polyacrylamide substrates for cell mechanotransduction assays. Biotechniques. 2005;39:847-51.
[177] Rajagopalan P, Marganski WA, Brown XQ, Wong JY. Direct Comparison of the Spread Area, Contractility, and Migration of balb/c 3T3 Fibroblasts Adhered to Fibronectin- and RGD-Modified Substrata. Biophysical journal. 2004;87:2818-27.
[178] Bryant SJ, Nuttelman CR, Anseth KS. Cytocompatibility of UV and visible light photoinitiating systems on cultured NIH/3T3 fibroblasts in vitro. J Biomater Sci-Polym Ed. 2000;11:439-57.

[179] Mironi-Harpaz I, Wang DY, Venkatraman S, Seliktar D. Photopolymerization of cell-encapsulating hydrogels: Crosslinking efficiency versus cytotoxicity. Acta Biomaterialia. 2012;8:1838-48.
[180] Williams CG, Malik AN, Kim TK, Manson PN, Elisseeff JH. Variable cytocompatibility of six cell lines with photoinitiators used for polymerizing hydrogels and cell encapsulation. Biomaterials. 2005;26:1211-8.
[181] Cavell EAS. Kinetics of polymerisation of acrylamide initiated by 4,4'-azo-bis-4-cyanopentanoic acid. Die Makromolekulare Chemie. 1962;54:70-7.
[182] Tse JR, Engler AJ. Preparation of Hydrogel Substrates with Tunable Mechanical Properties. Current Protocols in Cell Biology: John Wiley & Sons, Inc.; 2001.
[183] Grinnell F, Petroll WM. Cell Motility and Mechanics in Three-Dimensional Collagen Matrices. Annual Review of Cell and Developmental Biology. 2010;26:335-61.
[184] Grinnell F, Ho C-H, Tamariz E, Lee DJ, Skuta G. Dendritic Fibroblasts in Three-dimensional Collagen Matrices. Molecular Biology of the Cell. 2003;14:384-95.
[185] Beningo KA, Dembo M, Wang Y-l. Responses of fibroblasts to anchorage of dorsal extracellular matrix receptors. Proceedings of the National Academy of Sciences. 2004;101:18024-9.
[186] Rajagopalan P, Marganski WA, Brown XQ, Wong JY. Direct comparison of the spread area, contractility, and migration of balb/c 3T3 fibroblasts adhered to fibronectin- and RGD-modified substrata. Biophysical journal. 2004;87:2818-27.
[187] Geissler E, Hecht AM. The Poisson Ratio in Polymer Gels. Macromolecules. 1980;13:1276-80.
[188] Gaudet C, Marganski WA, Kim S, Brown CT, Gunderia V, Dembo M, et al. Influence of Type I Collagen Surface Density on Fibroblast Spreading, Motility, and Contractility. Biophysical journal. 2003;85:3329-35.
[189] Salmon H, Rivas-Caicedo A, Asperti-Boursin F, Lebugle C, Bourdoncle P, Donnadieu E. Ex vivo imaging of T cells in murine lymph node slices with widefield and confocal microscopes. Journal of visualized experiments : JoVE. 2011:e3054.
[190] Zaidel-Bar R, Ballestrem C, Kam Z, Geiger B. Early molecular events in the assembly of matrix adhesions at the leading edge of migrating cells. Journal of cell science. 2003;116:4605-13.
[191] Sant S, Hancock MJ, Donnelly JP, Iyer D, Khademhosseini A. Biomimetic Gradient Hydrogels for Tissue Engineering. The Canadian journal of chemical engineering. 2010;88:899-911.
[192] Kirkpatrick SJ, Wang RK, Duncan DD, Kulesz-Martin M, Lee K. Imaging the mechanical stiffness of skin lesions by in vivo acousto-optical elastography. Optics express. 2006;14:9770-9.
[193] Engler AJ, Sen S, Sweeney HL, Discher DE. Matrix elasticity directs stem cell lineage specification. Cell. 2006;126:677-89.
[194] Rzymski P, Skorzewska A, Skibinska-Zielinska M, Opala T. Factors influencing breast elasticity measured by the ultrasound Shear Wave elastography - preliminary results. Arch Med Sci. 2011;7:127-33.
[195] Patel NR, Bole M, Chen C, Hardin CC, Kho AT, Mih J, et al. Cell Elasticity Determines Macrophage Function. PLoS ONE. 2012;7:e41024.
[196] Tse JR, Engler AJ. Stiffness Gradients Mimicking Tissue Variation Regulate Mesenchymal Stem Cell Fate. PLoS ONE. 2011;6:e15978.
[197] Hagemann T, Robinson SC, Schulz M, Trümper L, Balkwill FR, Binder C. Enhanced invasiveness of breast cancer cell lines upon co-cultivation with macrophages is due to TNF-α dependent up-regulation of matrix metalloproteases. Carcinogenesis. 2004;25:1543-9.
[198] Goers L, Freemont P, Polizzi KM. Co-culture systems and technologies: taking synthetic biology to the next level. Journal of The Royal Society Interface. 2014;11.
[199] Moraes C, Mehta G, Lesher-Perez S, Takayama S. Organs-on-a-Chip: A Focus on Compartmentalized Microdevices. Ann Biomed Eng. 2012;40:1211-27.

[200] Lucas T, Waisman A, Ranjan R, Roes J, Krieg T, Müller W, et al. Differential Roles of Macrophages in Diverse Phases of Skin Repair. The Journal of Immunology. 2010;184:3964-77.
[201] Mahdavian Delavary B, van der Veer W, van Egmond M, Niessen F, Beelen R. Macrophages in skin injury and repair. Immunobiology. 2011;216:753 - 62.
[202] Mosser D, Edwards J. Exploring the full spectrum of macrophage activation. Nat Rev Immunol. 2008;8:958 - 69.
[203] Gordon S. Alternative activation of macrophages. Nat Rev Immunol. 2003;3:23 - 35.
[204] Féréol S, Fodil R, Labat B, Galiacy S, Laurent VM, Louis B, et al. Sensitivity of alveolar macrophages to substrate mechanical and adhesive properties. Cell Motility and the Cytoskeleton. 2006;63:321-40.
[205] Blakney AK, Swartzlander MD, Bryant SJ. Student award winner in the undergraduate category for the society of biomaterials 9th World Biomaterials Congress, Chengdu, China, June 1–5, 2012. Journal of Biomedical Materials Research Part A. 2012;100A:1375-86.
[206] La Celle P, Blumenstock FA, McKinley C, Saba TM, Vincent PA, Gray V. Blood-borne collagenous debris complexes with plasma fibronectin after thermal injury. Blood. 1990;75:470-8.
[207] Gowen BB, Borg TK, Ghaffar A, Mayer EP. Selective adhesion of macrophages to denatured forms of type I collagen is mediated by scavenger receptors. Matrix Biology. 2000;19:61-71.
[208] Garnotel R, Rittié L, Poitevin S, Monboisse J-C, Nguyen P, Potron G, et al. Human Blood Monocytes Interact with Type I Collagen Through αxβ2 Integrin (CD11c-CD18, gp150-95). The Journal of Immunology. 2000;164:5928-34.
[209] Davis GE, Thomas JS, Madden S. The alpha4beta1 integrin can mediate leukocyte adhesion to casein and denatured protein substrates. Journal of Leukocyte Biology. 1997;62:318-28.
[210] Davis GE. The Mac-1 and p150,95 β2 integrins bind denatured proteins to mediate leukocyte cell-substrate adhesion. Exp Cell Res. 1992;200:242-52.
[211] Postlethwaite AE, Kang AH. Collagen-and collagen peptide-induced chemotaxis of human blood monocytes. The Journal of Experimental Medicine. 1976;143:1299-307.
[212] Laskin DL, Soltys RA, Berg RA, Riley DJ. Activation of alveolar macrophages by native and synthetic collagen-like polypeptides. American Journal of Respiratory Cell and Molecular Biology. 1994;10:58-64.
[213] Laub R, Huybrechts-Godin G, Peeters-Joris C, Vaes G. Degradation of collagen and proteoglycan by macrophages and fibroblasts Individual potentialities of each cell type and cooperative effects through the activation of fibroblasts by macrophages. Biochimica et Biophysica Acta (BBA) - Molecular Cell Research. 1982;721:425-33.
[214] Song E, Ouyang N, Horbelt M, Antus B, Wang M, Exton M. Influence of Alternatively and Classically Activated Macrophages on Fibrogenic Activities of Human Fibroblasts. Cell Immunol. 2000;204:19 - 28.
[215] Zeng Q, Chen W. The functional behavior of a macrophage/fibroblast co-culture model derived from normal and diabetic mice with a marine gelatin–oxidized alginate hydrogel. Biomaterials. 2010;31:5772-81.
[216] Song E, Ouyang N, Hörbelt M, Antus B, Wang M, Exton MS. Influence of Alternatively and Classically Activated Macrophages on Fibrogenic Activities of Human Fibroblasts. Cellular Immunology. 2000;204:19-28.
[217] Huybrechts-Godin G, Peeters-Joris C, Vaes G. Partial characterization of the macrophage factor that stimulates fibroblasts to produce collagenase and to degrade collagen. Biochimica et Biophysica Acta (BBA) - Molecular Cell Research. 1985;846:51-4.
[218] Ploeger D, Hosper N, Schipper M, Koerts J, de Rond S, Bank R. Cell plasticity in wound healing: paracrine factors of M1/ M2 polarized macrophages influence the phenotypical state of dermal fibroblasts. Cell Communication and Signaling. 2013;11:29.
[219] McWhorter FY, Wang T, Nguyen P, Chung T, Liu WF. Modulation of macrophage phenotype by cell shape. Proceedings of the National Academy of Sciences. 2013.

[220] Stout R, Suttles J. Functional plasticity of macrophages: reversible adaptation to changing microenvironments. J Leukoc Biol. 2004;76:509 - 13.
[221] Stout R, Jiang C, Matta B, Tietzel I, Watkins S, Suttles J. Macrophages Sequentially Change Their Functional Phenotype in Response to Changes in Microenvironmental Influences. J Immunol. 2005;175:342 - 9.
[222] Barth KA, Waterfield JD, Brunette DM. The effect of surface roughness on RAW 264.7 macrophage phenotype. Journal of Biomedical Materials Research Part A. 2013;101A:2679-88.